THE UNIVERSITY OF OKLAHOMA
GRADUATE COLLEGE

# ANISOTROPIC POROMECHANICS OF THE WELLBORE COUPLED WITH THERMAL AND CHEMICAL GRADIENTS

A DISSERTATION
SUBMITTED TO THE GRADUATE FACULTY
IN PARTIAL FULFILLMENT OF THE REQUIREMENTS FOR THE
DEGREE OF
DOCTOR OF PHILOSOPHY

BY
SHAILESH MANIK EKBOTE
NORMAN, OKLAHOMA
2002

# ANISOTROPIC POROMECHANICS OF THE WELLBORE COUPLED WITH THERMAL AND CHEMICAL GRADIENTS

A DISSERTATION APPROVED
FOR
THE SCHOOL OF CIVIL ENGINEERING
AND ENVIRONMENTAL SCIENCE

BY

Yaman Abousleiman 10/24/2002

Md. Mushararfuzzaman

K.K. M 10/24/02

Gerald A. McKee 10/24/02

Luther W. White 10/28/02

Dedicated to my Parents and Teachers

# Acknowledgments

My wholehearted thanks go to my advisor Dr. Younane Abousleiman whose technical advice, encouragement and guidance have been invaluable. Dr. Abousleiman always encouraged independent thinking related to scientific aspects of my work and instilled a confidence in my abilities. Furthermore, his enthusiasm, scientific vigor, and commitment to excellence have always motivated me to strive for the very best. I am very much appreciative of the support he provided during my dissertation work and graduate studies in Civil Engineering and Computer Science. I would also like to thank my co-advisor Dr. Musharraf Zaman for providing encouragement, academic advice and technical help at various instances. He played a very important role in grooming me during my formative years at the University of Oklahoma. I would also like to thank members of my doctoral advisory committee, Dr. Luther White, Dr. K.K. Muraleetharan and Dr. Gerald Miller for interest in guiding my work. I also appreciate scientific help provided by Dr. Lizheng Cui during various formal and informal technical discussions in poroelasticity. During the course of my work, I have received invaluable suggestions from industry members of the Rock Mechanics Consortium, especially Dr. Fersheed Mody and Mr. Uday Tare.

My appreciation also goes to Dr. Mazen Kanj and Dr. Gene Scott for their encouragement and technical help. I also thank Ms Carla Cates for her open door policy on any matters pertaining to administrative affairs.

I sincerely appreciate the help and assistance of any kind provided by my colleague

Mr. Rajesh Nair during my stay. I have had numerous technical discussions with him and his suggestions and advice have provided me with a better understanding of the subject. My sincere thanks also goes to Mrs. Maya Nandakumar for her assistance and advice on various matters. I would also like to thank my friends Mr. Sachin Deshpande, Mr. Tarun Srivastava, Mr. Anil Shenoy, Mr. Torez Kasnavia for making my stay at Norman a pleasant one.

Finally I am thankful to my parents, Mr. Manik Ekbote and Mrs. Apara Ekbote for their encouragement, support and patience. Right from my childhood my parents have instilled in me a confidence, that I could achieve whatever I strive for, and I believe this quality has always helped me in my academic career. My brother, Mr. Shirish Ekbote, has always been a source of inspiration for me and I appreciate his guidance, encouragement and the financial support he provided me during my graduate studies.

I owe all the knowledge that I have acquired in my life to my parents and to every teacher and professor who have taught me right from my childhood. My dissertation is dedicated to them.

# Contents

# List of Figures

# List of Tables

# Abstract

A comprehensive and systematic study of anisotropic poromechanics is undertaken with application to the problem of an inclined borehole in a saturated porous rock formation. The development is based on the theoretical approach in anisotropic poromechanics that accounts for the coupling characteristics between the fluid saturated porous rock and rock solid structure with emphasis on the thermal, chemical, hydraulic and mechanical coupled processes. The borehole is assumed to be deep, as in an oil recovery process, and inclined to the insitu three-dimensional state of stress. Analytical solutions for stress and pore pressure distributions in the vicinity of the borehole have been developed under the framework of the poromechanics models. It is envisaged that the theoretical formulations and solutions would aid in the understanding of complex coupled phenomena known to exist in fluid saturated porous media when subjected to stress and pressure perturbations. Further, these solutions developed would provide an accurate assessment of borehole stability that is critical to a successful drilling operation.

A generalized solution strategy for the inclined borehole problem, where the problem is sub-divided into simpler problems, is presented. The linearity of stress-strain relations assumed, allows a superposition of the solutions of the sub-problems.

A generalized anisotropic porothermoelastic formulation incorporating fully coupled thermo-hydro-mechanical response of saturated porous media is developed. Governing equations are tailored for transversely isotropic media and the solution for the inclined borehole problem is developed. The effect of material anisotropy on the stress, pore

pressure and borehole stability is analyzed.

Chemical effects are incorporated into the anisotropic poroelastic formulation and the resulting model is termed porochemoelastic. The model accounts for fully-coupled hydraulic, chemical and mechanical processes and, is applicable to chemically active anisotropic formations saturated with a pore fluid comprising of two species. Inclined borehole solutions applicable to transversely isotropic and isotropic media are developed. The effect of chemical potential of the fluid in the wellbore on its stability is also analyzed.

A generalized anisotropic porochemothermoelastic formulation is presented which is an extension of the porochemoelastic model and accounts for thermal effects in chemically active poroelastic media. Governing equations are specialized for transversely isotropic and isotropic cases and corresponding inclined borehole solutions are developed. As in the porochemoelastic case, the effect of chemical potential on borehole stability is studied.

# Chapter 1

# Introduction

There are a broad class of problems in geotechnical, mining and petroleum engineering fields for which all dominant characteristics are well represented under the realm of the mechanics of porous media, 'poromechanics'. Geo-activities associated with the aforementioned areas are host to a multitude of complex phenomena. Numerous driving flux phenomena come into play which interact retroactively dictating a time-dependent coupled behavior.

Of particular interest are the induced physicochemical processes associated with deep drilling undertaken in oil recovery schemes. Wellbore drilling perturbs the pre-existing stress and pore pressure fields and triggers a coupled response between the fluid diffusion and the solid deformation processes. Associated with wellbore drilling is the existence of the drilling fluid which acts as a stabilizing entity. This drilling fluid brings into play the presence of thermal gradients that affect both the diffusion as well as deformation mechanisms. Also, most of the drilling activities are carried out in formations that can be broadly classified as chemically active due to the fluid-shale interaction that occurs at the microscale. The anisotropic nature of rock formations is another factor that adds a further degree of complexity to the problem.

In the petroleum industry, technological development associated with deviated drilling has facilitated higher reserve access, faster production rates and favored development

of far reaching reservoirs utilizing highly deviated 'extended reach wells'. The stability issues associated with deviated wellbores pose an additional cause for concern. The significantly higher development cost of deviated wellbores dictate a rigorous analysis of their stability, and an appropriate design of the drilling fluid density, thermal and chemical properties, to ensure an economical and successful drilling operation.

The inter-dependence of the change in stress and pore pressure fields due to perturbations imposed on a saturated porous rock formations is well known. The coupled phenomena results in a time-dependent response, a feature that cannot be accounted for by conventional elastic/plastic models. The concepts associated with the coupled diffusion-deformation phenomenon are addressed by Biot's theory of poroelasticity (*Biot*, 1941; *Rice and Cleary*, 1976). Many critical observations pertaining to borehole failure, especially the time-dependency associated with wellbore stability and evaluation of associated design parameters, have found their explanation on the basis of this theory (*Cheng et al.*, 1993; *Cui et al.*, 1999a).

Subsequently, Biot's isotropic theory has been extended for general anisotropic materials (*Biot*, 1955; *Thompson and Willis*, 1991). The associated material constants have been identified and linked to well understood engineering constants (*Abousleiman and Cheng*, 1993; *Cheng*, 1997; *Abousleiman and Cui*, 2000). This development of anisotropic poroelasticity has resulted in development of various fundamental analytical solutions which address the coupled behavior patterns in the anisotropic materials (*Abousleiman et al.*, 1995; *Abousleiman et al.*, 1996a; *Abousleiman and Cui*, 1998).

Over the years, theoretical developments in this field have resulted in thermal and chemical effects being accounted for within the framework of Biot's theory (*Schiffman* 1971; *Bear and Corapcioglu*, 1981; *McTigue*, 1986, 1990; *Katsube*, 1988; *Sherwood*, 1993, 1994a, 1994b). However, critical aspects of material anisotropy coupled with the thermal and chemical processes have not been addressed. In view of the above, a development

of poromechanical models that present an accurate and appropriate assessment of the coupled behavior patterns and a quantification of these effects in the stability analyses of wellbores is deemed necessary, which would assist in selection of effective and economical drilling strategies considering realistic field conditions.

## 1.1 Motivation

Assessing the implications of undertaking geomechanical projects such as drilling deep, deviated boreholes in complex formations requires a thorough understanding of the coupled processes that may be induced by this activity. This interplay could be between the thermal, hydraulic, chemical and mechanical processes, depending on the nature (chemically active or inactive) of the formation and drilling conditions (isothermal or non-isothermal). Poroelastic solutions for the inclined borehole problem have been obtained and subsequent stability analyses have been carried out for permeable and impermeable flux boundary conditions at the wellbore wall (*Cui et al.*, 1997, 1998, 1999a).

Non-isothermal conditions in drilling and wellbore stability are appropriately addressed by the porothermoelastic model (*Li*, 1998). Subsequently, borehole solutions have been proposed and wellbore stability analysis has been carried out based on this theory. However, the simple deposition of sedimentary rocks over a geological time scale, lends a transversely isotropic character to formations in which drilling activities are usually carried out (*Abousleiman and Ekbote*, 1999). Corresponding inclined borehole solutions applicable to such formations have not been developed.

In the case of drilling through chemically active formations such as shale, interaction with the drilling fluid may induce swelling of the formation in the vicinity of the borehole (*Sherwood*, 1993; *Mody and Hale*, 1993). The induced changes in pore pressure and stress distributions can be analyzed, as a first order approximation, employing the concept of a chemical potential within the framework of a porochemoelastic model (*Sherwood*,

1993). This approach has been implemented to derive the porochemoelastic solution of the inclined borehole using the membrane efficiency approach (*Abousleiman et al.*, 2001, 2002). However, the effects of ionic exchange predominant in chemically active formations are not addressed. Also, the anisotropy of chemically active rock formations have not been accounted for in earlier solutions.

In the general case, all of the aforementioned physicochemical processes may have a bearing on the pore pressure and stress distributions in the vicinity of the borehole. An accurate formulation of each of these processes and development of borehole solutions accounting for their combined effect are a precursor to any stability assessment under such scenarios. To the author's knowledge, such a formulation has not been reported in the literature.

This dissertation is oriented towards the development of a framework for poromechanics models. A generalized solution strategy for the inclined borehole problem applicable to these poromechanics models is developed. It is envisaged that inclined borehole solutions for the poromechanics models in this dissertation will provide researchers and field engineers with a more comprehensive tool that enhances understanding of the factors involved in the complex borehole geometries.

## 1.2 Objectives

The objectives of this dissertation are as follows:

1. Develop a generalized solution strategy for the inclined borehole problem applicable to the poromechanics models discussed earlier.

2. Develop a formulation for anisotropic poroelastic media under non-isothermal conditions. Obtain governing equations for a transversely isotropic medium under this formulation and apply these to develop the solutions for the inclined borehole for

both, the permeable and impermeable flux boundary conditions at the borehole wall.

3. Develop a formulation for anisotropic chemically active poroelastic media assuming isothermal and non-isothermal conditions. Obtain governing equations for this model applicable to transversely isotropic and isotropic media. Develop solutions for the inclined borehole problem in transversely isotropic as well as isotropic media for both, the permeable and impermeable flux boundary conditions at the borehole wall.

4. Analyze the effects of these coupled physicochemical processes on the stability of the inclined borehole.

## 1.3 Literature Review

A brief review of the theoretical development in the mechanics of porous media, 'poromechanics', and its application to the wellbore problem is presented in this section. A detailed review of the development is presented in relevant chapters.

Poromechanics finds its basis in the seminal work of Biot who proposed the theory of linear poroelasticity (*Biot*, 1941). A complete description of the coupled diffusion-deformation processes within the framework of this theory requires four independent material constants (two more than those for conventional elasticity) and one constant to characterize the fluid transport (*Biot*, 1941; *Biot and Willis* 1957). The isotropic theory of poroelasticity was subsequently extended by Biot to incorporate anisotropy, viscoelasticity, wave propagation, and non-linear poroelasticity (*Biot*, 1955, 1956a, 1956b, 1956c, 1956d, 1962a, 1962b, 1972). The relevance of the theory of poroelasticity in petroleum engineering was first recognized by Biot in 1946 during his work on his theory while working at Shell Oil Company (*Abousleiman*, 2002). Additional insight into the poroelastic

effects in rock mechanics was provided by Geertsma (1966), Coussy (1991,1995), Cheng *et al.* (1993), Wang (2000). Over the years, the poromechanical parameters have been revisited by several researchers in an attempt to provide a better understanding (*Rice and Cleary*, 1976; *Kumpel*, 1991; *Lee and Mei*, 1991)

The isotropic poroelastic inclined borehole solution was first developed by Cui *et al.* (1997). Under the linearized assumption, the solution was obtained by invoking the principle of superposition (*Hubbert and Willis*, 1957; *Carter and Booker*, 1982). The borehole was assumed to be infinitely long and in a poroelastic domain of infinite extent which manifests the assumption of a generalized plane strain condition (*Abousleiman et al.*, 1996b; *Cui et al.*, 1997). Subsequently, solutions for inclined borehole problems assuming permeable and impermeable flux boundary conditions at the borehole wall were developed. (*Cui et al.*, 1998, 1999a, 1999b; *Ekbote et al.*, 2002). A detailed description of the inclined borehole solution scheme is discussed in Chapter 3.

Biot's (1955) anisotropic poroelastic theory was reformulated by Thompson and Willis (1991) following the interpretation of poroelastic material constants by Rice and Cleary (1976). The anisotropic poroelastic parameters were expressed in terms of drained and undrained compliances and components of a generalized Skempton pore pressure coefficient tensor (*Abousleiman and Cheng*, 1993; *Cui*, 1995; *Cheng*, 1997). Abousleiman and Cui (2000) extended the formulation presented by Thompson and Willis and presented a micromechanics approach to obtain the anisotropic constitutive relations. The anisotropic poroelastic constants were identified and relations between Hookean engineering and micromechanical constitutive constants were explicitly and extensively listed (*Abousleiman and Cui*, 2000). Analytical solutions of fundamental problems such as the one-dimensional consolidation problem, Mandel's problem (*Mandel*, 1953), cylinder problem and borehole problem were developed (*Abousleiman et al.*, 1995; *Abousleiman and Cui*, 1998). A generalized poromechanical solution for circular geometries (Lame's

problem) has also been reported (*Cui and Abousleiman*, 2001; *Abousleiman and Kanj*, 2002; *Kanj and Abousleiman*, 2002). These analytical solutions are helpful in understanding physical phenomena and also serve as a benchmark for validating numerical codes (*Cui et al.*, 1996; *Nair et al.*, 2002).

An extension of Biot's theory to account for thermal effects has resulted in the development of the porothermoelastic model (*Schiffman*, 1971; *Brownell et al.*, 1977; *Bear and Corapcioglu*, 1981; *Palciauskas and Domenico*, 1982; *Kurashige*, 1989; *Coussy*, 1989, 1995). Analytical solutions have been developed for problems such as consolidation around a spherical and a point heat source (*Booker and Savvidou*, 1984, 1985), heating of a porothermoelastic half-space (*McTigue*, 1986), axisymmetric borehole solutions (*McTigue*, 1990), thermally induced stresses in a poroelastic hollow cylinder (*Kurashige*, 1992) and thermally induced stresses in a poroelastic sphere (*Kodashima and Kurashige*, 1996). McTigue (1990) specialized the governing equations for a fluid-saturated thermoelastic medium for the borehole problem and obtained the axisymmetric solution for the pore pressure response to a constant heat flux at the borehole wall. Wang and Papamichos (1994) developed axisymmetric analytical solutions for temperature and pore pressure distributions in the vicinity of a borehole under instantaneous temperature and fluid pressure changes. Kurashige (1992) obtained the a numerical solution for heat and fluid flow taking into consideration convective effects in a poroelastic hollow cylinder. Nair *et al.*, (2002) obtained finite element solutions for the inclined borehole problem in a fractured porous medium and analyzed the effect of heat transport by convection. A comprehensive treatment of the anisotropic porothermoelasticity (*Katsube*, 1988) and porothermoelastoplasticity (*Coussy*, 1989) have been addressed.

An extension of the isotropic poroelastic model to account for viscoelastic effects was proposed by Biot (1956, 1973). Subsequent extensions of Biot's approach have been presented to extend the poroviscoelastic model to quasi-static and dynamic ranges

(*Abousleiman et al.*, 1993, 1996b; *Coussy*, 1995; *Vgenopoulou and Beskos*, 1993). A micromechanical approach to the poroviscoelastic model, with the assistance of a rheological model, has been proposed by *Abousleiman et al.* (1993, 1996b) and the relevance of the physical constants introduced by the extension has been explained. The response is characterized by two time scales in which the characteristic time due to a viscoelastic nature is a material property, and that due to the diffusion is dependent on the material as well as the geometry length scale (*Abousleiman et al.*, 1996b).

Frequent borehole instability problems are encountered in chemically active shale formations (*Mody and Hale*, 1993). When water based muds (WBM) are used to drill in shale formations, the shale chemically reacts and produce hydrational stresses. These hydrational stresses cause the shale to swell modifying the stress and pore pressure fields around the borehole wall. In turn, the swelling also results in a change in wellbore diameter which can lead to operational problems (*Chenevert*, 1970a). Although oil based muds (OBM) have been used avoid such problems, unfortunately they are not environmentally sound (*Chenevert*, 1970b). Attempts have been made in the past to quantify the chemical effects of various water based muds (drilling fluids) and incorporate them in physical models (*Mody and Hale*, 1993; *Hale et al.*, 1992). Sherwood (1993) first presented a poroelasticity theory incorporating chemical effects in the constitutive and governing equations. In a more rigorous approach, the modified form of Biot's poroelastic theory was applied to account for solute transport in shales (*Sherwood*, 1994a). A continuum mechanics based model of hindered solute transport in shales was also used by Sherwood (1994a, 1994b, 1995) to predict the radial flow of water and solute away from a wellbore wall.

Based on the literature review regarding borehole solutions for the poromechanics models, it can be pointed out that the problem of an inclined borehole drilled under non-isothermal conditions in chemically active or inactive formations has not been addressed.

Given the importance of deviated wellbores in current drilling and oil/gas recovery schemes, the need for development of a mathematically rigorous framework for their analyses is imperative. The work in the subsequent chapters is aimed towards the development of these solutions and conducting stability analyses where these coupled physicochemical processes come into play.

## 1.4 Dissertation Outline

The outline of this dissertation is as follows:

In Chapter 2, the theoretical concepts underlying the formulation of poromechanics models carried out in later chapters is presented. A general set of assumptions and idealizations of the physical nature of the porous medium are outlined. Macroscopic mass, momentum and energy conservation equations are derived following micromechanical considerations. Constitutive relations for the poromechanics models discussed in this work, are presented. Equations for heat and fluid transport in porous media are presented. Also, material anisotropy and the relations between the anisotropic material constants are discussed.

In Chapter 3, a generalized analytical solution scheme for the inclined borehole problem which is an extension of the poroelastic inclined borehole solution is presented. This analytical scheme is applicable to the various poromechanics models discussed in this dissertation is presented. A superposition methodology is employed wherein the inclined borehole problem is divided into simpler problems for which solutions exist or can be easily obtained. Issues pertaining to borehole stability with a discussion on the modes of borehole failure and failure criteria used in the stability analysis is presented.

In Chapter 4, a porothermoelastic formulation for anisotropic media is developed. Governing equations are specialized for a transversely isotropic poroelastic material subjected to non-isothermal conditions. The resulting system of equations have been solved

for the problem of an inclined borehole drilled in a transversely isotropic formation. Analytical solutions for the permeable and impermeable scenarios have been obtained. The effect of anisotropy of the porothermomechanical parameters on the stress and pore pressure boundary conditions have been analyzed. Further, the impact of thermal loading and effect of the anisotropy of thermal coefficients on borehole stability have been analyzed.

In Chapter 5, Biot's poroelastic theory is extended to account for chemically active anisotropic porous media saturated by a pore fluid composed of multiple species. Governing equations and solutions for the inclined borehole problem in transversely isotropic and isotropic media, are presented. The resulting porochemoelastic models accounts for fully coupled transport of solute in shales under isothermal conditions. The chemical effect on stress and pore pressure is isolated considering a simplified axisymmetric case where the wellbore fluid pressure is equal to the formation pore pressure. The chemical effect on the stability of an inclined borehole is subsequently analyzed.

In Chapter 6, a porochemothermoelastic formulation for anisotropic chemically active porous media is developed. The model accounts for interplay between the hydraulic, thermal, chemical and mechanical processes that exist or may be induced when a porous medium is subjected to perturbations. Governing equations are tailored for transversely isotropic and isotropic chemically active formations subjected to non-isothermal conditions. The analytical solution for an inclined borehole problem under these scenarios has been obtained. As in Chapter 5, the impact of thermal and chemical effects on stress and pore pressure distributions are highlighted considering a simplified axisymmetric case. The stability of an inclined borehole drilled in a chemically active formation and subjected to pore pressure and temperature gradients is analyzed.

Finally in Chapter 7, summary, conclusions and the scope for future research have been presented.

# Chapter 2

# Poromechanics

## 2.1 Introduction

Poromechanics can be broadly described as the science that deals with the direct or indirect response of a porous medium, saturated partially or fully with one or more fluids, to the action of forces, internal and/or external (*Abousleiman*, 2002). The porous medium is conceptualized as a solid-fluid mixture comprising of the solid matrix and a simply connected pore space containing a freely moving pore fluid (*Coussy*, 1995). The essential characteristic of the poromechanical response is the coupling between the deformation of the solid matrix and the diffusion of the interstitial pore fluid pressure. The nature of the deformation, rate of diffusion and intensity of the coupling depend on the poromechanical and physical characteristics of the porous medium and the fluid.

The coupled response is a consequence of two actions occurring simultaneously while affecting one another. On one hand, the applied load results in a change in the pore volume thereby affecting the pore fluid pressure. This action may be viewed as the *solid-to-fluid* coupling. On the other hand, the change in the fluid pressure counteracts resulting in a change in the pore volume also referred to as the *fluid-to-solid* coupling (*Nur and Byerlee*, 1971; *Wang*, 2000). The intensity of the coupling depends not only on the porosity of the medium but also on the compressibilities of the solid skeleton, pores, solid grains and the pore fluid (*Rice and Cleary*, 1976; *Cleary*, 1977). The change in

the pore fluid pressure triggers a diffusive fluid mass transport, which also progressively affects the deformation resulting in a time-dependent response (*Coussy*, 1995; *Detournay and Cheng*, 1993).

A large number of factors are known to influence the poromechanical behavior of geomaterials. Firstly, the load-deformation response of the porous material can be rationalized in a number of ways, some of which are linear elastic, non-linear elastic, viscoelastic and/or plastic (*Coussy*, 1995). Secondly, the displacement field can be idealized as resulting in either infinitesimal strains or finite strains (*Biot*, 1972). Next, the interstitial pore space can be fully or partially saturated with a pore fluid which can be modeled as Newtonian or non-Newtonian fluid. In addition, the effects of external stimuli such as temperature and chemical effects need to be appropriately accounted for. A combination of each of the aforementioned factors constitute a hypothesis inherent in a poromechanical model. Although each poromechanical model is identified by its unique characteristics, they are basically extensions of Biot's fundamental theory of poroelasticity and display the essential feature of the poromechanics theory, which models the coupled diffusion-deformation process.

Following the work of Biot (1941), numerous models have been developed under the umbrella of poromechanics, which deviate from the idealizations used by Biot, in an attempt to simulate more involved phenomena. The differences are, however, only in the modeling approach. Their mechanics is, of course, governed by the universal laws of mass, momentum and energy conservation.

This chapter serves as a presynopsis to fundamental concepts employed in formulating poromechanics models. A discussion on the physical nature of the porous media and the idealizations used therein along with the fundamental quantities that play an important role in determining behavior is presented. A general set of assumptions that form the basis for the mathematical formulations are outlined. Laws of heat and fluid

conduction within the porous medium along with their pertinent assumptions are discussed. Starting from a micromechanical approach, the mass momentum and energy conservation equations are derived and presented in their macroscopic forms. Constitutive equations for the poromechanics models used and developed in this work are presented. Finally, material anisotropy is discussed with a presentation of the relations between the anisotropic material constants.

## 2.2 Basic Concepts

As an essential preliminary to the presentation of the poromechanics models, basic concepts involved in the mathematical representation are briefly discussed in this section. Firstly, a conceptual idealization of the porous media is presented. Next the concept of a representative elementary volume (*Bear*, 1972) is discussed, which forms the central idea of the continuum representation of porous media. Finally, a discussion of the fundamental quantities that govern the mechanical response in the perturbed state is presented.

### 2.2.1 Description of Porous Media

The porous media is visualized as a solid-fluid mixture comprising of the solid matrix and a connected pore space completely saturated with a fluid (*Coussy*, 1991, 1995). Discussion on partially saturated porous media is beyond the scope of this work. The solid constituent is therefore assumed to comprise of the solid matrix and the disconnected porous space. The complementary part, which is the connected porous space, is assumed to be completely saturated with the fluid and forms the volume of the fluid constituent. A physical characteristic of the porous medium is its porosity defined as the ratio of the connected pore volume to the total volume. A schematic of the porous media idealization is shown in Figure 2.1.


Figure 2.1: A schematic of the porous media idealization (*Coussy*, 1995)

### 2.2.2 The REV Concept

The porous media can be viewed over three distinct scales; molecular, microscopic and macroscopic (*Bear*, 1972). On the microscopic scale any element within the porous media can be regarded as heterogeneous, i.e., consisting of the solid part (the grain structure) and the void part (the pore space). However, in practice of main concern is the analysis and quantification of the physical phenomena over the macroscopic scale. To provide a continuum representation, the microscopically heterogeneous material, comprising of the solid and the void, is averaged to create a continuous space for both the solid grains and the void. The volume used in the averaging is called the Representative Elementary Volume (REV) and is assumed to be sufficiently large to include enough pores yet small enough to allow introduction of any macroscopic scale heterogeneity. Any physical or mechanical quantity is expressed as an average over the REV given by (*Bear*, 1972)

$$f = \frac{1}{V}\int_V \hat{f} dV \tag{2.1}$$

where $V$ is the volume of the REV, $\hat{f}$ is any quantity at a point within the REV and $f$ is the average continuum representation. Every quantity can thus be averaged and assigned to the center of some REV within the domain. All quantities can therefore be considered to be continuous over the entire domain.

### 2.2.3 Fundamental Variables

The response of the porous system subject to perturbation is quantified by changes in dynamic and kinematic quantities that control its state. Changes in these dynamic and kinematic variables are related through material constants and formulate constitutive relations specific to a poromechanics model. The dynamic variables are identified as stress, pore pressure and temperature whereas the kinematic variables include strain and the variation of the fluid content. Each of the aforementioned quantities is averaged over the REV and expressed as (*Bear*, 1972; *Bear and Corapcioglu*, 1981)

$$\sigma_{ij} = \frac{1}{V}\int_V \hat{\sigma}_{ij} dV = \frac{1}{V}\int_S t_i n_j dS \tag{2.2}$$

$$\epsilon_{ij} = \frac{1}{V}\int_V \hat{\epsilon}_{ij} dV = \frac{1}{V}\int_S (u_i n_j + u_j n_i)\, dS \tag{2.3}$$

$$p = \frac{1}{V}\int_V \hat{p} dV; \qquad T = \frac{1}{V}\int_V \hat{T} dV \tag{2.4}$$

where $\sigma_{ij}$, $\epsilon_{ij}$, $p$ and $T$ are averaged quantities for the total stress, solid strain, pore pressure and temperature respectively. Also $t_i$, $u_i$ and $n_i$ are the $i^{th}$ components of the surface traction, displacement and unit normal to the surface, respectively. From the above, it is seen that stress at a point in the domain is determined by the loading on the surface of the REV encompassing it. Similarly, strain is a result of displacement on the surface of the REV.

The variation of pore fluid content, denoted by $\zeta$, can be considered analogous to the strain, $\epsilon_{ij}$, but on the fluid constituent. $\zeta$ is defined as the variation of the net fluid volume relative to the solid skeleton due to deformation of the porous medium (*Detournay and Cheng*, 1993; *Coussy*, 1995; *Wang*, 2000). This variation can result from either deformation of the solid skeleton resulting in expulsion of the pore fluid.

The foregoing discussion presents the essential simplifications necessitated by the complex nature of porous media for a convenient representation within a mathematical model. The next section enlists a detailed set of assumptions adopted in this work,

which facilitates a mathematical representation of the phenomena studied.

## 2.3 Assumptions

The following assumptions are adopted and provide the basic framework for development of the poromechanics models.

- The porous media is conceptualized as a solid-fluid mixture in which the solid constituent comprises of the solid matrix and pores while the fluid constituent can move through the connected pores.

- The pores are assumed to be interconnected and randomly distributed in the medium but there may exist statistically preferred directions in their arrangement. They are assumed to be completely saturated with a single compressible Newtonian fluid.

- Load application on the porous media results in deformations that are assumed to be small such that infinitesimal strain-displacement relations can be adopted to describe the displacement field.

- The load-deformation behavior of the solid matrix is assumed to be linear, elastic and reversible. The anisotropy of the solid matrix is assumed to be of structural origin and attributed to the arrangement of the grains.

- A perturbation applied to the porous medium may result in flow of interstitial fluid which is assumed to be laminar and can be described using Darcy's law.

- A continuum mechanics approach is adopted with the assumption of existence of a *Representative Elementary Volume* (REV) over which all quantities, physical and mechanical, are averaged.

The aforementioned assumptions form a necessary and sufficient set and are the basis for Biot's linear poroelastic model

## 2.4 Deformation Restrictions

As noted in the previous section, a continuum mechanics approach is adopted in this work with the assumption of small displacements and rotations. In addition, the porous media is modeled as a continuum devoid of any cracks, dislocations or overlap. To ensure the above conditions, restrictions are imposed in the strain and displacement fields which are briefly discussed in this section.

### 2.4.1 Strain-Displacement Relations

Following the usual continuum mechanics approach, the strain experienced by a point in the most general case is given by (*Saada*, 1974; *Boresi and Chong*, 1987)

$$\epsilon_{ij} = \frac{1}{2}\left[u_{i,j} + u_{j,i} + u_{k,i}u_{k,j}\right] \tag{2.5}$$

where $\epsilon_{ij}$ is the strain tensor and $u_i$ is the displacement vector. In writing equation (2.5), the Einstien index notation has been used where a repeated index denotes summation while a comma followed by an index indicates differentiation. Under the assumption of infinitesimal displacements, the higher order terms appearing in equation (2.5) can be ignored and the simplified strain-displacement relation for small strains is given as (*Saada*, 1974; *Boresi and Chong*, 1987)

$$\epsilon_{ij} = \frac{1}{2}\left[u_{i,j} + u_{j,i}\right] \tag{2.6}$$

### 2.4.2 Compatibility Conditions

The porous media in this work is modeled as a continuum and ignores the existence of any flaws, cracks or dislocations. The domain is assumed to be simply connected and every point within the domain is in the neighborhood of some other point. As a result the components of the strain tensor cannot be given arbitrarily since they are determined completely by the displacement fields. Hence, there must exist relations between the strain components since they are not independent functions. These relations are referred to as the compatibility conditions. Under the assumption of small displacements, the compatibility conditions are given by (*Saada*, 1974; *Boresi and Chong*, 1987)

$$\epsilon_{ij,mn} + \epsilon_{mn,ij} - \epsilon_{im,jn} - \epsilon_{jn,im} = 0 \tag{2.7}$$

## 2.5 Conduction Laws

Conduction laws for heat and fluid mass transport are discussed in this section. In the most general case, a difference in potentials results in a flow. For instance, a difference in the temperature gradient causes a heat flow or a concentration gradient results in transport or a pressure gradient cause a fluid flux. The resulting flux is related to the causative gradients by the phenomenological coefficients according to Onsager's theory and it can be expressed as (*De Groot*, 1952)

$$J_i = L_{ij} X_{,j} \tag{2.8}$$

where $J_i$ is the flux, $X$ is the potential gradient, and $L_{ij}$ are the phenomenological coefficients. These coefficients are for example, heat conductivity, permeability, chemical drag coefficients etc. The matrix of the coefficients, $L_{ij}$, has been shown to be symmetric, i.e., $L_{ij} = L_{ji}$. Onsager's theory can be specialized to be applicable to the problems of heat conduction and fluid flow in porous media as discussed in the next section.

### 2.5.1 Darcy's Law

Darcy's law defines a relation between the fluid flux generated as a result of a pressure gradient in fluid saturated porous media. The matrix of phenomenological coefficients $L_{ij}$ is replaced by the anisotropic permeability matrix. In the most general form Darcy's law is expressed as (*Scheidegger*, 1974)

$$q_i^f = \kappa_{ij} p_{,j} \tag{2.9}$$

where $q_i^f$ is the specific discharge vector, $\kappa_{ij}$ is the anisotropic mobility coefficient tensor and $p$ represents the pressure gradient. The mobility coefficient tensor is related to the anisotropic permeability tensor, $k_{ij}$, as $\kappa_{ij} = k_{ij}/\mu$, where $k_{ij}$ is the intrinsic permeability tensor and $\mu$ is the interstitial pore fluid viscosity. For a simple isotropic case equation (2.9) reduces to

$$q_i^f = -\kappa p_{,i} \tag{2.10}$$

where $\kappa$ is the isotropic mobility coefficient.

### 2.5.2 Fourier's Law

Fourier's law, on the other hand, relates the heat flux generated by the temperature gradient across the porous media. The phenomenological coefficients in this case are the heat conduction coefficients. In the most general form, Fourier's law is expressed as (*Nowacki*, 1962; *Nowinski*, 1978)

$$q_i^h = \lambda_{ij} T_{,j} \tag{2.11}$$

where $q_i^h$ is the heat flux vector, $\lambda_{ij}$ is the heat conduction coefficients tensor and $T_{,j}$ is the temperature gradient. Again, under isotropy, equation (2.11) reduces to

$$q_i^h = \lambda T_{,i} \tag{2.12}$$

where $\lambda$ is the isotropic thermal conductivity.

## 2.6 Conservation Laws

The conservation laws of mass, momentum and energy conservation are presented in this section. Starting from a micromechanical approach, these equations are derived and presented in their macroscopic forms. By averaging microscopic balance equations over a REV, macroscopic equations valid at every point within the domain are established. A quasi-static approximation is assumed wherein the REV adjusts its state instantaneously in every instant of time to accommodate the changes resulting from the perturbation. These conservation equations combined with the constitutive equations and conduction laws give the governing field equations that can be solved to yield solutions to useful problems. It should be noted here that under isothermal conditions the energy conservation equation would become redundant. The formulation for all the aforementioned conservation equations is presented in this section to provide a complete set.

### 2.6.1 Mass Conservation

The exact statement for balance of mass of fluid in a saturated medium considering mass in/ mass out across an REV is given by (*Bear*, 1972; *Bear and Corapcioglu*, 1981)

$$\frac{\partial}{\partial t}(\phi\rho^f) + \nabla \cdot (\phi\rho^f v^f) = f_i \tag{2.13}$$

where $\phi$ is the porosity, $\rho^f$ is the fluid density $v^f$ is the velocity of the fluid and $f_i$ is the mass supply or withdrawal due to a source or sink. Assuming no sources or sinks and rearranging equation (2.13) we have

$$\frac{\partial}{\partial t}(\phi\rho^f) + \nabla \cdot (\phi\rho^f(v^f - v^s) + \nabla \cdot (\phi\rho^f v^s) = 0 \tag{2.14}$$

where $v^s$ is the velocity of the solid constituent. In the linear theory, the infinitesimal volumetric strain or dilatation of the fluid $\epsilon^f$ is related to the partial density $\phi\rho^f$ by

$$\phi\rho^f = \phi_o\rho^f_o(1 - \epsilon^f) \tag{2.15}$$

where $\phi_o$ is the reference porosity and $\rho_o^f$ is the initial fluid density. Assuming small deformations,

$$\nabla \cdot (v^s) = \frac{\partial \epsilon^s}{\partial t} \tag{2.16}$$

where $\epsilon^s$ is the strain of the solid constituent. Combining equations (2.14) - (2.16) and linearizing yields

$$\frac{\partial}{\partial t}\left[\phi_o\left(\epsilon^s - \epsilon^f\right)\right] + \nabla \cdot \left[\phi_o\left(v^s - v^f\right)\right] = 0 \tag{2.17}$$

We define

$$\zeta = \phi_o\left(\epsilon^s - \epsilon^f\right) \tag{2.18}$$

$$q_r = \phi_o\left(v^s - v^f\right) \tag{2.19}$$

where $\zeta$ is the change in fluid content and $q_r$ is the relative flux. Substituting equations (2.18) and (2.19) in equation (2.17) we get the mass balance equation as follows

$$\frac{\partial \zeta}{\partial t} + \nabla \cdot q_r = 0 \tag{2.20}$$

### 2.6.2 Momentum Conservation

Let $S$ be the surface closing the REV of volume $V$. The external forces acting on the REV consist of two parts: (1) body force and (2) tractive or surface force. Let $(x_1, x_2, x_3)$ denote the spatial coordinate system. The body force vector $\bar{b}$, is defined by $\bar{b} : (\bar{b}_1, \bar{b}_2, \bar{b}_3)$ where $\bar{b}_1, \bar{b}_2, \bar{b}_3$ denote the projection of the body force vector in the $x_1, x_2, x_3$ directions respectively. Similarly, the tractive force vector $\sigma_n$, is defined by $\sigma_n : (\sigma_{n1}, \sigma_{n2}, \sigma_{n3})$. In addition, $n : (n_1, n_2, n_3)$ is the unit normal vector.

Summing, the $x_1$ projections of the tractive forces, body forces and inertia forces gives (*Boresi and Chong*, 1987)

$$\int\int\int_V \left(\bar{b}_1 - \rho a_1\right) dV + \int\int_S \left(n_1\sigma_{n1} + n_2\sigma_{n2} + n_3\sigma_{n3}\right) dS = 0 \tag{2.21}$$

where $\rho a_1$ is the $x_1$ projection of the resultant inertia force. Applying the divergence theorem to the surface integral of equation (2.21) and regrouping in a single volume integral yields

$$\int\int\int_V \left(\frac{\partial \sigma_{11}}{\partial x_1} + \frac{\partial \sigma_{21}}{\partial x_2} + \frac{\partial \sigma_{31}}{\partial x_3} + \bar{b}_1 - \rho a_1\right) dV = 0 \tag{2.22}$$

Equation (2.22) applies to any volume element $dV$ in the medium. Consequently, for equation (2.22) to be satisfied for all parts of the medium, the integrand must vanish identically yielding

$$\left(\frac{\partial \sigma_{11}}{\partial x_1} + \frac{\partial \sigma_{21}}{\partial x_2} + \frac{\partial \sigma_{31}}{\partial x_3}\right) + \bar{b}_1 = \rho a_1 \tag{2.23}$$

Similar equations can be written summing $x_2$ and $x_3$ projections of the tractive, body and inertia forces yielding the differential equations of equilibrium. These equations have the same form as their counterparts in elasticity. In a more compact form, the aforementioned equations are written using the index notation as follows (*Boresi and Chong*, 1987)

$$\sigma_{ij,j} = -\bar{b}_i \qquad (i, j = 1, 3) \tag{2.24}$$

where a repeated index denotes the Einstein summation and an index followed by a comma denotes differentiation with respect to that index.

### 2.6.3 Energy Conservation

The equation for energy balance in the porous medium is obtained by writing microscopic forms of the energy conservation individually for the solid and fluid constituents and adding them to get the macroscopic form of the equation. The equation for energy balance for the fluid constituent for a unit volume of the REV is given by (*Bird et al.*, 1960; *Bear and Corapcioglu*, 1981)

$$\frac{\partial}{\partial t}(\phi \rho^f \hat{U}^f) = -\nabla \cdot (\phi \rho^f v^f \hat{U}^f) - \nabla \cdot (\phi q^{hf}) \tag{2.25}$$

where $\hat{U}^f$ is internal energy per unit mass of the fluid constituent, $q^{hf}$ is the heat flux vector for the fluid constituent. Note that the superscript $f$ denotes the quantities for the fluid constituent. In equation (2.25) the first term on the right hand side denotes the internal energy input due to convection while the second term denotes the internal energy input due to conduction. Expanding equation (2.25) assuming that the porosity is constant in time and space yields

$$\hat{U}^f \frac{\partial}{\partial t}(\phi\rho^f) + \phi\rho^f \frac{\partial \hat{U}^f}{\partial t} = -\hat{U}^f \nabla \cdot (\phi\rho^f v^f) - \phi\rho^f v^f \cdot \nabla \hat{U}^f - \nabla \cdot (\phi q^{hf}) \tag{2.26}$$

The fluid mass balance equation, ignoring existence of fluid sources or sinks is given by

$$\frac{\partial}{\partial t}(\phi\rho^f) = -\nabla \cdot (\phi\rho^f v^f) \tag{2.27}$$

Using equation (2.27) in equation (2.26) and rewriting yields

$$\phi\rho^f \frac{\partial \hat{U}^f}{\partial t} = -\phi\rho^f v^f \cdot \nabla \hat{U}^f - \nabla \cdot (\phi q^{hf}) \tag{2.28}$$

Now the internal energy per unit mass, $\hat{U}^f$, can be considered to be a function of the volume, $\hat{V}^f$, and temperature, $\hat{T}^f$, such that $\hat{U}^f = \hat{U}^f(\hat{V}^f, \hat{T}^f)$. Hence, the differential form of the internal energy $d\hat{U}^f$ is written as

$$d\hat{U}^f = \left.\frac{d\hat{U}^f}{d\hat{V}^f}\right|_{\hat{T}^f = \text{constant}} d\hat{V}^f + \left.\frac{d\hat{U}^f}{d\hat{T}^f}\right|_{\hat{V}^f = \text{constant}} d\hat{T}^f \tag{2.29}$$

Neglecting energy change due to volume change we have $d\hat{U}^f = C_v^f d\hat{T}^f$, where $C_v^f$ is the specific heat of the fluid constituent at constant volume. This is expressed as

$$\frac{d\hat{U}^f}{dt} = C_v^f \frac{d\hat{T}^f}{dt} \tag{2.30}$$

Substituting equation (2.30) in equation (2.26), and using equation (2.14), the energy conservation equation for the fluid constituent is given as

$$\phi\rho^f C_v^f \frac{d\hat{T}^f}{dt} = -\phi\rho^f C_v^f v^f \cdot \nabla \hat{T}^f - \nabla \cdot (\phi\lambda^f \nabla \hat{T}^f) \tag{2.31}$$

where $\lambda^f$ is the thermal conductivity of the fluid constituent. Similarly, the energy conservation equation for the solid constituent is given as

$$(1-\phi)\rho^s C_v^s \frac{d\hat{T}^s}{dt} = -(1-\phi)\rho^s C_v^s v^s \cdot \nabla \hat{T}^s - \nabla \cdot ((1-\phi)\lambda^s \nabla \hat{T}^s) \tag{2.32}$$

where the superscript $s$ has been used to denote the quantities for the solid constituent. The thermal energy conservation equation is obtained for the porous medium as a whole by adding equations (2.31) and (2.32). In addition it is assumed that $\hat{T}^s = \hat{T}^f = T$ which implies that both the fluid and solid constituents within the REV acquire the same temperature due to instantaneous local equilibrium (*Bear and Corapcioglu*, 1981). The energy conservation equation for the porous medium is then written as

$$\begin{aligned}\left[\phi\rho^f C_v^f + (1-\phi)\rho^s C_v^s\right]\frac{dT}{dt} &= -\left[\phi\rho^f C_v^f v^f + (1-\phi)\rho^s C_v^s v^s\right]\cdot\nabla T \\ &\quad -\nabla\cdot\left[\left(\phi\lambda^f + (1-\phi)\lambda^s\right)\nabla T\right]\end{aligned} \tag{2.33}$$

Equation (2.33) can be rewritten as follows

$$\begin{aligned}\left[\phi\rho^f C_v^f + (1-\phi)\rho^s C_v^s\right]\frac{dT}{dt} &= -\left[\phi\rho^f C_v^f (v^f - v^s)\right. \\ &\quad \left.+(\phi\rho^f C_v^f + (1-\phi)\rho^s C_v^s)v^s\right]\cdot\nabla T \\ &\quad -\nabla\cdot\left[\left(\phi\lambda^f + (1-\phi)\lambda^s\right)\nabla T\right]\end{aligned} \tag{2.34}$$

Next $\rho C_v$ and $\lambda$ are introduced which are the bulk heat capacity and the thermal conductivity of the porous medium defined by (*Bear and Corapcioglu*, 1981; *McTigue*, 1986)

$$\rho C_v = \phi\rho^f C_v^f + (1-\phi)\rho^s C_v^s \tag{2.35}$$

$$\lambda = \phi\lambda^f + (1-\phi)\lambda^s \tag{2.36}$$

Also, the relative flux $q_r$ is defined as in equation (2.19). Accordingly, using equations (2.19), (2.35) and (2.36) in equation (2.34) gives

$$\rho C_v \frac{dT}{dt} = -\left[\rho^f C_v^f q_r + \rho C_v v^s\right]\cdot\nabla T - \nabla\cdot[\lambda\nabla T] \tag{2.37}$$

Finally, neglecting $v^s$ equation (2.37) reduces to

$$\rho C_v \frac{dT}{dt} = -\left[\rho^f C_v^f q_r\right] \cdot \nabla T - \lambda \nabla^2 T \tag{2.38}$$

Equation (2.38) is the macroscopic equation of energy conservation. Note that the first term on the right hand side gives the energy change due to convection whereas the second term gives the energy change due to conduction.

## 2.7 Constitutive Equations

The constitutive equations relate the dynamic variables (stress, pore pressure, temperature) to the kinematic variables (strain, variation of fluid content) weighted by material coefficients. Constitutive equations for the poromechanics models discussed in this work are presented in this section. A tension positive convention is adopted in their presentation.

### 2.7.1 Poroelasticity

The constitutive relations for Biot's theory of poroelasticity (*Biot*, 1941) in the most general case are expressed as (*Thompson and Willis*, 1991; *Abousleiman and Cheng*, 1993; *Abousleiman and Cui*, 2000)

$$\sigma_{ij} = M_{ijkl}\epsilon_{kl} - \alpha_{ij}p \tag{2.39}$$

$$p = M(\zeta - \alpha_{ij}\epsilon_{ij}) \tag{2.40}$$

where $\sigma_{ij}$ is the total stress tensor, $\epsilon_{ij}$ is the strain tensor, $p$ is the pore pressure, $\zeta$ is the variation of fluid content, $M_{ijkl}$ is the drained elastic modulus tensor, $\alpha_{ij}$ is the Biot's effective stress coefficient tensor and $M$ is Biot's modulus. In the above, equation (2.39) is the stress-strain relation and equation (2.40) is the pore pressure response equation. In the above equations, $p$ is used as the coupling term. It must be noted that the above

equations can be written in a number of ways. The drained elastic modulus tensor ($M_{ijkl}$), the Biot's effective stress tensor ($\alpha_{ij}$) and the Biot's modulus ($M$) characterize the material constants.

### 2.7.2 Porothermoelasticity

With the introduction of a temperature perturbation, both the stresses and pore pressure are modified due to differential expansion or contraction of the solid matrix and pore fluid. The constitutive equations for linear isotropic porothermoelasticity are given as (*Kurashige*, 1989)

$$\sigma_{ij} = 2G\left(\epsilon_{ij} + \frac{\nu}{1-2\nu}\epsilon_{kk}\delta_{ij}\right) - \alpha_{ij}p\delta_{ij} - \frac{2G(1+\nu)}{3(1-2\nu)}T\delta_{ij} \tag{2.41}$$

$$\Delta m = \rho_f\left[\frac{\alpha(1-2\nu)}{2G(1+\nu)}\left(\sigma_{kk} + \frac{3}{B}p\right) - \left(\alpha^f - \alpha^s\right)\phi T\right] \tag{2.42}$$

Correspondingly, these equations are written in their anisotropic form as (*Abousleiman and Ekbote*, 1999, 2002)

$$\sigma_{ij} = M_{ijkl}\epsilon_{kl} - \alpha_{ij}p - \beta^s_{ij}T \tag{2.43}$$

$$p = M(\zeta - \alpha_{ij}\epsilon_{ij} + \beta^{sf}T) \tag{2.44}$$

where $\beta^s_{ij}$ is the thermic coefficient related to the solid matrix and $\beta^{sf}$ is the thermic coefficient related to the pore fluid. Both the aforementioned thermic coefficients can be related to the thermal expansion coefficients of the solid matrix and pore fluid as follow (*Abousleiman and Ekbote*, 1999, 2002)

$$\beta^s_{ij} = M_{ijkl}\alpha^s_{kl} \tag{2.45}$$

$$\beta^{sf} = \alpha_{ij}\alpha^s_{ij} + (\alpha^f - \alpha^s_{kk})\phi \tag{2.46}$$

where $\alpha^s_{ij}$ is the linear thermal expansion coefficient of the solid matrix, $\alpha^f$ is the volumetric expansion coefficient of the pore fluid and $\phi$ is the porosity. Again, the number

of independent constants required for a complete description depend on the degree of material symmetry modeled.

### 2.7.3 Porochemoelasticity

The porochemoelastic model is formulated as an extension of Biot's linear poroelastic model which accounts for the chemically active nature of the fluid saturating a porous medium (*Sherwood*, 1993). The porous medium is assumed to be completely saturated by a pore fluid containing $n$ chemical species. A perturbed state introduced by application of stress, results in a change in the strain of the solid matrix and changes in chemical potential of each of the pore fluid species. These are related by (*Sherwood*, 1993)

$$\epsilon_{ij} = C_{ijkl}\sigma_{kl} + \sum_{p} Q^{p}_{ij}\mu^{p} \tag{2.47}$$

$$M^{p} = Q^{p}_{ij}\sigma_{ij} + \sum_{q} B^{pq}\mu^{q} \tag{2.48}$$

$C_{ijkl}$ is the drained compliance tensor, $\mu^{i}$ is the chemical potential of the $i^{th}$ species, $M^{i}$ is the mass per unit reference volume of the $i^{th}$ species and $Q_{ij}$ is a material coefficient tensors with the symmetry $Q_{ij} = Q_{ji}$. It is assumed that the pore fluid can consists of two species. The stress-strain relations for the porochemoelasticity are given by

$$\sigma_{ij} = M_{ijkl}\epsilon_{kl} - \alpha_{ij}p + \gamma^{s}_{ij}m^{s} \tag{2.49}$$

where $\gamma^{s}_{ij}$ is the chemo-mechanical coupling coefficient tensor. In the two species pore fluid, (comprising of the solute and solvent), the equations for variation of solute and solvent content are given by

$$\zeta^{s} = \bar{m}^{s}\left[\frac{p}{M} + \alpha_{ij}\epsilon_{ij}\right] + \beta^{c}\frac{V_{sol}}{V_{s}}m^{s} \tag{2.50}$$

$$\zeta^{w} = (1-\bar{m}^{s})\left[\frac{p}{M} + \alpha_{ij}\epsilon_{ij}\right] - \beta^{c}\frac{V_{sol}}{V_{w}}m^{s} \tag{2.51}$$

where $\zeta^{s}$ is the variation of solute content, $\zeta^{w}$ is the variation of solvent content, $m^{s}$ is the variation in the solute molar fraction, $\bar{m}^{s}$ is the initial solute molar fraction, $\beta^{c}$ is a

hydro-chemical coupling constant, $V_s$ is the partial molar volume of the solute, $V_w$ is the partial molar volume of the solvent and $V_{sol}$ is the partial molar volume of the solution. The above constitutive equations relates the change in the strain and pore pressure to the change in the volume content of each species and is proportional to them molar fraction of the species.

### 2.7.4 Porochemothermoelasticity

The porochemothermoelastic model is formulated by extending the porochemoelastic model to incorporate temperature effects. With the introduction of boundary temperatures, i.e., a non-isothermal state, both the pore fluid and pore volume are subject to differential expansion or contraction resulting in additional coupling associated with the temperature change. A temperature perturbation affects both the strain of the solid matrix as well as the mass fraction of each of the chemical species in the pore fluid due to differential expansion or contraction rates. In the most general anisotropic case the stress-strain relations for porochemothermoelasticity are given by

$$\sigma_{ij} = M_{ijkl}\epsilon_{kl} - \alpha_{ij}p - \beta^s_{ij}T + \gamma^s_{ij}m^s \tag{2.52}$$

In addition, in the two species pore fluid, (comprising of the solute and solvent), the equations for variation of solute and solvent content are given by

$$\zeta^s = \bar{m}^s\left[\frac{p}{M} + \alpha_{ij}\epsilon_{ij} - \beta^{sf}T\right] + \beta^c\frac{V_{sol}}{V_s}m^s \tag{2.53}$$

$$\zeta^w = (1-\bar{m}^s)\left[\frac{p}{M} + \alpha_{ij}\epsilon_{ij} - \beta^{sf}T\right] - \beta^c\frac{V_{sol}}{V_w}m^s \tag{2.54}$$

## 2.8 Material Anisotropy

In general, rocks and other geomaterials exhibit anisotropy due to arrangement of the grains at the microstructural level (*Abousleiman and Cheng*, 1993; *Cheng*, 1997). Some

symmetry may exist due to a preferential arrangement at the microscale. The number of material constants required to describe behavior decreases as a higher degree of symmetry is modeled. Relations between material constants for the orthotropic, transversely isotropic and isotropic materials are discussed in this section.

### 2.8.1 Orthotropy

An orthotropic material has at least 2 orthogonal planes of symmetry, where material properties are independent of direction within each plane (*Boresi and Chong*, 1987). This form of symmetry results in the material possessing different properties in the three mutually perpendicular directions. The drained elastic modulus tensor is given by (*Amadei*, 1983; *Cui*, 1995; *Cheng*, 1997)

$$[M] = \begin{bmatrix} M_{11} & M_{12} & M_{13} & 0 & 0 & 0 \\ M_{12} & M_{22} & M_{23} & 0 & 0 & 0 \\ M_{13} & M_{23} & M_{33} & 0 & 0 & 0 \\ 0 & 0 & 0 & M_{44} & 0 & 0 \\ 0 & 0 & 0 & 0 & M_{55} & 0 \\ 0 & 0 & 0 & 0 & 0 & M_{66} \end{bmatrix} \tag{2.55}$$

in which the components, $M_{11}, M_{12}$ etc. are defined in terms of the Young's moduli, Poisson's ratio and shear moduli. For an orthotropic material 9 independent constants are required to describe material behavior. These are selected as: $E_1$, $E_2$, $E_3$ which are the drained Young's moduli in directions 1, 2 and 3 respectively; $G_{12}$, $G_{23}$ and $G_{13}$ which are the shear moduli for planes that are parallel to the coordinate planes $1-2$, $2-3$, and $1-3$ respectively; $\nu_{ij}$ $(i,j = 1,2,3)$ which are the drained Poisson's ratio and which characterized the compressive strain in $j$ direction produced by a tensile stress in the $i$ direction. Following relations must be satisfied to ensure compatibility between material parameters (*Lekhnitskii*, 1981; *Amadei*, 1983)

$$E_1\nu_{21} = E_2\nu_{12}; \qquad E_2\nu_{32} = E_3\nu_{23}; \qquad E_3\nu_{13} = E_1\nu_{31} \tag{2.56}$$

The components of the drained elastic modulus tensor are given by (*Lekhnitskii*, 1981)

$$M_{11} = \frac{E_1(\nu_{23}\nu_{12} - 1)}{v_d}; \quad M_{12} = -\frac{E_2(\nu_{13}\nu_{32} + \nu_{12})}{v_d} \tag{2.57}$$

$$M_{13} = -\frac{E_3(\nu_{12}\nu_{23} + \nu_{13})}{v_d}; \quad M_{22} = \frac{E_2(\nu_{13}\nu_{31} - 1)}{v_d} \tag{2.58}$$

$$M_{23} = -\frac{E_1(\nu_{13}\nu_{21} + \nu_{23})}{v_d}; \quad M_{33} = \frac{E_3(\nu_{12}\nu_{21} - 1)}{v_d} \tag{2.59}$$

$$M_{44} = G_{12}; \quad M_{55} = G_{23}; \quad M_{66} = G_{13} \tag{2.60}$$

in which

$$v_d = \nu_{21}\nu_{12} + \nu_{31}\nu_{13} + \nu_{23}\nu_{32} + \nu_{12}\nu_{23}\nu_{31} + \nu_{13}\nu_{32}\nu_{21} - 1 \tag{2.61}$$

The inverse of the drained elastic modulus tensor is the compliance tensor $C_{ijkl}$ is defined as follows

$$[C] = \begin{bmatrix} C_{11} & C_{12} & C_{13} & 0 & 0 & 0 \\ C_{12} & C_{22} & C_{23} & 0 & 0 & 0 \\ C_{13} & C_{23} & C_{33} & 0 & 0 & 0 \\ 0 & 0 & 0 & C_{44} & 0 & 0 \\ 0 & 0 & 0 & 0 & C_{55} & 0 \\ 0 & 0 & 0 & 0 & 0 & C_{66} \end{bmatrix} \tag{2.62}$$

in which

$$C_{11} = \frac{1}{E_1}; \quad C_{22} = \frac{1}{E_2}; \quad C_{33} = \frac{1}{E_3} \tag{2.63}$$

$$C_{12} = -\frac{\nu_{21}}{E_2} = -\frac{\nu_{12}}{E_1}; \quad C_{13} = -\frac{\nu_{31}}{E_3} = -\frac{\nu_{13}}{E_1} \tag{2.64}$$

$$C_{23} = -\frac{\nu_{32}}{E_3} = -\frac{\nu_{23}}{E_2} \tag{2.65}$$

For an orthotropic material the Biot's effective stress coefficient tensor is defined as (*Thompson and Willis*, 1991; *Abousleiman and Cheng*, 1993; *Abousleiman and Cui*, 2000)

$$[\alpha] = \begin{bmatrix} \alpha_1 & \alpha_2 & \alpha_3 & 0 & 0 & 0 \end{bmatrix}^T \tag{2.66}$$

and the Skempton's coefficient tensor is defined as (*Thompson and Willis*, 1991; *Abousleiman and Cheng*, 1993; *Abousleiman and Cui*, 2000)

$$[B] = \begin{bmatrix} B_1 & B_2 & B_3 & 0 & 0 & 0 \end{bmatrix}^T \tag{2.67}$$

Under the assumption of microisotropy and microhomogeneity the components of the Biot's effective stress coefficient tensor are related to the components of the drained elastic moduli as follows (*Abousleiman et al.*, 1996a; *Cui*, 1995; *Cheng*, 1997; *Abousleiman and Cui*, 2000)

$$\alpha_1 = 1 - \frac{M_{11} + M_{12} + M_{13}}{3K_s} \tag{2.68}$$

$$\alpha_2 = 1 - \frac{M_{12} + M_{22} + M_{23}}{3K_s} \tag{2.69}$$

$$\alpha_3 = 1 - \frac{M_{13} + M_{23} + M_{33}}{3K_s} \tag{2.70}$$

in which $K_s$ is the solid grain bulk modulus. Similarly, components of the Skempton's coefficient tensor (*Cheng*, 1997; *Abousleiman and Cui*, 2000) are given as

$$B_1 = \frac{3K_s\left(C_{11} + C_{21} + C_{31}\right) - 1}{K_s\bar{C} + \phi K_s/K_f - (1-\phi)} \tag{2.71}$$

$$B_2 = \frac{3K_s\left(C_{12} + C_{22} + C_{32}\right) - 1}{K_s\bar{C} + \phi K_s/K_f - (1-\phi)} \tag{2.72}$$

$$B_3 = \frac{3K_s\left(C_{13} + C_{23} + C_{33}\right) - 1}{K_s\bar{C} + \phi K_s/K_f - (1-\phi)} \tag{2.73}$$

where $\phi$ is the porosity, $K_f$ is the pore fluid compressibility, and $\bar{C}$ is given by

$$\bar{C} = C_{11} + C_{22} + C_{33} + 2C_{12} + 2C_{23} + 2C_{13} \tag{2.74}$$

Biot's modulus $M$ can be expressed as

$$M = \frac{K_s^2}{K_s\left[1 + \phi\left(K_s/K_f - 1\right)\right] - \bar{M}/9} \tag{2.75}$$

where

$$\bar{M} = M_{11} + M_{22} + M_{33} + 2M_{12} + 2M_{23} + 2M_{13} \tag{2.76}$$

The thermic coefficient tensor $\beta_{ij}^s$ for the orthotropic material is given by

$$[\beta^s] = \begin{bmatrix} \beta_1^s & \beta_2^s & \beta_3^s & 0 & 0 & 0 \end{bmatrix} \tag{2.77}$$

in which expressions for $\beta_1^s$, $\beta_2^s$ and $\beta_3^s$ are given as (*Abousleiman and Ekbote*, 2002)

$$\beta_1^s = M_{11}\alpha_1^s + M_{12}\alpha_2^s + M_{13}\alpha_3^s \tag{2.78}$$

$$\beta_2^s = M_{12}\alpha_1^s + M_{22}\alpha_2^s + M_{23}\alpha_3^s \tag{2.79}$$

$$\beta_3^s = M_{13}\alpha_1^s + M_{23}\alpha_2^s + M_{33}\alpha_3^s \tag{2.80}$$

where $\alpha_1^s$, $\alpha_2^s$ and $\alpha_3^s$ are the linear expansion coefficients of the solid skeleton in directions 1, 2 and 3 respectively. The thermic coefficient $\beta^{sf}$ is given by (*Abousleiman and Ekbote*, 2002)

$$\beta^{sf} = \alpha_1\alpha_1^s + \alpha_2\alpha_2^s + \alpha_3\alpha_3^s + (\alpha^f - \alpha_1^s - \alpha_2^s - \alpha_3^s)\phi \tag{2.81}$$

where $\alpha^f$ is the volumetric thermal expansion coefficient of the pore fluid.

### 2.8.2 Transverse Isotropy

Transversely isotropic materials are those that have the same properties in one plane (e.g. the $x-y$ plane, also known as the isotropic plane) and different properties in the direction normal to this plane (e.g. the $z$-axis). They are characterized by an axis of rotational elastic symmetry. The drained elastic modulus tensor is given by equation (2.55) with

$$M_{22} = M_{11}; \quad M_{23} = M_{13}; \quad M_{66} = M_{55} \tag{2.82}$$

For a transversely isotropic material, 5 independent constants are required to describe material behavior. These are selected as: $E$, $E'$, $\nu$, $\nu'$ and $G'$ in which $E$ is the Young's modulus in the isotropic plane, $E'$ is the Young's modulus in the transverse direction, $\nu$ is the Poisson's ratio which characterizes the transverse strain reduction in the isotropic plane due to a tensile stress in the same plane, $\nu'$ is the Poisson's ratio which gives the transverse strain reduction due to a tensile stress in the direction normal to the

isotropic plane, and, $G'$ is the shear modulus of a plane normal to the isotropic plane. The components of the drained elastic modulus tensor are related to $E$, $E'$, $\nu$, $\nu'$ and $G'$ as follows (*Abousleiman and Cui*, 2000)

$$M_{11} = \frac{E(E' - E\nu'^2)}{(1+\nu)(E' - E'\nu - 2E\nu'^2)} \tag{2.83}$$

$$M_{12} = \frac{E(E'\nu + E\nu'^2)}{(1+\nu)(E' - E'\nu - 2E\nu'^2)} \tag{2.84}$$

$$M_{13} = \frac{EE'\nu'}{(E' - E'\nu - 2E\nu'^2)}; \qquad M_{33} = \frac{E'^2(1-\nu)}{(E' - E'\nu - 2E\nu'^2)} \tag{2.85}$$

$$M_{44} = G = \frac{E}{2(1+\nu)}; \qquad M_{55} = G' \tag{2.86}$$

The compliance tensor $C_{ijkl}$ is given by equation (2.62) with

$$C_{22} = C_{11}; \qquad C_{23} = C_{12}; \qquad C_{66} = C_{55} \tag{2.87}$$

and

$$C_{11} = \frac{1}{E}; \qquad C_{33} = \frac{1}{E'}; \qquad C_{12} = -\frac{\nu}{E} \tag{2.88}$$

$$C_{13} = -\frac{\nu'}{E'}; \qquad C_{44} = \frac{1}{G}; \qquad C_{55} = \frac{1}{G'} \tag{2.89}$$

Accordingly the elements of the Biot's effective stress coefficient tensor and the Skempton's coefficient tensor are given by (*Abousleiman and Cui*, 2000)

$$\alpha_1 = \alpha_2 = \alpha = 1 - \frac{M_{11} + M_{12} + M_{13}}{3K_s} \tag{2.90}$$

$$\alpha_3 = \alpha' = 1 - \frac{2M_{13} + M_{33}}{3K_s} \tag{2.91}$$

$$\alpha_4 = \alpha_5 = \alpha_6 = 0 \tag{2.92}$$

$$B_1 = B_2 = B = \frac{3K_s\left[(1-\nu)/E - \nu'/E\right] - 1}{K_s\bar{C} + \phi K_s/K_f - (1-\phi)} \tag{2.93}$$

$$B_3 = B' = \frac{3K_s\left[1/E - 2\nu'/E\right] - 1}{K_s\bar{C} + \phi K_s/K_f - (1-\phi)} \tag{2.94}$$

$$B_4 = B_5 = B_6 = 0 \tag{2.95}$$

where $\bar{C}$ is given by

$$\bar{C} = 2C_{11} + C_{33} + 2C_{12} + 4C_{13} \tag{2.96}$$

Also elements of the thermic coefficient tensor $\beta^s_{ij}$ for the transversely isotropic material are given by (*Abousleiman and Ekbote*, 2002)

$$\beta^s_1 = \beta^s_2 = \beta^s = M_{11}\alpha^s + M_{12}\alpha^s + M_{13}\alpha^{s'} \tag{2.97}$$

$$\beta^s_3 = \beta^{s'} = 2M_{13}\alpha^s + M_{33}\alpha^{s'} \tag{2.98}$$

$$\beta^s_4 = \beta^s_5 = \beta^s_6 = 0 \tag{2.99}$$

where $\alpha^s$, and $\alpha^{s'}$ are the linear expansion coefficients of the solid skeleton in directions in the isotropic plane and transverse directions respectively. The thermic coefficient $\beta^{sf}$ is given by

$$\beta^{sf} = 2\alpha\alpha^s + \alpha^{'}\alpha^{s'} + (\alpha^f - 2\alpha^s - \alpha^{s'})\phi \tag{2.100}$$

### 2.8.3 Isotropy

An isotropic material displays no directional preference in the material properties. In other words, the material is characterized by infinite planes of symmetry and is requires only 2 elastic constants. Consequently, the non-zero elements of the drained elastic modulus tensor are given as

$$M_{11} = M_{22} = M_{33} = \frac{E(1-\nu)}{(1+\nu)(1-2\nu)} \tag{2.101}$$

$$M_{12} = M_{13} = M_{21} = M_{23} = M_{32} = M_{31} = \frac{E\nu}{(1+\nu)(1-2\nu)} \tag{2.102}$$

$$M_{44} = M_{55} = M_{66} = G = \frac{E}{2(1+\nu)} \tag{2.103}$$

Also, elements of the compliance matrix are given by

$$C_{11} = C_{22} = C_{33} = \frac{1}{E} \tag{2.104}$$

$$C_{12} = C_{13} = C_{21} = C_{23} = C_{32} = C_{31} = -\frac{\nu}{E} \tag{2.105}$$

$$C_{44} = C_{55} = C_{66} = \frac{1}{G} = \frac{2(1+\nu)}{E} \tag{2.106}$$

The Biot's effective stress coefficient and Skempton's coefficient are given by

$$\alpha_1 = \alpha_2 = \alpha_3 = \alpha = 1 - \frac{K}{K_s} \tag{2.107}$$

$$\alpha_4 = \alpha_5 = \alpha_6 = 0 \tag{2.108}$$

$$B_1 = B_2 = B_3 = B = \frac{K_s/K - 1}{K_s/K + \phi K_s/K_f - (1-\phi)} \tag{2.109}$$

$$B_4 = B_5 = B_6 = 0 \tag{2.110}$$

The thermic coefficients $\beta^s$ and $\beta^{sf}$ are defined as follows

$$\beta_1^s = \beta_2^s == \beta_3^s = \beta^s = (M_{11} + 2M_{12})\alpha^s \tag{2.111}$$

$$\beta_4^s = \beta_5^s = \beta_6^s = 0 \tag{2.112}$$

$$\beta^{sf} = 3\alpha\alpha^s + (\alpha^f - 3\alpha^s)\phi \tag{2.113}$$

## 2.9 Summary

Basic concepts in poromechanics have been revisited in this chapter. A description of the porous media, amenable to a mathematical representation has been discussed. The assumptions that have been employed to formulate basic laws and relations have also been discussed. Starting from first principles, conservation equations for mass, momentum and energy have been developed. Constitutive equations of the poromechanics models, that will be addressed in this work in the forthcoming chapters, have been presented. The governing equations applicable to specific poromechanics models will be discussed in respective chapters.

# Chapter 3

# The Inclined Borehole Problem and Borehole Stability

## 3.1 Introduction

The problem of the stress concentrations near an excavated opening is perhaps the most important problem in rock mechanics (*Hubbert and Willis*, 1957; *Jaegar and Cook*, 1979). Applications are found in the geotechnical, mining and petroleum engineering fields where borehole and tunnel drilling activities are usually carried out in formations subjected to high level of in-situ stresses. Excavation results in a redistribution of stresses and generates stress concentrations in the vicinity of the opening. Stress levels exceeding formation material strength result in failure.

The focus in this work is mainly on petroleum engineering activities related to oil and gas exploration, which are usually carried out in fluid saturated formations. Borehole excavation in such formations, triggers a fluid diffusion process in addition to the aforementioned stress concentrations and associated deformation. These are appropriately explained by poromechanics models. As boreholes are drilled, they are usually filled with a pressurized borehole fluid, also known as borehole mud, which assists in maintaining the stress concentration levels within limits of permissible material strength. However, the temperature and chemical composition of the borehole mud lead to thermal and chemical gradients which act as driving forces for thermal and chemical processes which

affect the stress and pore pressure distributions near the borehole.

Over the years, this problem has attracted interest of several researchers. The solution for a vertical borehole based on a plane strain idealization and employing the linear elasticity theory have been presented (*Hubbert and Willis*, 1957; *Wood*, 1975; *Pender*, 1980). Subsequently, these solutions have also been extended to an inclined borehole (*Bradley*, 1979). The elastic inclined borehole solution presented by Bradley (1979), employs a generalized plane strain idealization and is discussed in Appendix A. However, the elastic approach fails to account for the various coupled physicochemical processes that may be induced due to drilling the borehole in a fluid saturated porous medium. A solution for a circular tunnel in a fluid saturated medium based on Biot's linear theory of poroelasticity was presented by Carter and Booker (1982, 1983). This approach has been extended to yield a complete poroelastic solution for an inclined borehole in a three-dimensional in-situ state of stress (*Cui et al.*, 1997). Due to the generalized nature of this approach, the solution has been extensively applied by borehole stability analysts in the petroleum industry (*Abousleiman et al.*, 1999, 2001; *Abousleiman et al.*, 2002). Studies on borehole stability have been conducted which have unearthed a physical reasoning for several field observations such as time-delayed failure which cannot be explained by the linear elasticity theory.

In addition to the coupling between the diffusion and deformation, thermal effects, chemical reactivity to the formation, and formation rheology also affect the magnitude of the stress concentrations that develop close to the borehole wall. In this chapter, a generalized analytical solution scheme (applicable to poromechanics models discussed in this dissertation) for the inclined borehole problem is presented. The scheme proposed here is an extension of the poroelastic inclined borehole solution available in the literature (*Cui et al.*, 1997; *Cheng*, 1998). The scheme adopts a superposition methodology, subdividing the problem into simpler problems for which solutions either exist or can

easily be obtained. A complete solution is obtained by a superposition of the solutions from the contributing sub-problems. Next, the issues pertaining to borehole stability evaluation are discussed. The modes of borehole failure considered in this work, and the failure criteria used in their determination are presented.

## 3.2 Problem Description

The borehole is defined as an infinitely long circular cavity created by removal or excavation of material from a formation. The domain for the problem, (i.e., the formation) is assumed to be of semi-infinite extent. Prior to borehole excavation, the formation is assumed to be subjected to orthogonal in-situ stresses $S_{x'}$, $S_{y'}$, and $S_{z'}$ and formation pore pressure, temperature and solute molar fraction denoted by $p_o$, $T_o$ and $m_o^s$, respectively. The in-situ stresses $S_{x'}$, $S_{y'}$, and $S_{z'}$ are assumed to be subjected along the three directions of a right-handed global coordinate system $x'y'z'$. Here $S_{z'}$ is the vertical overburden stress, $S_{x'}$ is the maximum horizontal in-situ stress and, $S_{y'}$ is the minimum horizontal in-situ stress. In addition, the formation pore pressure $p_o$, temperature $T_o$, and solute molar fraction $m_o^s$ due to the formation chemical reactivity, are assumed to be uniform throughout the domain. The borehole is infinitely long and inclined with respect to the directions of the in-situ stresses. The orientation of the borehole is measured by two angles, the inclination $\varphi_z$ and the azimuth $\varphi_y$. The inclination $\varphi_z$ is defined as the angle between the borehole axis and $z'$ direction. The azimuth $\varphi_y$, on the other hand, is the angle between the $x'$ axis and the projection of the borehole axis on the $x'y'$ plane. The borehole is assumed to be drilled instantaneously that sets the boundary along the borehole wall, free of surface tractions, pore pressure and temperature. The sudden removal of material introduces a disturbance or perturbation that results in a modification of the stress, pore pressure and temperature fields in the vicinity of the borehole. It must be noted here that, upon drilling, the borehole cavity may be instan-

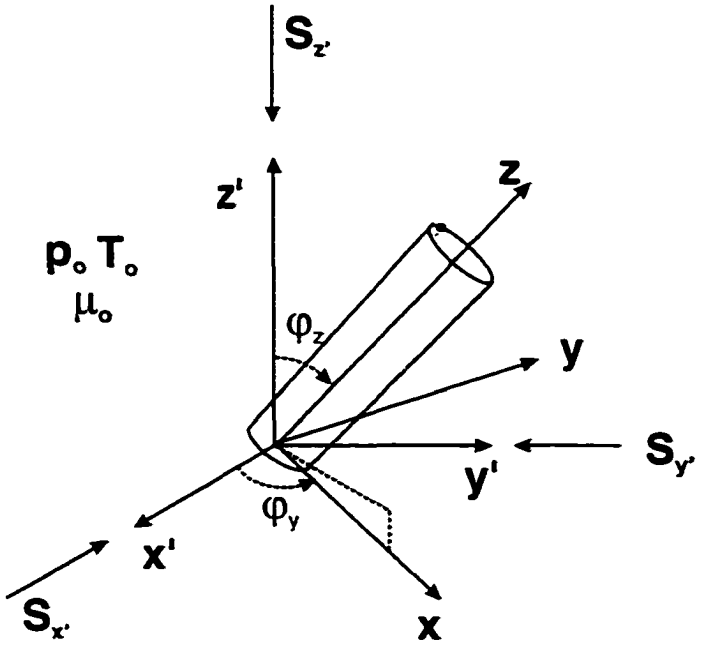


Figure 3.1: Schematic of the inclined borehole problem

taneously filled with a drilling fluid having a pressure $p_w$, temperature $T_w$ and solute molar fraction $m_w^s$. The effect of these parameters can easily be accounted for as the perturbation in the pore pressure, temperature and solute molar fraction fields.

A schematic of the inclined borehole is shown in Figure 3.1. The sudden change in conditions due to borehole excavation are mathematically represented by a change in the boundary conditions. Two boundaries in the domain are of interest. Of these, one is the far-field boundary which is at an infinite distance from the location where the borehole is drilled. No change in the conditions are assumed to occur at this boundary. The other boundary of interest is the borehole wall where the stress, pore pressure, solute molar fraction and temperature states are modified. A scheme for obtaining solutions for the stress, pore pressure and temperature distributions resulting from the perturbation is presented in the next section.

## 3.3 Solution Strategy

The inclined borehole problem is solved by defining a local coordinate system $xyz$ obtained by a rotation of the global coordinate system $x'y'z'$ and the magnitude of this rotation is governed by the orientation angles $\varphi_y$ and $\varphi_z$. The $z$-axis in the local coordinate system is assumed to coincide with the borehole axis. The local coordinate system is formed by first a rotation of $\varphi_y$ (the azimuth angle) about the $z'$-axis followed by a second rotation equivalent to the inclination angle $\varphi_z$ towards the $x$-axis (*Cui et al.*, 1997). (See Figure 3.1 for illustration.)

The problem is solved within the local coordinate system. The domain of the problem in the local coordinate system is shown by the cubical section as shown in Figure 3.2. Note that the boundaries of the cubical section represent the far-field boundaries and are assumed to be at infinite extent. The far-field stresses $S_{x'}$, $S_{y'}$, and $S_{z'}$ in the $x'y'z'$ coordinate system are transformed to the local coordinate system $xyz$ following a stress transformation given as follows

$$\begin{Bmatrix} S_x \\ S_y \\ S_z \\ S_{xy} \\ S_{yz} \\ S_{xz} \end{Bmatrix} = \begin{bmatrix} \ell^2_{xx'} & \ell^2_{xy'} & \ell^2_{xz'} \\ \ell^2_{yx'} & \ell^2_{yy'} & \ell^2_{yz'} \\ \ell^2_{zx'} & \ell^2_{zy'} & \ell^2_{zz'} \\ \ell_{xx'}\ell_{yx'} & \ell_{xy'}\ell_{yy'} & \ell_{xz'}\ell_{yz'} \\ \ell_{yx'}\ell_{zx'} & \ell_{yy'}\ell_{zy'} & \ell_{yz'}\ell_{zz'} \\ \ell_{zx'}\ell_{xx'} & \ell_{zy'}\ell_{xy'} & \ell_{zz'}\ell_{xz'} \end{bmatrix} \begin{Bmatrix} S_{x'} \\ S_{y'} \\ S_{z'} \end{Bmatrix} \tag{3.1}$$

where $S_x$, $S_y$, $S_z$, $S_{xy}$, $S_{yz}$, $S_{xz}$ are far-field in-situ stress components in the local coordinate system and $\ell_{xx'}$, $\ell_{xy'}$, etc. represent direction cosines of the angles between corresponding pairs of axes ($x$ and $x'$, $x$ and $y'$, etc.). The complete direction cosine matrix is given as

$$\begin{bmatrix} \ell_{xx'} & \ell_{xy'} & \ell_{xz'} \\ \ell_{yx'} & \ell_{yy'} & \ell_{yz'} \\ \ell_{zx'} & \ell_{zy'} & \ell_{zz'} \end{bmatrix} = \begin{bmatrix} \cos\varphi_y \cos\varphi_z & \sin\varphi_y \cos\varphi_z & -\sin\varphi_z \\ -\sin\varphi_y & \cos\varphi_x & 0 \\ \cos\varphi_y \sin\varphi_z & \sin\varphi_y \sin\varphi_z & \cos\varphi_z \end{bmatrix} \tag{3.2}$$

It is seen from equation (3.1) that in the local coordinate system, the borehole is subject to far-field normal as well as shear stress components. The far-field stresses in the local

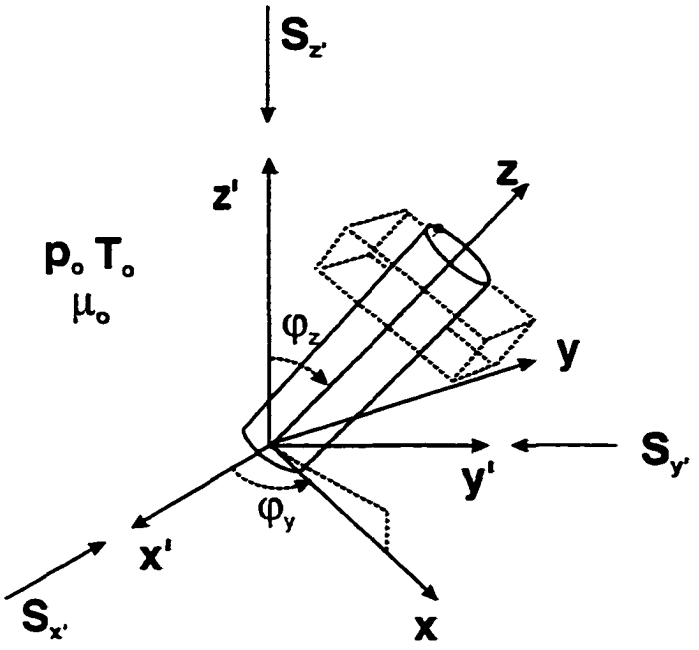


Figure 3.2: Defining a local borehole coordinate system (*Abousleiman* et al., 1999)

coordinate system can be visualized as shown in Figure 3.3.

Mathematically, the boundary conditions at far-field i.e. $r \rightarrow \infty$, where $r$ is the radial distance from the borehole axis, are given as follows:

At far-field ($r \rightarrow \infty$)

$$\sigma_{xx} = -S_x; \quad \sigma_{yy} = -S_y; \quad \sigma_{zz} = -S_z \tag{3.3}$$

$$\tau_{xy} = -S_{xy}; \quad \tau_{yz} = -S_{yz}; \quad \tau_{zx} = -S_{zx} \tag{3.4}$$

$$p = \varpi_1 p_o; \quad T = \varpi_2 T_o; \quad m^s = \varpi_3 m_o^s \tag{3.5}$$

Note that a generalized solution scheme applicable to the poromechanics models described in Chapter 2 is being sought here. Coefficients $\varpi_1$, $\varpi_2$ and $\varpi_3$ are introduced here which take values 0 or 1. Appropriate selection of these coefficients will result in the inclined borehole solutions specific to the poromechanics model for which the coefficients

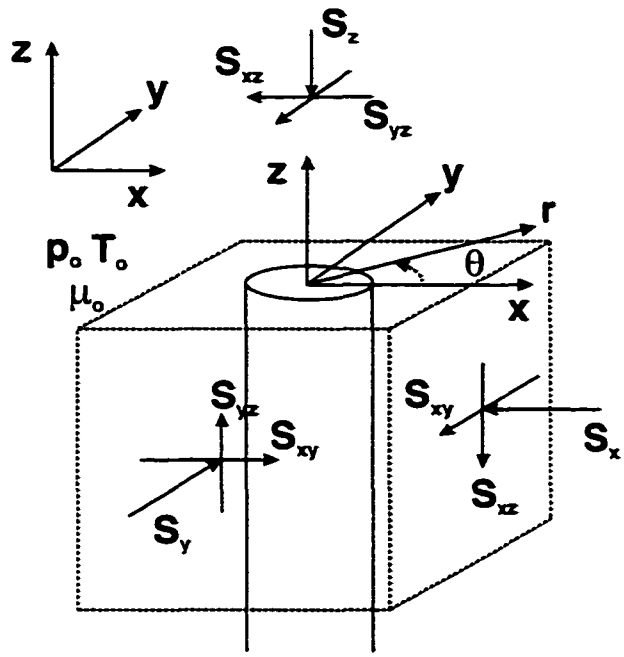


Figure 3.3: Anisotropic far-field stresses in the borehole local coordinate system

have been selected. The coefficients for the different poromechanics models are

$$\text{Poroelastic:} \quad \varpi_1 = 1, \varpi_2 = 0, \varpi_3 = 0 \tag{3.6}$$

$$\text{Porothermoelastic:} \quad \varpi_1 = 1, \varpi_2 = 1, \varpi_3 = 0 \tag{3.7}$$

$$\text{Porochemoelastic:} \quad \varpi_1 = 1, \varpi_2 = 0, \varpi_3 = 1 \tag{3.8}$$

$$\text{Porochemothermoelastic:} \quad \varpi_1 = 1, \varpi_2 = 1, \varpi_3 = 1 \tag{3.9}$$

The borehole exhibits a natural symmetry due to its circular geometrical shape. Boundary conditions resulting from the perturbation are written within a cylindrical coordinate system. At the borehole wall, $r = R$, where $R$ is the borehole radius, surface tractions, pore pressure, flux and temperature are assumed to change from their initial state at the instant of excavation. The boundary conditions at the borehole wall are expressed as

At the borehole wall ($r = R$)

$$\sigma_{rr} = -S_r \mathrm{H}(-t) - p_w \mathrm{H}(t) \tag{3.10}$$

$$\tau_{r\theta} = -S_{r\theta} \mathrm{H}(-t) \tag{3.11}$$

$$\tau_{rz} = -S_{rz} \mathrm{H}(-t) \tag{3.12}$$

$$L_1 p + L_2 q_r = \varpi_1 \left[ L_1 \left( p_o \mathrm{H}(-t) + p_w(t) \mathrm{H}(t) \right) + L_2 \left( q_w(t) \mathrm{H}(t) \right) \right] \tag{3.13}$$

$$T = \varpi_2 \left[ T_o \mathrm{H}(-t) + T_w \mathrm{H}(t) \right] \tag{3.14}$$

$$m^s = \varpi_3 \left[ m^s_o \mathrm{H}(-t) + m^s_w \mathrm{H}(t) \right] \tag{3.15}$$

In the above, $S_r$, $S_{r\theta}$ and $S_{rz}$ are the far-field stress components in the cylindrical coordinate system, $p_w(t)$ is the time-dependent borehole fluid pressure, $q_w(t)$ is the time-dependent flux across the borehole wall, $T_w$ is the borehole fluid temperature, $m^s_w$ is the solute molar fraction in the borehole fluid and H denotes the Heaviside unit step function. $L_1$ and $L_2$ are coefficients, which take values 0 or 1, and characterize the permeability condition across the borehole wall. Selecting $L_1 = 1$ and $L_2 = 0$ implies a pore pressure boundary condition across the borehole wall. On the other hand, selecting $L_1 = 0$ and $L_2 = 1$ indicates that a boundary condition on the flux is being imposed. Both $p_w(t)$ and $q_w(t)$ can be known time-dependent functions. Setting $p_w(t) = p_w$ gives a permeable condition across the borehole wall with a constant pore pressure whereas $q_w(t) = 0$ implies an impermeable condition across the borehole wall. Solutions with time-dependent pore pressure and flux boundary can also be obtained and are presented in forthcoming chapters.

The far-field stress components $S_r$, $S_{r\theta}$ and $S_{rz}$ are related to the components $S_x$, $S_y$ and $S_z$ as follows

$$S_r = \frac{S_x + S_y}{2} + \frac{S_x - S_y}{2} \cos 2\theta + S_{xy} \sin 2\theta \tag{3.16}$$

$$S_{r\theta} = -\frac{S_x - S_y}{2} \sin 2\theta + S_{xy} \cos 2\theta \tag{3.17}$$

$$S_{rz} = S_{xz} \cos 2\theta + S_{yz} \sin 2\theta \tag{3.18}$$

Not that, the Heaviside unit step function is defined as follows $H(-t) = 1 - H(t)$ such that $H(-t) = 1$ for $t < 0$ and $H(-t) = 0$ for $t \geq 0$.

## 3.4 Problem Decomposition

The inclined borehole problem, as described in the earlier sections, with the boundary conditions is mathematically complex as regards to analytical solution development. However, it is characterized by a geometry in which boundary conditions do not change along the direction of its generator, namely the $z$-axis in the local coordinate system. Under such circumstances, a generalized plane strain idealization can be used which allows extrapolation of solutions developed in two-dimensional geometries to a general three-dimensional case (*Cui et al.*, 1997; *Cheng*, 1998).

It is assumed that the borehole is infinitely long (in the $z$-direction) and that boundary conditions are invariant along that direction. Hence a generalized plane strain condition, as discussed above, manifests itself resulting in all stress and strain components, pore pressure and temperature to be $z$-independent. Again, owing to linearity of all the governing equations and boundary conditions, as is assumed in this work, a superposition technique can be employed to sub-divide this complex problem into simpler problems for which solutions can be obtained. Under this formalism, the inclined borehole problem is decomposed into three sub-problems which are solved individually and later their solutions are superposed to give a solution for the complete problem (*Cui et al.*, 1997). The decomposition scheme is shown in Figure 3.4. It must be noted here that, the inclined borehole scheme, discussed in this work, is generalized to be applicable to transversely isotropic media in which the borehole axis ($z$-axis) coincides the axis of material symmetry. Poroelastic solutions for the inclined borehole for isotropic and transversely isotropic cases are presented in Appendix B.

Adopting a tension positive convention within the framework of the decomposition

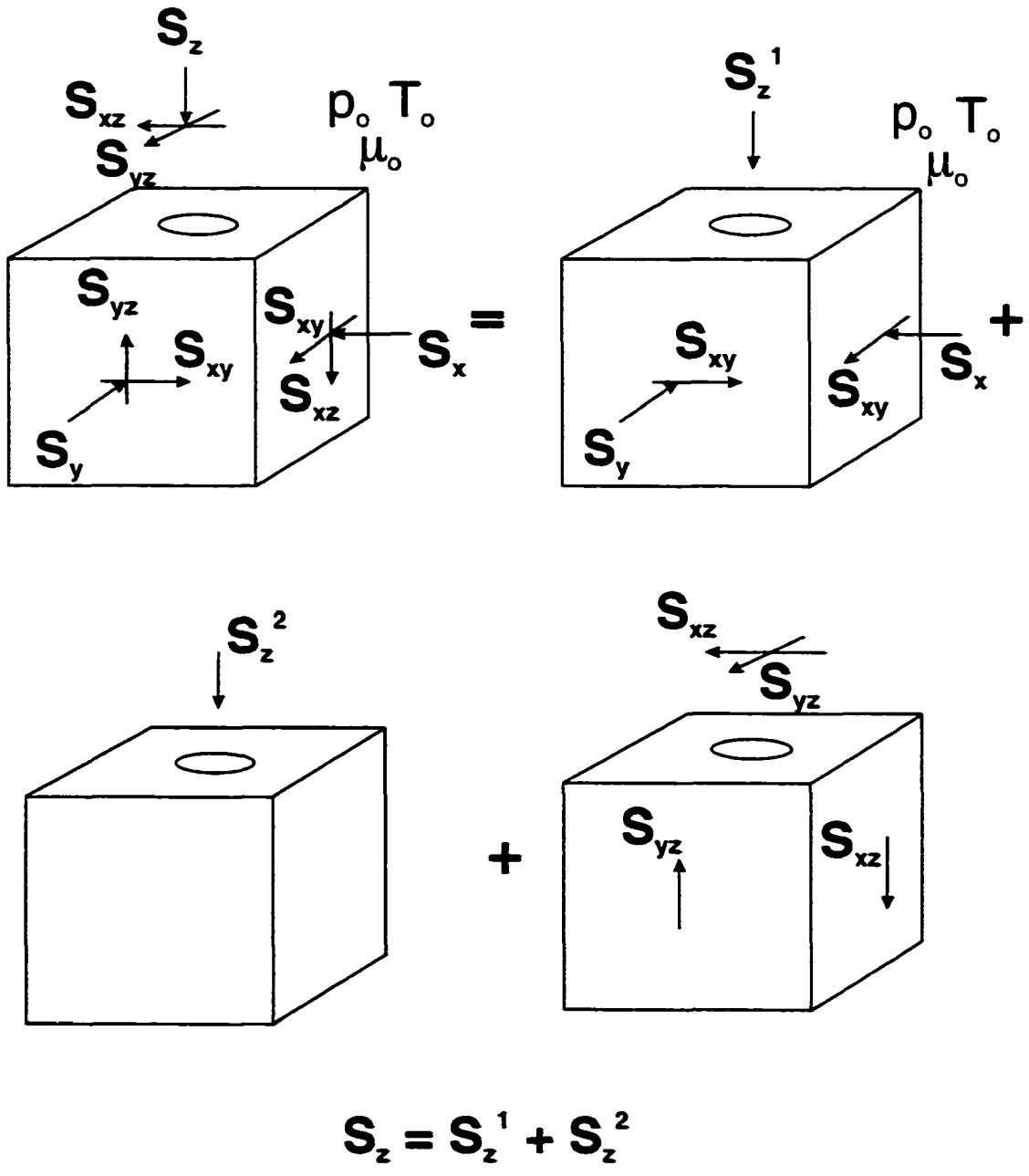


Figure 3.4: Decomposition of the inclined borehole problem

scheme, the boundary conditions for the three problem are given as follows

**Problem I**: At far-field ($r \to \infty$)

$$\sigma_{xx} = -S_x; \quad \sigma_{yy} = -S_y; \quad \sigma_{zz} = -S_z^{(I)} \tag{3.19}$$

$$\tau_{xy} = -S_{xy}; \quad \tau_{yz} = 0; \quad \tau_{xz} = 0 \tag{3.20}$$

$$p = \varpi_1 p_o; \quad T = \varpi_2 T_o; \quad m^s = \varpi_3 m_o^s \tag{3.21}$$

At the borehole wall ($r = R$)

$$\sigma_{rr} = -S_r \mathrm{H}(-t) - p_w \mathrm{K}(t) \tag{3.22}$$

$$\tau_{r\theta} = -S_{r\theta} \mathrm{H}(-t); \quad \tau_{rz} = 0 \tag{3.23}$$

$$L_1 p + L_2 q_r = \varpi_1 \left[ L_1 \left( p_o \mathrm{H}(-t) + p_w(t)\mathrm{H}(t) \right) + L_2 \left( q_w(t)\mathrm{H}(t) \right) \right] \tag{3.24}$$

$$T = \varpi_2 \left[ T_o \mathrm{H}(-t) + T_w \mathrm{H}(t) \right] \tag{3.25}$$

$$m^s = \varpi_3 \left[ m_o^s \mathrm{H}(-t) + m_w^s \mathrm{H}(t) \right] \tag{3.26}$$

**Problem II**: At far-field ($r \to \infty$)

$$\sigma_{zz} = -S_z + S_z^{(I)} \tag{3.27}$$

$$\sigma_{xx} = \sigma_{yy} = \tau_{xy} = \tau_{yz} = \tau_{xz} = p = q_r = T = m^s = 0 \tag{3.28}$$

At the borehole wall ($r = R$)

$$\sigma_{rr} = \tau_{r\theta} = \tau_{rz} = p = q_r = T = m^s = 0 \tag{3.29}$$

**Problem III**: At far-field ($r \to \infty$)

$$\tau_{yz} = -S_{yz}; \quad \tau_{xz} = -S_{xz} \tag{3.30}$$

$$\sigma_{xx} = \sigma_{yy} = \sigma_{zz} = p = q_r = T = m^s = 0 \tag{3.31}$$

At the borehole wall ($r = R$)

$$\tau_{rz} = -S_{rz} \mathrm{H}(-t) \tag{3.32}$$

$$\sigma_{rr} = \tau_{r\theta} = p = q_r = T = m^s = 0 \tag{3.33}$$

In equation (3.27), the constant stress $S_z^{(I)}$, which is the axial stress solution of problem I, can be considered to be a part of the axial stress $S_z$. It is the out-of plane stress of problem I which can be calculated from in-plane stress components $S_x$, $S_y$ and $S_{xy}$, the virgin pore pressure $p_o$, the formation temperature $T_o$ and the molar fraction of the solute in the formation pore fluid $m_o^s$. A detailed discussion on each of the contributing problems, described in the aforementioned decomposition scheme, is presented next.

### 3.4.1 Problem I

A schematic of the Problem I is shown in Figure 3.5. This problem accounts for the far-field in-plane normal and shear stresses and is designed such that a plane strain solution can be utilized. This can be only possible if the out-of-plane displacement and flux vanish and the applied stresses are in agreement with the natural result of a plane strain solution. Accordingly, an out-of-plane vertical stress, $S_z^{(I)}$, which is equivalent to that generated by the in-plane stress components due to a Poisson effect, is applied to ensure applicability of the plane strain solution. It must be noted that equations for $S_z^{(I)}$ would be specific to the poromechanics model for which solutions are being sought. A generalized expression for $S_z^{(I)}$ can be given as follows

$$S_z^{(I)} = \nu'(S_x + S_y) + \varpi_1\left[(\alpha' - 2\nu'\alpha)p_o\right] + \varpi_2\left[(\beta^{s\prime} - 2\nu'\beta^s)T_o\right] - \varpi_3\left[(\gamma^{s\prime} - 2\nu'\gamma^s)m_o^s\right] \tag{3.34}$$

Equation (3.34) has been written for a transversely isotropic material in which the unprimed variables correspond to quantities in the isotropic plane whereas the primed variables are quantities in the transverse direction. In the above, $\alpha$ is the Biot's effective stress coefficient, $\beta^s$ is the thermic coefficient related to the solid skeleton and $\gamma^s$ is the chemo-mechanical coupling coefficient. Equating the primed and unprimed variables would result in an equation applicable to isotropic media.

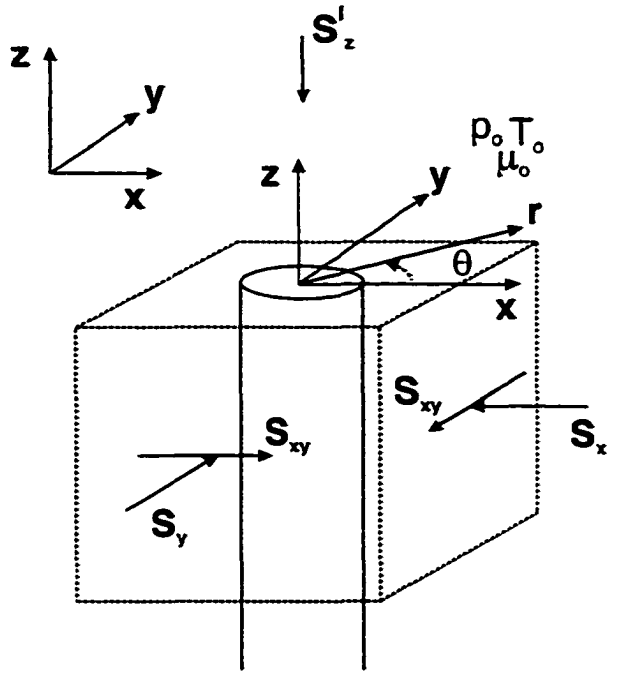


Figure 3.5: A schematic of Problem I

In addition, the boundary conditions in Problem I show that there exists an in-plane far field shear stress which must be eliminated such that the far-field boundary is characterized by only two normal stress components, both of which are the in-plane principal far-field stresses. This is achieved by a rotation of the $xyz$ local coordinate system about the $z$-axis such that a new coordinate system $x''y''z$ is formed in which the $x''$-axis coincides with the minimum horizontal principal stress whereas the $y''$-axis with the maximum horizontal principal stress. The angle of rotation is given by

$$\theta_r = \frac{1}{2}\tan^{-1}\left(\frac{2S_{xy}}{S_x - S_y}\right) \tag{3.35}$$

and the polar angle under the $x''y''z$ coordinate system is given by

$$\theta'' = \theta - \theta_r \tag{3.36}$$

With the aforementioned rotation and elimination of the far-field shear stress, the in-plane boundary conditions are modified as follows

At far-field ($r \rightarrow \infty$ )

$$\sigma_{x''x''} = S_{x''} = -(P_o - S_o) \tag{3.37}$$

$$\sigma_{y''y''} = S_{y''} = -(P_o + S_o) \tag{3.38}$$

$$\tau_{x''y''} = 0 \tag{3.39}$$

$$p = \varpi_1 p_o; \qquad T = \varpi_2 T_o; \qquad m^s = \varpi_3 m_o^s \tag{3.40}$$

In equations (3.37) and (3.38), the normal stress components, $S_{x''}$ and $S_{y''}$ have been written as comprising of a hydrostatic part, $P_o$, and a deviatoric part, $S_o$, which are obtained as follows

$$P_o = \frac{S_x + S_y}{2}; \qquad S_o = \sqrt{\left(\frac{S_x - S_y}{2}\right)^2 + S_{xy}^2} \tag{3.41}$$

With the above boundary conditions, the plane strain solution can be utilized. Since far-field stresses are in equilibrium only the perturbed state needs to be solved for. The background stresses are eliminated and the excavation is simulated by applying boundary conditions at the borehole wall. The excavation simulation is conveniently subdivided to three loading cases for easy physical interpretation (*Carter and Booker*, 1982). The solution is then obtained by a superposition of the background stresses and loading cases. A schematic of the loading cases is shown in Figure 3.6.

The boundary conditions at the borehole wall ($r = R$) for the three induced loading cases due to the perturbation are described as follows

*Case 1*

$$\sigma_{rr}^{(1)} = [P_o - p_w(t)]\,\mathrm{H}(t) \tag{3.42}$$

$$\sigma_{r\theta}^{(1)} = 0 \tag{3.43}$$

$$L_1 p^{(1)} + L_2 q_r^{(1)} = 0; \qquad T^{(1)} = 0; \qquad m^{s(1)} = 0 \tag{3.44}$$

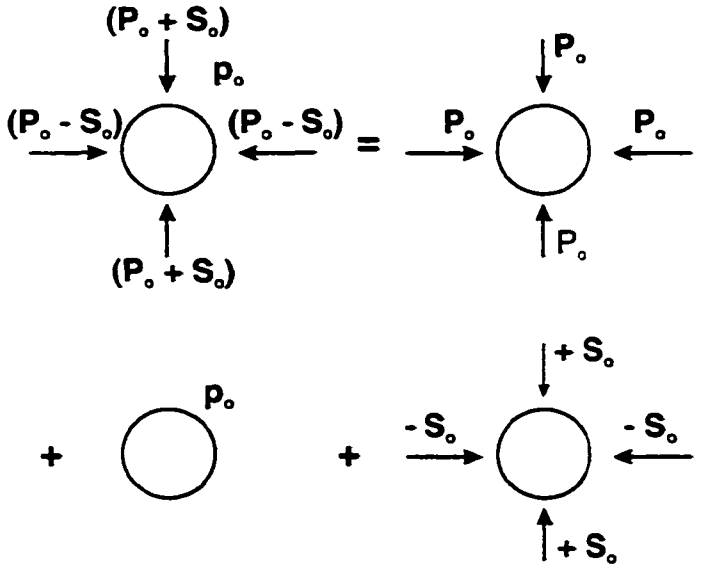


Figure 3.6: Subdivisions of Problem I

*Case 2*

$$\sigma_{rr}^{(2)} = 0; \qquad \sigma_{r\theta}^{(2)} = 0 \tag{3.45}$$

$$\left[L_1 p^{(2)} + L_2 q_r^{(2)}\right] = \varpi_1 L_1 \left(-p_o \mathrm{H}(t) + p_w(t)\mathrm{H}(t)\right) + L_2 \left(q_w(t)\mathrm{H}(t)\right) \tag{3.46}$$

$$T^{(2)} = \varpi_2 \left[T_o \mathrm{H}(-t) + T_w \mathrm{H}(t)\right] \tag{3.47}$$

$$m^{s(2)} = \varpi_3 \left[m_o^s \mathrm{H}(-t) + m_w^s \mathrm{H}(t)\right] \tag{3.48}$$

*Case 3*

$$\sigma_{rr}^{(3)} = \left[-S_o \cos 2(\theta - \theta_r)\right] \mathrm{H}(t) \tag{3.49}$$

$$\sigma_{r\theta}^{(3)} = \left[S_o \sin 2(\theta - \theta_r)\right] \mathrm{H}(t) \tag{3.50}$$

$$L_1 p^{(3)} + L_2 q_r^{(3)} = 0; \qquad T^{(3)} = 0; \qquad m^{s(3)} = 0 \tag{3.51}$$

Of the above, Case 1 and Case 2 are axisymmetric while Case 3 is asymmetric. Case 1 does not generate any volumetric strain and the solution is purely elastic and given by Lame's elastic solution. Case 2 is an axisymmetric problem having a pore pressure,

temperature and solute molar fraction field. The perturbation in these would generate irrotational displacement fields due to their hydrostatic nature. In addition, the domain is also semi-infinite which implies that the diffusion phenomena would be uncoupled from the deformation process. Deformation fields would be induced by the ongoing diffusion process. The solution for this case is obtained within the Laplace domain and inverted to the time domain using the Stehfest algorithm. Case 3 is deviatoric and shows characteristics of full poroelastic coupling. An excess pore pressure is generated instantaneously due to the Skempton effect which diffuses in time and is coupled with the deformation caused by the deviatoric nature of the applied stresses. Again, solutions for Case 3 are obtained within the Laplace domain and inverted to the time domain using the Stehfest algorithm.

### 3.4.2 Problem II

A schematic of Problem II is shown in Figure 3.7. The boundary conditions show that the problem is characterized by the partial axial stress not accounted for in Problem I. Otherwise, all other contributing stresses are trivial. The solution for this problem is elastic and is given by a constant uniaxial vertical stress everywhere. Prior to excavation, the domain is characterized by a constant vertical stress without any pore pressure, temperature or solute molar fraction. The perturbation introduced by the excavation sets the borehole wall free of surface traction. Since the pore pressure, temperature and solute molar fractions are absent in this problem, the solutions for these are naturally trivial. Hence, no diffusion phenomena would occur and the solution is independent of time and thereby elastic.

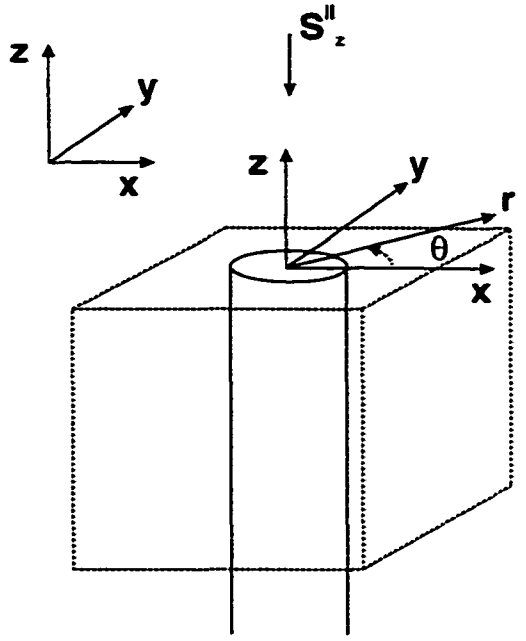


Figure 3.7: A schematic of Problem II

### 3.4.3 Problem III

A schematic of Problem III is shown in Figure 3.8. This problem accounts for the far-field out-of plane shear stresses, $S_{xz}$ and $S_{yz}$. The excavation results in a sudden release of the shear stress $\sigma_{rz}$ at the borehole wall to zero. However, no excess pore pressure is generated by this disturbance of the shear stress. Hence, the solution will be independent of time and identical to the elastic solution given as (*Cui et al.*, 1997)

$$\sigma_{rz}^{(III)} = -(S_{xz}\cos\theta + S_{yz}\sin\theta)\left[1 - \mathrm{H}(t)\frac{R^2}{r^2}\right] \tag{3.52}$$

$$\sigma_{\theta z}^{(III)} = (S_{xz}\sin\theta - S_{yz}\cos\theta)\left[1 + \mathrm{H}(t)\frac{R^2}{r^2}\right] \tag{3.53}$$

### 3.4.4 Complete Solution

The complete solution is obtained by a superposition of the solutions from the three contributing problems. Generalized expressions for the complete solution are given as

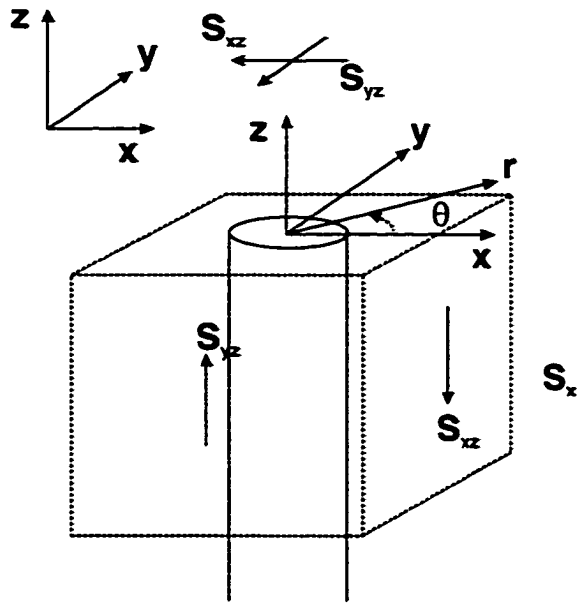


Figure 3.8: A schematic of Problem III

follows

$$\sigma_{rr} = -P_o + S_o \cos 2(\theta - \theta_r) + \sigma_{rr}^{(1)} + \sigma_{rr}^{(2)} + \sigma_{rr}^{(3)} \tag{3.54}$$

$$\sigma_{\theta\theta} = -P_o - S_o \cos 2(\theta - \theta_r) + \sigma_{\theta\theta}^{(1)} + \sigma_{\theta\theta}^{(2)} + \sigma_{\theta\theta}^{(3)} \tag{3.55}$$

$$\sigma_{r\theta} = -P_o + S_o \sin 2(\theta - \theta_r) + \sigma_{r\theta}^{(3)} \tag{3.56}$$

$$\sigma_{rz} = -(S_{xz} \cos\theta + S_{yz} \sin\theta)\left[1 - (R^2/r^2)\right] \tag{3.57}$$

$$\sigma_{\theta z} = (S_{xz} \sin\theta + S_{yz} \cos\theta)\left[1 + (R^2/r^2)\right] \tag{3.58}$$

$$p = p_o + p^{(2)} + p^{(3)} \tag{3.59}$$

$$T = T_o + T^{(2)} \tag{3.60}$$

$$\begin{aligned}\sigma_{zz} = -S_z + [\nu'(S_x + S_y) + \varpi_1(\alpha' - 2\nu'\alpha)p_o + \varpi_2(\beta' - 2\nu'\beta)T_o \\ -\varpi_3(\gamma^{s'} - 2\nu'\gamma^s)m_o^s] + \nu'(\sigma_{rr} + \sigma_{\theta\theta}) - \varpi_1(\alpha' - 2\nu'\alpha)p \\ -\varpi_2(\beta^{s'} - 2\nu'\beta^s)T + \varpi_3(\gamma^{s'} - 2\nu'\gamma^s)m^s\end{aligned} \tag{3.61}$$

in which $\sigma_{rr}^{(1)}$, $\sigma_{\theta\theta}^{(1)}$ are solutions of Case 1 in Problem I, $\sigma_{rr}^{(2)}$, $\sigma_{\theta\theta}^{(2)}$, $p^{(2)}$, $T^{(2)}$ are solutions of Case 2 in Problem I and $\sigma_{rr}^{(3)}$, $\sigma_{\theta\theta}^{(3)}$, $\sigma_{r\theta}^{(3)}$, $p^{(3)}$ are solutions of Case 3 in Problem I.

The inclined borehole solution scheme discussed in this section is general and will be specialized in the forthcoming chapters to be applicable to the specific poromechanics model discussed there.

## 3.5 Borehole Stability Considerations

The redistribution of compressive stresses and triggering of the coupled physicochemical processes due to excavation modifies the stress, temperature, pore pressure and chemical potential fields in the vicinity of the borehole. Mechanical instability is caused if the stresses are larger than what the material can sustain or, in other words, strength of the material. The potential instability can be controlled by managing the borehole fluid pressure and/or salt concentrations in the borehole fluid, such that, the stresses are within permissible limits of the material strength. The potential for failure is assessed by applying a failure criterion, which is a function of the material strength parameters, to the state of stress around the borehole, and examining if the stress-levels would result in failure (*Bradley*, 1979). The modes of failure and the applicable failure criteria that can be employed are discussed in this section.

### 3.5.1 Modes of Borehole Failure

In this work, borehole failure from purely a mechanical viewpoint is examined. The mechanical failure investigated, is assumed to be caused due to alteration of stress fields resulting directly from excavation as well as due to induced thermo-hydro-chemo-mechanical processes. It is assumed that failure is controlled by Terzaghi's effective stress. In other words, a Terzaghi effective stress state larger than the material strength implies failure. Two modes of failure are considered,

- tensile or fracturing failure

Fracturing is generally caused due to excessive pressures exerted by the borehole fluid which result in a development of tensile stresses greater than the tensile strength of the material.

- shear or collapse failure.

Collapse failures, on the other hand, are generally caused due to insufficient borehole fluid support pressure resulting in failure in the shear mode.

There are two possible forms of tensile failure. A schematic of the tensile failure forms is shown in Figure 3.9. Figure 3.9(a) shows the fracturing tensile failure which occurs due to buildup of effective tangential stress which are of a tensile nature and which are greater than the tensile strength of the material. Figure 3.9(b) - (c), on the other hand, show the outburst or spalling tensile failure which is a result of the tensile effective radial stresses.

Mathematical expressions for the tensile failure and shear failure criterion are presented next.

### 3.5.2 Tensile Failure Criterion

Tensile failure is assumed to occur when the maximum effective principal stress (most tensile effective principal stress) exceeds the tensile strength of the material. Suppose $\sigma_{max}$ is the maximum effective principal stress, the corresponding Terzaghi's effective stress is given by:

$$\sigma'_{max} = \sigma_{max} + p \tag{3.62}$$

If $T$ denotes the tensile strength of the material, the tensile failure criteria is mathematically expressed as:

$$\sigma_{fr} = \min_{0 \leq \theta \leq 2\pi} \{-\sigma'_{\max} + T\} < 0 \tag{3.63}$$

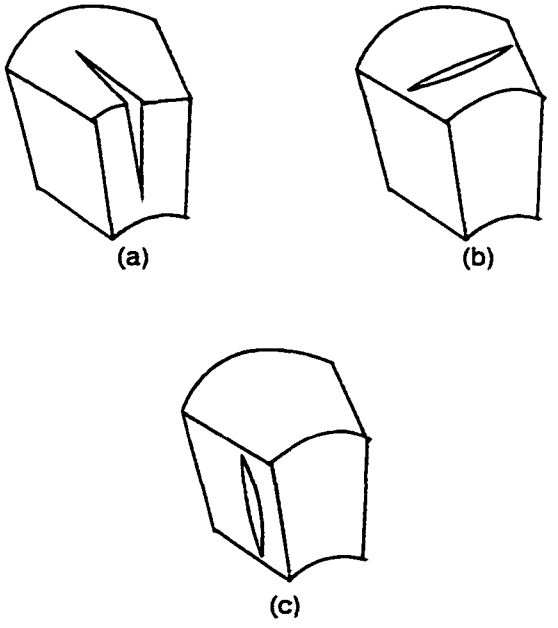


Figure 3.9: A schematic of the tensile failure forms (*Cui et al.*, 1999)

where $\sigma_{fr}$ is referred to as the effective fracturing stress. A negative value of the effective fracturing stress ($\sigma_{fr} < 0$) implies failure.

### 3.5.3 Shear Failure Criteria

The Mohr-Coulomb, Drucker-Prager and Modified-Lade failure criterion are commonly used to assess shear failures. Mathematical forms of these are presented in this section.

- *Mohr-Coulomb*

The Mohr-Coulomb failure envelope is expressed by

$$\tau_f + \sigma_f \tan\phi - c = 0 \tag{3.64}$$

where $\tau_f$ is the mean shear stress, $\sigma_f$ is the mean normal stress, $c$ is the cohesion and $\phi$ is the friction angle. In the above

$$\tau_f = \frac{1}{2}\left(\sigma_1^{'} - \sigma_3^{'}\right)\sin 2\theta \tag{3.65}$$

$$\sigma_f = \frac{1}{2}\left(\sigma_1^{'} + \sigma_3^{'}\right) + \frac{1}{2}\left(\sigma_1^{'} - \sigma_3^{'}\right)\cos 2\theta \tag{3.66}$$

$$\theta = \frac{\pi}{4} + \frac{\phi}{2} \tag{3.67}$$

Failure occurs when the effective collapse stress, $\sigma_{cl}$, is less than zero ($\sigma_{cl} < 0$) where $\sigma_{cl}$ is defined by

$$\sigma_{cl} = \min_{0 \le \theta \le 2\pi} \{-\tau_f - \sigma_f \tan\phi + c\} < 0 \tag{3.68}$$

- *Drucker-Prager*

The Drűcker-Prager failure envelope is expressed by (*Desai and Siriwardane*, 1984)

$$\sqrt{J_2} + 3AS_p - D = 0 \tag{3.69}$$

where $S_p$ is the effective mean normal stress $\sqrt{J_2}$ is the mean shear stress and $A$ and $D$ are two positive material constants determined from laboratory testing. $S_p$ and $J_2$ are defined as:

$$S_p = \frac{\sigma_{11} + \sigma_{22} + \sigma_{33}}{3} + p \tag{3.70}$$

$$J_2 = \frac{1}{6}\left[(\sigma_{11} - \sigma_{22})^2 + (\sigma_{11} - \sigma_{22})^2 + (\sigma_{11} - \sigma_{22})^2\right] + \sigma_{12}^2 + \sigma_{23}^2 + \sigma_{31}^2 \tag{3.71}$$

Failure occurs when the effective collapse stress, $\sigma_{cl}$, is less than zero where $\sigma_{cl}$ is defined by

$$\sigma_{cl} = \min_{0 \le \theta \le 2\pi} \{-\sqrt{J_2} - 3AS_p + D\} < 0 \tag{3.72}$$

- *Modified Lade*

The failure envelope for the Modified-Lade criteria is given by (*Lade*, 1985)

$$\frac{I_1''}{\sqrt[3]{I_3''}} - \sqrt[3]{(27+\bar{\eta})} = 0 \tag{3.73}$$

where $I_1''$ and $I_3''$ are defined by

$$I_1'' = (\sigma_1 + \bar{S}_1 + p) + (\sigma_2 + \bar{S}_1 + p) + (\sigma_3 + \bar{S}_1 + p) \tag{3.74}$$

$$I_3'' = (\sigma_1 + \bar{S}_1 + p)(\sigma_2 + \bar{S}_1 + p)(\sigma_3 + \bar{S}_1 + p) \tag{3.75}$$

in which $\sigma_1$, $\sigma_2$ and $\sigma_3$ are the principal stresses and $S_1$, $\bar{\eta}$ are defined by

$$\bar{S}_1 = \frac{c}{\tan\phi} \tag{3.76}$$

$$\bar{\eta} = \frac{4\tan^2\phi(9 - 9\sin\phi)}{(1 - \sin\phi)} \tag{3.77}$$

The effective collapse stress, $\sigma_{cl}$ is defined by

$$\sigma_{cl} = \min_{0\leq\theta\leq 2\pi}\{-\frac{I_1''}{\sqrt[3]{I_3''}} + \sqrt[3]{(27+\bar{\eta})}\} < 0 \tag{3.78}$$

and failure is assumed to occur when $\sigma_{cl}$ is less than zero.

## 3.6 Summary

The inclined borehole problem has been discussed in detail in this chapter. A generalized analytical solution scheme to obtain solutions under the poromechanics models has presented. Linearity of the stress-strain behavior allows the use of a superposition methodology to arrive upon solutions. A decomposition scheme for the inclined borehole problem has been presented. Borehole stability considerations, modes of borehole failure and the applicable failure criteria have been discussed. The generalized solution scheme presented in this chapter will be specialized to specific poromechanics models discussed in forthcoming chapters.

# Chapter 4

# Anisotropic Porothermoelasticity

## 4.1 Introduction

A great deal of attention has been focused on coupled thermomechanical behavior of fluid-saturated porous media. Over the years, the theoretical developments in this area have resulted in development of poromechanics models rationalizing the thermo-hydro-mechanical response. Research efforts have matured from a simple extension of Biot's isotropic poroelastic theory (*Biot*, 1941; *Bear and Corapcioglu*, 1981; *Kurashige*, 1989; *Coussy*, 1989, 1995) to a more general approach which can handle the coupling along with the material anisotropy (*Katsube*, 1988; *Abousleiman and Ekbote*, 1999). Applications for these are found in diverse areas such as deep drilling and excavation, modeling of nuclear waste disposal facilities (*Utsugida*, 1985) and extraction of geothermal energy (*Brownell et al.*, 1977). With the complex mechanisms that come into play, identification of various driving forces and the interaction between them presents a challenge in predicting an appropriate behavior at depth.

In most cases, the aforementioned field situations exhibit a porothermoelastic response displaying a strong coupling between the heat transport, fluid diffusion and transport, and the solid deformation. For example, in deep-drilling projects, stress and pore pressure distributions are altered due to presence of a thermal and fluid pressure gradients that must be accounted for in the analysis. Also, in nuclear waste deposi-

tories where the applied boundaries, i.e., extremely high temperatures in anisotropic shale/clay deep formations, pose significant concerns in estimating an accurate response of the coupled phenomena. The interplay between the coupled stress/pressure, deformation and temperature fields associated with poromechanical and thermal porous material properties forms an important factor in obtaining efficient and stable designs within the porothermoelastic approach.

Extension of Biot's theory to incorporate thermal effects for the isotropic case, which formulates the porothermoelastic model, has been addressed by several authors (*Bear and Corapcioglu*, 1981; *Kurashige*, 1989; *Coussy*, 1989, 1995). Solutions to boundary and initial value problems have been developed under various scenarios which demonstrate the effect of the thermohydromechanical coupling on the response (*Booker and Savvidou*, 1984, 1985; *McTigue*, 1986, 1990; *Kurashige*, 1992; *Kodashima and Kurashige*, 1996). At the same time, Biot's theory has been extended to account for material anisotropy (*Biot*, 1955; *Thompson and Willis* 1991). Analytical solutions for fundamental problems such as Mandel's problem (*Abousleiman et al.* 1996a), the borehole problem and the cylinder problem (*Abousleiman and Cui*, 1998) have been extended for the transversely isotropic poroelastic case. It was found that analysis of the transversely isotropic poroelastic problems showed unpredicted results when compared to their elastic counterparts (*Abousleiman et al.*, 1996a, *Abousleiman and Cui*, 1998). In addition to the time-dependency of the flow and deformation fields, the anisotropic material coefficients play an important role in the calculation of the in-plane and out-of-plane stresses. There is existing literature that addresses the thermal effects in anisotropic media though the treatment in many cases is limited to coupled thermoelasticity (*Li*, 1992; *Sharma and Kumar*, 1996, 1997). A comprehensive treatment of the anisotropic porothermoelasticity has been addressed by Katsube (1988).

In general, geo-activities are usually carried out in formations that can be broadly

classified as transversely isotropic due to the simple natural deposition of sedimentary rocks which has occurred over a geological time scale. The deposition processes lead to development of formations with similar material properties across a cross section but having different characteristics in the direction perpendicular to it. In this chapter, a porothermoelastic formulation applicable to transversely isotropic media is developed. Governing equations are developed first for the general anisotropic case and then specialized for a transversely isotropic poroelastic material subjected to non-isothermal conditions. The resulting system of equations is used to obtain analytical solutions.

Solution for the inclined borehole problem is presented where it is assumed that the borehole generator coincides with the material axis of symmetry. Source terms related to heat convection are neglected. In other words, the rate of heat transport, in the porous media is assumed to be much faster than that of the interstitial fluid transport which is the case in most low to moderate values of the permeability coefficient. Borehole solutions are presented assuming both, the permeable and the impermeable boundary conditions at the borehole wall. Numerical examples demonstrate the effect of anisotropy of the poromechanical parameters, as well as the anisotropy of the thermal coefficients, on stress and pore pressure distributions.

## 4.2 General Formulation

Upon load application, the mechanical response of a fluid saturated porous system is characterized by coupled diffusion-deformation attributed to the interdependence of change in pore volume and the pore fluid pressure. With the introduction of boundary temperatures, i.e., a non-isothermal state, both the pore fluid and pore volume are subject to differential expansion or contraction resulting in additional coupling associated with the temperature change. The magnitude of the relative change in stress, pore pressure, and temperature is coupled and described by constitutive relations weighted

by material coefficients. The set of governing equations includes conservation laws, i.e., mass, momentum, and energy balance, along with conduction laws, i.e., Darcy's law and Fourier's law, which account for fluid and heat flux respectively in the fluid saturated porous system. In this section, a full set of governing equations is developed for the general anisotropic case.

*Constitutive Equations*

The constitutive equations for linear porothermoelasticity are expressed as

$$\sigma_{ij} = M_{ijkl}\epsilon_{kl} - \alpha_{ij}p - \beta^s_{ij}T \tag{4.1}$$

$$\zeta = p/M + \alpha_{ij}\epsilon_{ij} - \beta^{sf}T \tag{4.2}$$

Equations (4.1) and (4.2) are written using a tension positive convention. The above equations relate the response of the dynamic variables, $\sigma_{ij}$ (total stress tensor), $p$ (pore pressure), and $T$ (temperature), to the kinematic quantities, $\epsilon_{ij}$ (solid strain tensor) and $\zeta$ (variation of fluid content). The connection between the dynamic and kinematic quantities is characterized by the material constants, $M_{ijkl}$ (drained elastic modulus tensor), $\alpha_{ij}$ (Biot's effective stress coefficient tensor), $M$ (Biot's modulus), $\beta^s_{ij}$ (thermic coefficient tensor related to the solid skeleton), and $\beta^{sf}$ (thermic coefficient related to the pore fluid). The thermic coefficient tensor, $\beta^s_{ij}$, provides a measure of the stress induced due to change in temperature. It is related to the thermal expansion coefficients and the drained elastic modulus tensors as follows (*Nowinski*, 1978)

$$\beta^s_{ij} = M_{ijkl}\alpha^s_{kl} \tag{4.3}$$

where $\alpha^s_{ij}$ is the linear expansion coefficient tensor of the solid skeleton. The thermic coefficient, $\beta^{sf}$, on the other hand, is associated with the pore fluid and provides a measure of the pore pressure induced due to a change in temperature. It is related to the thermal expansion coefficients of the solid-fluid system, the porosity to the medium

and the Biot's effective stress coefficient tensor and is given as (*Ekbote et al.*, 2000)

$$\beta^{sf} = \alpha_{ij}\alpha^{s}_{ij} + (\alpha^{f} - \alpha^{s}_{kk})\phi \tag{4.4}$$

in which $\alpha^f$ is the volumetric expansion coefficient for the pore fluid, and $\phi$ is the porosity. Note that in writing equations (4.1) - (4.4), the thermal expansion coefficients of the bulk drained material and that of the solid skeleton are assumed to be equal. The above equations give the complete anisotropic stress-strain response of a porothermoelastic material. For the most general anisotropic case, the behavior is described using 35 constants (21 $M_{ijkl}$'s, 6 $\alpha_{ij}$'s, 1 $M$, 6 $\beta^s_{ij}$'s and 1 $\beta^{sf}$) (*Abousleiman and Ekbote*, 1999)

*Mass balance*

For solid-fluid constituent porous system, where no fluid sources or sinks exist, the fluid mass balance equation is written as

$$\frac{\partial \zeta}{\partial t} + q_{i,i} = 0 \tag{4.5}$$

where $q$ is the specific discharge vector. Under non-isothermal conditions fluid transport within the system can be caused by a gradient in both, the pore fluid pressure as well as temperature. A generalized expression for the specific discharge, $q$, is given as (*McTigue*, 1986)

$$q_i = -\kappa_{ij}p_{,j} + \Gamma^{q}_{ij}T_{,j} \tag{4.6}$$

in which $\kappa_{ij}$ is the anisotropic mobility coefficient tensor and $\Gamma^q_{ij}$ is the coefficient tensor which relates the flux to the temperature gradient. The first term on the right hand side in equation (4.6) corresponds to the fluid transport caused by the *Darcy* effect and the second term on the right hand side analogous to the *Soret* effect is ignored in this analysis. The anisotropic mobility coefficient tensor, $\kappa_{ij}$, is related to the intrinsic permeability tensor, $k_{ij}$, and the pore fluid viscosity, $\mu$, by $\kappa_{ij} = k_{ij}/\mu$.

*Momentum balance*

Momentum balance yields the equilibrium equations which are given by

$$\sigma_{ij,j} = 0 \tag{4.7}$$

Again equation (4.7) has been written ignoring any body and inertia forces.

*Energy balance*

Within a continuum model both the matrix and the pore fluid are assumed to occupy the same point in space and therefore one should introduce two temperatures to characterize the thermal state of the system. However, existing studies for thermomechanical behavior of porous media employ a common temperature for both the constituents of the porous system based on the assumption of instantaneous local temperature equilibrium (*Bird et al.*, 1960; *Bear and Corapcioglu*, 1981; *McTigue*, 1986, 1990; *Kurashige*, 1989). In other words, it is assumed that the heat transport between the matrix and the pore fluid at the local level is much faster than the overall heat diffusion process. Neglecting the internal energy change due to viscous dissipation and compression the energy balance equation is given as

$$\rho C_v \frac{\partial T}{\partial t} = -h_{i,i} - (\rho C_v q_i) T_{,i} \tag{4.8}$$

where $\rho C_v$ is the heat capacity of the solid-fluid mixture and $h$ is the heat flux. In equation (4.8) the first term on the right hand side corresponds to heat transport by conduction whereas the second term represents the heat transport by convection. In addition, it is assumed that the porous material bears a low permeability and that the heat diffusion occurs much faster than the fluid diffusion which indirectly results in the assumption of a small *Peclet* number. Under these circumstances, the term corresponding to convection can be dropped from (4.8) resulting in a linearized form of the energy balance given by

$$\rho C_v \frac{\partial T}{\partial t} + h_{i,i} = 0 \tag{4.9}$$

Clearly, equation. (4.9) is uncoupled from the pore pressure field.

The 'bulk heat capacity', $\rho C_v$, can be related to individual heat capacities of the solid and fluid constituents by (*Bear and Corapcioglu*, 1981; *McTigue*, 1986)

$$\rho C_v = (1-\phi)\rho^s C_v^s + \phi \rho^f C_v^f \tag{4.10}$$

in which the superscripts $s$ and $f$ refer to the solid and fluid respectively.

Analogous to the fluid mass transport, the heat flux in the most general case can be caused by gradients in pressure and temperature. A generalized equation for the heat flux is given by (*McTigue*, 1986)

$$h_i = -\lambda_{ij} T_{,j} + \Gamma_{ij}^h p_{,j} \tag{4.11}$$

where $\lambda_{ij}$ is the effective thermal conductivity of the solid-fluid system, and $\Gamma_{ij}^h$ is the coefficient tensor associated with the heat flux caused due to the pressure gradient. The first term on the right hand side in equation (4.11) is the heat flux caused by the *Fourier* effect, whereas the second term analogous to the *Dufour* effect is ignored in this analysis.

As in equation (4.11) the 'effective thermal conductivity' can also be obtained from the thermal conductivities of the solid and fluid constituents as a weighted average using the porosity and is given as (*Bear and Corapcioglu*, 1981; *McTigue*, 1986)

$$\lambda_{ij} = (1-\phi)\lambda_{ij}^s + \phi \lambda_{ij}^f \tag{4.12}$$

where $\lambda_{ij}^s$ and $\lambda_{ij}^f$ are the thermal conductivities of the solid and fluid constituents, respectively.

The above set of equations (4.1) - (4.12) represents the porothermoelastic system in the general anisotropic form. These are specialized for a transversely isotropic material in the following section.

## 4.3 Transversely Isotropic Porothermoelasticity

A transversely isotropic material is characterized by same properties in one plane and different properties in the direction normal to this plane. For the transversely isotropic material it is assumed that the $z$-axis coincides with the axis of elastic symmetry. The transversely isotropic poroelastic material is characterized by 8 material constants (*Cheng*, 1997; *Abousleiman and Cui*, 2000). These are given as $E$, $E'$, $\nu$, $\nu'$, $G'$, $\alpha$, $\alpha'$ and $M$ where the unprimed variables are material coefficients in the isotropic plane and the primed variables are material coefficients in the transverse direction. In the above, $E$ is the drained elastic modulus, $\nu$ is the drained Poisson's ratio. $G$ is the shear modulus, $\alpha$ is the Biot's effective stress coefficient and $M$ is the Biot's modulus.

With the introduction of non-isothermal effects three additional thermic constants, $\beta^s$, $\beta^{s'}$, $\beta^{sf}$ are required to account for the differential volume change of the solid skeleton and pore fluid due to temperature changes. Hence, constitutive relations for a transversely isotropic material under the porothermoelastic model are given as follows

$$\begin{Bmatrix} \sigma_{xx} \\ \sigma_{yy} \\ \sigma_{zz} \\ \tau_{xy} \\ \tau_{yz} \\ \tau_{zx} \\ p \end{Bmatrix} = \begin{bmatrix} \bar{M}_{11} & \bar{M}_{12} & \bar{M}_{13} & 0 & 0 & 0 & -\alpha M \\ \bar{M}_{12} & \bar{M}_{11} & \bar{M}_{13} & 0 & 0 & 0 & -\alpha M \\ \bar{M}_{13} & \bar{M}_{13} & \bar{M}_{33} & 0 & 0 & 0 & -\alpha' M \\ 0 & 0 & 0 & G & 0 & 0 & 0 \\ 0 & 0 & 0 & 0 & G' & 0 & 0 \\ 0 & 0 & 0 & 0 & 0 & G' & 0 \\ -\alpha M & -\alpha M & -\alpha' M & 0 & 0 & 0 & M \end{bmatrix} \begin{Bmatrix} \epsilon_{xx} \\ \epsilon_{yy} \\ \epsilon_{zz} \\ \gamma_{xy} \\ \gamma_{yz} \\ \gamma_{zx} \\ \zeta \end{Bmatrix} - \begin{bmatrix} \bar{\beta}^s \\ \bar{\beta}^s \\ \bar{\beta}^{s'} \\ 0 \\ 0 \\ 0 \\ M\beta^{sf} \end{bmatrix} T \tag{4.13}$$

where

$$\bar{M}_{11} = M_{11} + \alpha^2 M; \qquad \bar{M}_{12} = M_{12} + \alpha^2 M \tag{4.14}$$

$$\bar{M}_{13} = M_{13} + \alpha\alpha' M; \qquad \bar{M}_{33} = M_{33} + \alpha'^2 M \tag{4.15}$$

$$\bar{\beta}^s = \beta^s + \alpha M \beta^{sf}; \qquad \bar{\beta}^{s'} = \beta^{s'} + \alpha' M \beta^{sf} \tag{4.16}$$

In the above, the coefficients of the drained elastic modulus tensor can be related to the material constants $E$, $E'$, $\nu$, $\nu'$, and $G'$ chosen to represent the transversely isotropic materials by the following relations (*Abousleiman et al.*, 1996a; *Abousleiman and Cui*, 1998, 2000)

$$M_{11} = \frac{E(E' - E\nu'^2)}{(1+\nu)(E' - E'\nu - 2E\nu'^2)}; \quad M_{12} = \frac{E(E'\nu + E\nu'^2)}{(1+\nu)(E' - E'\nu - 2E\nu'^2)} \tag{4.17}$$

$$M_{13} = \frac{EE'\nu'}{(E' - E'\nu - 2E\nu'^2)}; \quad M_{33} = \frac{E'^2(1-\nu)}{(E' - E'\nu - 2E\nu'^2)} \tag{4.18}$$

In addition, it has been shown that, with the assumption of microisotropy and microhomogeneity the coefficients $\alpha$ and $\alpha'$ can be related to components of the drained elastic tensor (*Abousleiman et al.*, 1996a; *Cheng*, 1997; *Abousleiman and Cui*, 1998, 2000). These relations are given as

$$\alpha = 1 - \frac{M_{11} + M_{12} + M_{13}}{3K_s} \tag{4.19}$$

$$\alpha' = 1 - \frac{2M_{13} + M_{33}}{3K_s} \tag{4.20}$$

where $K_s$ is the grain bulk modulus of the solid constituent. The expressions for $\beta^s$, $\beta^{s'}$ and $\beta^{sf}$ are obtained as follows

$$\beta^s = (M_{11} + M_{12})\,\alpha^s + M_{13}\alpha^{s'} \tag{4.21}$$

$$\beta^{s'} = 2M_{13}\alpha^s + M_{33}\alpha^{s'} \tag{4.22}$$

$$\beta^{sf} = 2\alpha\alpha^s + \alpha'\alpha^{s'} + (\alpha^f - 2\alpha^s - \alpha^{s'})\phi \tag{4.23}$$

where $\alpha^s$ and $\alpha^{s'}$ are coefficients of linear expansion of the solid skeleton in the isotropic plane and transverse directions, respectively. In addition, the transversely isotropic material is characterized by different thermal conductivities ($\lambda$, $\lambda'$) and mobility coefficients ($\kappa$, $\kappa'$) in the isotropic plane and transverse directions. In line with the aforementioned discussion, governing equations for a three-dimensional case can be derived.

However, many problems in geomechanics are characterized by geometries in which boundary conditions do not change along the direction of their generators. Under such circumstances, a generalized plane strain idealization can be used which allows extrapolation of solutions developed in two-dimensional geometries to a general three-dimensional case (*Abousleiman et al.*, 1996a).

It is assumed that the $z$-direction is infinitely long and that boundary conditions are invariant along that direction. Hence, a generalized plane strain condition, as discussed above, manifests itself resulting in all stress components, pore pressure and temperature to be $z$-independent. Naturally, both heat and fluid flux components in the $z$-direction vanish and all diffusion phenomena occur in the $x-y$ plane which is isotropic. It would, therefore, be useful to derive governing equations for a plane ($x-y$) case which will be utilized in obtaining analytical solutions (two-dimensional) and subsequently extended to the three-dimensional case under the assumption of a generalized plane strain condition.

Combination of the equilibrium equations with the constitutive relations yields the Navier-type equations which are given as follows

$$\frac{1}{2}(M_{11}-M_{12})u_{i,jj}+\frac{1}{2}(M_{11}+M_{12})u_{j,ji}=\ \alpha p_{,i}+\beta^s T_{,i}\quad (i,j=1,2) \tag{4.24}$$

where, $u_i$ denotes the total displacement of the REV. Note that the two-dimensional form of the equilibrium equations has been used to derive the above equation.

Following the approach outlined by Rice and Cleary (1976), the Beltrami-Michelle

compatibility equations for transversely isotropic porothermoelasticity are expressed as

$$\left[C_{11}-\frac{C_{13}^2}{C_{33}}\right]\nabla^2\left(\sigma_{xx}+\sigma_{yy}\right)+\left[C_{11}+C_{12}-\frac{2C_{13}^2}{C_{33}}\right]\left(\alpha\nabla^2 p+\beta^s\nabla^2 T\right)=0 \tag{4.25}$$

where $C_{ij}$'s are elements of the compliance matrix. Combining the energy balance relation with Fourier's law yields the heat diffusion equation

$$\frac{\partial T}{\partial t}-c_h\nabla^2 T=0 \tag{4.26}$$

where $c_h=\lambda/\rho C_v$ is the heat diffusivity in the isotropic plane.

Diffusion equations for the pore fluid are obtained combining the fluid mass balance relations with the Darcy's law. These can be expressed in terms of the pore pressure, $p$, and the variation of the fluid content $\zeta$ and are given as

$$\frac{\partial p}{\partial t}-\kappa M\nabla^2 p=-\alpha M\frac{\partial \epsilon}{\partial t}+\beta^{sf}M\frac{\partial T}{\partial t} \tag{4.27}$$

$$\frac{\partial \zeta}{\partial t}-c_f\left[\nabla^2\zeta+\bar{c}\nabla^2 T\right]=0 \tag{4.28}$$

where $\epsilon=\epsilon_{xx}+\epsilon_{yy}$, and, $c_f$, $\bar{c}$ are respectively the fluid diffusivity and a solid-fluid coupling constant in accordance to

$$c_f=\frac{\kappa M M_{11}}{(M_{11}+\alpha^2 M)};\qquad \bar{c}=\frac{\alpha\beta^s-M_{11}\beta^{sf}}{M_{11}} \tag{4.29}$$

In addition, the pore pressure diffusion equation (4.27) can be simplified assuming an irrotational displacement field and a semi-infinite domain and is expressed as

$$\frac{\partial p}{\partial t}-c_f\nabla^2 p=c_{hf}\frac{\partial T}{\partial t} \tag{4.30}$$

where $c_{hf}$ is a coupling constant given by

$$c_{hf}=\frac{c_f}{\kappa}\left(\beta^{sf}-\frac{\alpha\beta^s}{M_{11}}\right) \tag{4.31}$$

Notice that although governing equations are written here in their two-dimensional forms (equations (4.24 - (4.31)), their coefficients are still dependent on the material elastic properties in the transverse direction.

The Navier-type equations (4.24), heat diffusion equation (4.26) and the pore fluid diffusion equations (4.27) and (4.28) constitute a set of complete equations which can be solved to obtain solutions at the stress level. The pore pressure diffusion equation (4.30) is used when conditions for the irrotational displacement field and semi-infinite domain are satisfied. Clearly, the heat diffusion equation is uncoupled from the fluid diffusion and deformation fields and can be solved independently to yield expressions for the temperature distribution. These expressions for the temperature field are then used in the pore pressure diffusion equation (4.30) to obtain expressions for the pore pressure which can in turn be used within the Navier-type equations (4.24) to obtain solutions for the stress field.

## 4.4 Isotropic Porothermoelasticity

Under the special case where the material is isotropic, the material is identified by two elastic constants, $G$ and $\nu$ two poroelastic constants, $\alpha$ and $M$ and two thermic coefficients $\beta^s$ and $\beta^{sf}$. It can be shown that the constitutive equations reduce to (*Li*, 1998)

$$\sigma_{ij} = 2G\epsilon_{ij} + \frac{2G\nu}{1-2\nu}\epsilon\delta_{ij} - \alpha p\delta_{ij} - \beta^s T\delta_{ij} \tag{4.32}$$

$$p = M(\zeta - \alpha\varepsilon + \beta^{sf}T) \tag{4.33}$$

$$\beta^s = \left(\frac{2G(1+\nu)}{(1-2\nu)}\right)\alpha^s \tag{4.34}$$

$$\beta^{sf} = 3\alpha\alpha^s + (\alpha^f - 3\alpha^s)\phi \tag{4.35}$$

The other governing equations are given as

*Heat Diffusion*

$$\frac{\partial T}{\partial t} - c_h\nabla^2 T = 0 \tag{4.36}$$

*Fluid Diffusion*

$$\frac{\partial p}{\partial t} - \kappa M \nabla^2 p = -\alpha M \frac{\partial \epsilon}{\partial t} + \beta^{sf} M \frac{\partial T}{\partial t} \tag{4.37}$$

$$\frac{\partial \zeta}{\partial t} - c_f \left[ \nabla^2 \zeta + \bar{c} \nabla^2 T \right] = 0 \tag{4.38}$$

Under the assumptions of an irrotational displacement field and semi-infinite domain, the pore pressure diffusion equation (4.37) reduces to

$$\frac{\partial p}{\partial t} - c_f \nabla^2 p = c_{hf} \frac{\partial T}{\partial t} \tag{4.39}$$

*Navier Equations*

$$G u_{i,jj} + \frac{G\nu}{1-2\nu} u_{j,ji} = \alpha p_{,i} + \beta^s T_{,i} \tag{4.40}$$

and $c_f$, $c_{hf}$ and $\bar{c}$ reduce to their isotropic counterparts and are given by

$$c_f = \frac{2G\kappa(1-\nu)(\nu_u - \nu)}{\alpha^2(1-2\nu)^2(1-\nu_u)} \tag{4.41}$$

$$\bar{c} = \left( \alpha\alpha^s \frac{(1+\nu)}{(1-\nu)} - \beta^{sf} \right) \tag{4.42}$$

$$c_{hf} = \frac{c_f}{\kappa} \left( \beta^{sf} - \alpha\alpha^s \frac{(1+\nu)}{(1-\nu)} \right) \tag{4.43}$$

The transversely isotropic porothemoelastic analytical solution for the inclined borehole problem is presented in the next section. The corresponding isotropic solution for the inclined borehole is included in Appendix C.

## 4.5 Inclined Borehole Problem

It is assumed that an infinitely long borehole is drilled perpendicular to the isotropic plane of a transversely isotropic poroelastic formation. The borehole is inclined and its axis deviated from the in-situ stress orientation. A schematic of the inclined borehole is shown in Figure 3.1. The formation, described using a Cartesian coordinate system

$x'y'z'$, is characterized by in-situ stresses $S_{x'}$, $S_{y'}$, and $S_{z'}$, virgin pore pressure $p_o$, and formation temperature $T_o$. The borehole deviation is measured by two angles $\varphi_z$ and $\varphi_y$, which are the inclination and azimuth angles respectively. A local coordinate system is chosen to represent the borehole in which the $z$-axis is assumed to coincide with the borehole axis. The far-field in-situ stresses in the $x'y'z'$ coordinate system are transformed to the local $xyz$ coordinate system via a transformation matrix (*Cui et al.*, 1997). In the local coordinate system, the borehole is subject to normal as well as shear components of stress given as $S_x$, $S_y$, $S_z$, $S_{xy}$, $S_{xz}$, and $S_{yz}$ as shown in Figure 3.3.

The boundary conditions for the inclined borehole problem, discussed in Chapter 3, are specialized for the porothermoelastic problem. The boundary conditions of the problem at the far field, $r \to \infty$, are as follows

$$\sigma_{xx} = -S_x; \quad \sigma_{yy} = -S_y; \quad \sigma_{zz} = -S_z; \tag{4.44}$$

$$\tau_{xy} = -S_{xy}; \quad \tau_{yz} = -S_{yz}; \quad \tau_{xz} = -S_{xz}; \tag{4.45}$$

$$p = p_o; \qquad T = T_o \tag{4.46}$$

At the borehole wall, $r = R$,

$$\sigma_{rr} = -p_w H(t); \quad \tau_{r\theta} = \tau_{rz} = 0; \tag{4.47}$$

$$L_1 p + L_2 q_r = L_1 p_w H(t) + L_2 q_i H(t) \tag{4.48}$$

$$T = T_w H(t) \tag{4.49}$$

where $p_w$ is the wellbore pressure, $T_w$ is the wellbore fluid temperature, and $H(t)$ is the Heaviside unit step function. $L_1$ and $L_2$ are constants which take values 0 or 1. For $L_1 = 1$ and $L_2 = 0$, $p = p_w$ results in the permeable boundary condition model. Similarly for $L_1 = 0$ and $L_2 = 1$, $q_r = q_i = 0$ gives the impermeable boundary condition model.

The three sub-problems in the decomposition of the inclined borehole problem are identified as the modified plane strain problem, the uniaxial problem and the anti-plane

problem (*Cui et al.*, 1997). The modified plane strain problem accounts for the in-plane normal and shear stresses and the pore pressure and temperature perturbations and shows full coupling of the fluid and heat diffusion processes with the deformation. The other two problems, are again, purely elastic since they do not trigger fluid or heat diffusion.

The boundary conditions for the three problems are given as follows

**Problem 1:** At far field ( $r \rightarrow \infty$)

$$\sigma_{xx} = -S_x; \quad \sigma_{yy} = -S_y; \quad \tau_{xy} = -S_{xy} \tag{4.50}$$

$$\sigma_{zz} = -\nu^{'}(S_x + S_y) - (\alpha^{'} - 2\nu^{'}\alpha)p_o - (\beta^{s'} - 2\nu^{'}\beta^{s})T_o \tag{4.51}$$

$$\tau_{yz} = \tau_{xz} = 0; \qquad p = p_o; \qquad T = T_o \tag{4.52}$$

At the borehole wall ($r = R$)

$$\sigma_{rr} = -p_w H(t); \qquad T = T_w H(t) \tag{4.53}$$

$$L_1 p + L_2 q_r = L_1 p_w H(t) + L_2 q_i H(t) \tag{4.54}$$

**Problem 2:** At far field ( $r \rightarrow \infty$)

$$\sigma_{zz} = -S_z + [\nu^{'}(S_x + S_y) + (\alpha^{'} - 2\nu^{'}\alpha)p_o + (\beta^{s'} - 2\nu^{'}\beta^{s})T_o] \tag{4.55}$$

$$\sigma_{xx} = \sigma_{yy} = \tau_{xy} = \tau_{yz} = \tau_{xz} = p = T = 0 \tag{4.56}$$

At borehole wall ($r = R$)

$$\sigma_{rr} = \tau_{r\theta} = \tau_{rz} = p = T = 0 \tag{4.57}$$

**Problem 3:** At far field ( $r \rightarrow \infty$)

$$\sigma_{xx} = \sigma_{yy} = \sigma_{zz} = \tau_{xy} = p = T = 0 \tag{4.58}$$

$$\tau_{xy} = -S_{xy}; \quad \tau_{yz} = -S_{yz} \tag{4.59}$$

At the borehole wall ($r = R$)

$$\sigma_{rr} = \tau_{r\theta} = \tau_{rz} = p = T = 0 \tag{4.60}$$

The complete solution for the inclined borehole problem in a transversely isotropic medium is given by equations (3.54) - (3.61) setting $\varpi_1 = 1, \varpi_2 = 1, \varpi_3 = 0$.

### 4.5.1 Permeable Boundary Condition Model

Assuming a permeable boundary condition at the borehole wall, the boundary conditions for the three contributing loading cases at the borehole wall ($r = R$) are given as follows

**Case 1:**

$$\sigma_{rr}^{(1)} = P_o - p_w \tag{4.61}$$

$$\sigma_{r\theta}^{(1)} = p^{(1)} = T^{(1)} = 0 \tag{4.62}$$

**Case 2:**

$$\sigma_{rr}^{(2)} = \sigma_{r\theta}^{(2)} = 0 \tag{4.63}$$

$$p^{(2)} = (p_w - p_o) \tag{4.64}$$

$$T^{(2)} = (T_w - T_o) \tag{4.65}$$

**Case 3:**

$$\sigma_{rr}^{(3)} = -S_o \cos 2(\theta - \theta_r) \tag{4.66}$$

$$\sigma_{r\theta}^{(3)} = S_o \sin 2(\theta - \theta_r) \tag{4.67}$$

$$p^{(3)} = T^{(3)} = 0 \tag{4.68}$$

where $\theta_r$ is given by equation (3.35), $P_o$ and $S_o$ are given by equation (3.41). The expressions for $\sigma_{rr}^{(1)}$, $\sigma_{rr}^{(2)}$, $\sigma_{rr}^{(3)}$, $\sigma_{\theta\theta}^{(1)}$, $\sigma_{\theta\theta}^{(2)}$, $\sigma_{\theta\theta}^{(3)}$, $\sigma_{r\theta}^{(3)}$, $p^{(2)}$, $p^{(3)}$, and $T^{(2)}$ are obtained as follows (*Cui et al.*, 1997; *Carslaw and Jaegar*, 1959)

**Solutions for Case 1:**

Case 1 results in only hydrostatic stresses with no effect on the pressure and temperature fields. The solution for $\sigma_{rr}^{(1)}$ and $\sigma_{\theta\theta}^{(1)}$ is purely elastic and is given by equations (B.1) - (B.2) in Appendix B.

**Solutions for Case 2:**

Case 2 includes a perturbation of the temperature and pore pressure fields. Solutions are obtained in the Laplace domain and inverted to the time domain using the Stehfest algorithm (*Stehfest*, 1970; *Davies and Martin*, 1970). Solution for the temperature field is first obtained by solving the heat diffusion equation (4.26) and is given as follows

$$s\tilde{T}^{(2)} = (T_w - T_o)\Phi(\xi_h) \tag{4.69}$$

where $\xi_h = \sqrt{s/c_h}$ and $\Phi(x)$ is a function given by equation (B.8). Expressions for the pore pressure field are obtained solving the pore pressure diffusion equation (4.30). Equation (4.30) is non-homogeneous, and solution is obtained as a summation of the homogeneous and particular solutions and given as

$$s\tilde{p}^{(2)} = F_2\Phi(\xi_f) + F_3\Phi(\xi_h) \tag{4.70}$$

where $\xi_f = \sqrt{s/c_f}$ and $F_2$ and $F_3$ are coefficients given by

$$F_2 = \left[(p_w - p_o) - \left(\frac{c_{hf}}{(1 - c_f/c_h)}\right)(T_w - T_o)\right] \tag{4.71}$$

$$F_3 = \left(\frac{c_{hf}}{(1 - c_f/c_h)}\right)(T_w - T_o) \tag{4.72}$$

Expressions for the stress fields are obtained using the constitutive relations. The expressions for the radial and tangential stresses are given as ($\sigma_{rr}^{(2)}$ and $\sigma_{\theta\theta}^{(2)}$) are obtained

as

$$s\tilde{\sigma}_{rr}^{(2)} = \alpha\left(1 - \frac{M_{12}}{M_{11}}\right)\{F_2\Psi(\xi_f) + F_3\Psi(\xi_h)\}$$
$$+\beta^s\left(1 - \frac{M_{12}}{M_{11}}\right)\{(T_w - T_o)\Psi(\xi_h)\} \tag{4.73}$$
$$s\tilde{\sigma}_{\theta\theta}^{(2)} = -\alpha\left(1 - \frac{M_{12}}{M_{11}}\right)\{F_2\Omega(\xi_f) + F_3\Omega(\xi_h)\}$$
$$-\beta^s\left(1 - \frac{M_{12}}{M_{11}}\right)\{(T_w - T_o)\Omega(\xi_h)\} \tag{4.74}$$

where the functions $\Psi(x)$ and $\Omega(x)$ are given by equations (B.9) and (B.10) in Appendix B.

**Solutions for Case 3:**

Case 3 is characterized by an asymmetric loading and a trivial temperature field. Solutions for $\sigma_{rr}^{(3)}$, $\sigma_{\theta\theta}^{(3)}$, $\sigma_{r\theta}^{(3)}$, $p^{(3)}$ are the same as that for the transversely isotropic permeable poroelastic case and are given by equations (B.11) - (B.22) in Appendix B.

### 4.5.2 Impermeable Boundary Condition Model

Assuming an impermeable boundary condition at the borehole wall, the boundary conditions for the three contributing loading cases at the borehole wall ($r = R$) are given as follows

**Case1:**

$$\sigma_{rr}^{(1)} = P_o - p_w \tag{4.75}$$
$$\sigma_{r\theta}^{(1)} = q^{(1)} = T^{(1)} = 0 \tag{4.76}$$

**Case 2:**

$$\sigma_{rr}^{(2)} = \sigma_{r\theta}^{(2)} = q^{(2)} = 0 \tag{4.77}$$
$$T^{(2)} = (T_w - T_o) \tag{4.78}$$

**Case 3:**

$$\sigma_{rr}^{(3)} = -S_o \cos 2(\theta - \theta_r) \tag{4.79}$$

$$\sigma_{r\theta}^{(3)} = S_o \sin 2(\theta - \theta_r) \tag{4.80}$$

$$q^{(3)} = T^{(3)} = 0 \tag{4.81}$$

**Solutions for Case 1:**

Case 1 results in only hydrostatic stresses with no effect on the pressure and temperature fields. The solution for $\sigma_{rr}^{(1)}$ and $\sigma_{\theta\theta}^{(1)}$ is purely elastic and is given by equations (B.1) - (B.2) in Appendix B.

**Solutions for Case 2:**

Case 2 is characterized by a temperature perturbation and a no flux condition. The solution is time-dependent and is obtained in the Laplace domain and inverted to the time-domain using the Stehfest algorithm (*Stehfest*, 1970; *Davies and Martin*, 1979). As before, the expressions for the temperature field are obtained solving the heat diffusion equation (4.26). The solution is the same as obtained for the permeable boundary condition model and is given by

$$s\tilde{T}^{(2)} = (T_w - T_o)\Phi(\xi_h) \tag{4.82}$$

Expression for the pore pressure distribution is obtained solving the diffusion equation (4.30). However, since the boundary condition is imposed on the flux, Darcy's law is used to evaluate the constants in the resulting solution. The expression for the pore pressure field is given as

$$s\tilde{p}^{(2)} = F_3 \left\{ -\frac{\xi_h}{\xi_f} \left[ \frac{\mathrm{K}_1(\xi_h R)}{\mathrm{K}_0(\xi_h R)} \right] \left[ \frac{\mathrm{K}_0(\xi_f r)}{\mathrm{K}_1(\xi_f R)} \right] + \Phi(\xi_h) \right\} \tag{4.83}$$

The radial and tangential stress are obtained as

$$s\bar{\sigma}_{rr}^{(2)} = \alpha\left(1-\frac{M_{12}}{M_{11}}\right)F_3\left\{\left[\frac{\xi_h}{\xi_f}\frac{1}{\xi_f r}\frac{\mathrm{K}_1(\xi_h R)}{\mathrm{K}_0(\xi_h R)}\right]\left[\frac{R}{r}-\frac{\mathrm{K}_1(\xi_f r)}{\mathrm{K}_1(\xi_f R)}\right]\right.$$
$$\left.+\left[\frac{1}{\xi_h r}\frac{\mathrm{K}_1(\xi_h R)}{\mathrm{K}_0(\xi_h R)}\left(1-\frac{R}{r}\right)\right]\right\}$$
$$+\beta^s\left(1-\frac{M_{12}}{M_{11}}\right)(T_w-T_o)\left\{\frac{1}{\xi_h r}\frac{\mathrm{K}_1(\xi_h R)}{\mathrm{K}_0(\xi_h R)}\left(1-\frac{R}{r}\right)\right\} \tag{4.84}$$

$$s\bar{\sigma}_{\theta\theta}^{(2)} = -\alpha\left(1-\frac{M_{12}}{M_{11}}\right)F_3\left\{\left[\frac{\xi_h}{\xi_f}\frac{\mathrm{K}_1(\xi_h R)}{\mathrm{K}_0(\xi_h R)}\right]\left[\frac{1}{\xi_f r}\frac{R}{r}-\frac{1}{\xi_f r}\frac{\mathrm{K}_1(\xi_f r)}{\mathrm{K}_1(\xi_f R)}-\frac{\mathrm{K}_0(\xi_f r)}{\mathrm{K}_1(\xi_f R)}\right]\right.$$
$$\left.+\left[\frac{1}{\xi_h r}\frac{\mathrm{K}_1(\xi_h r)}{\mathrm{K}_0(\xi_h R)}-\frac{R}{r}\frac{1}{\xi_h r}\frac{\mathrm{K}_1(\xi_h R)}{\mathrm{K}_0(\xi_h R)}+\Phi(\xi_h)\right]\right\}$$
$$-\beta^s\left(1-\frac{M_{12}}{M_{11}}\right)(T_w-T_o)\left\{\frac{1}{\xi_h r}\frac{\mathrm{K}_1(\xi_h r)}{\mathrm{K}_0(\xi_h R)}-\frac{R}{r}\frac{1}{\xi_h r}\frac{\mathrm{K}_1(\xi_h R)}{\mathrm{K}_0(\xi_h R)}+\Phi(\xi_h)\right\} \tag{4.85}$$

**Solutions for Case 3:**

Case 3 is characterized by an asymmetric loading and a trivial temperature field. Solutions for $\sigma_{rr}^{(3)}$, $\sigma_{\theta\theta}^{(3)}$, $\sigma_{r\theta}^{(3)}$, $p^{(3)}$ are the same as that for the transversely isotropic impermeable poroelastic case and are given by equations (B.9) - (B.12) and (B.23) - (B.30) in Appendix B.

## 4.6 Anisotropic Porothermomechanical Implications on Borehole Stability

The solutions developed in the previous section are applied to assess the effect of the anisotropic parameters on the stress and pore pressure distribution in the vicinity of the borehole. The observations are extended to evaluate the implications of the same on borehole stability. The borehole orientation is given by two angles as shown in Fig 3.1 which are the azimuth, $\varphi_y = 30°$, and the inclination $\varphi_z = 60°$. The formation surrounding the borehole is transversely isotropic with its plane of isotropy perpendicular to the borehole axis. Comparisons with the corresponding isotropic porothermoelastic

and the isotropic poroelastic cases are made to highlight the anisotropy effects on the results obtained.

A borehole of radius 0.1 m is assumed to be drilled in the formation characterized by in-situ stress and pore pressure gradients given as $S_{x'} = 25$ kPa/m, $S_{y'} = 22$ kPa/m, $S_{z'} = 29$ kPa/m, $p_o = 9.8$ kPa/m. A section at a depth of 1000 m is analyzed where the formation temperature is assumed to be $T_o = 125°$ C. The borehole is assumed to be filled with a fluid maintained at a constant pressure given by $p_w = 12.0$ MPa . The material properties used in the analysis are given in Table 4.1. The degree of anisotropy of material parameters is modeled by selecting appropriate values for the ratios $E/E'$, $\nu/\nu'$ and $\alpha^s/\alpha^{s'}$. Numerical results are presented in Figs 4.1 - 4.16, in which negative values of stresses are presented indicating that compression is denoted positive. In addition, only results of from the permeable boumdary condition model are studied in the analysis.

Table 4.1: Material Parameters for the Porothermoelastic analysiss

| Parameter | Units | Value |
|---|---|---|
| Elastic Modulus ($E$) | GPa | 9.474 |
| Poisson's Ratio ($\nu$) | - | 0.24 |
| Grain Bulk Modulus ($K_s$) | GPa | 27.5 |
| Biot's Modulus ($M$) | GPa | 8.875 |
| Permeability ($k$) | md | $5.0 \times 10^{-5}$ |
| Fluid Viscosity ($\mu$) | MPa.s | $10^{-9}$ |
| Heat Diffusivity.($c_h$) | $m^2$/day | 0.13824 |
| Linear Expansion Coefficient (solid skeleton, $\alpha^s$) | /°C | $6.0 \times 10^{-6}$ |
| Volumetric Expansion Coefficient (fluid, $\alpha^s$) | /°C | $3.0 \times 10^{-4}$ |
| Porosity ($\phi$) | - | 0.14 |

### 4.6.1 Effect of Temperature

The effect of temperature on the pore pressure and stress distributions is examined for the transversely isotropic material and compared with the isotropic case. Only the

anisotropy of thermic coefficients is modeled by fixing ratios for $E/E' = 1$ and $\nu/\nu' = 1$ and varying $\alpha^s/\alpha^{s'}$. The difference between the wellbore fluid and the formation temperature, $\Delta T$, is varied where $\Delta T = T_w - T_o$. All the results shown in this regard are for a short time interval, i.e., $t = 0.001$ day. Figures 4.1 and 4.2 show the pore pressure and the effective radial stress distributions respectively as a function of the radial distance along the $\theta = 90°$ direction. The angle around the borehole, $\theta$, is measured from the direction of the maximum in-plane principal stress obtained after transforming the far-field in-situ stress components to the local borehole coordinate system (*Cui et al.*, 1997). Alternately, the $\theta = 90°$ direction corresponds to direction of the minimum in-plane principal stress. Figure 4.1 shows that the temperature perturbation induces a higher pore pressure close the to borehole wall for the cases where $\Delta T$ is positive or when the wellbore fluid is at a higher temperature than the formation. On the other hand, a negative value of $\Delta T$ results in a reduction of the pore pressure. Also, both effects are more pronounced for the transversely isotropic case. The induced pore pressure (positive or negative) leads to a modification of the effective radial stresses. As presented in Fig 4.2, the effective radial stresses are tensile when the wellbore fluid is at a higher temperature than the formation with the tensile magnitude being higher in the transversely isotropic material. As most rocks have negligible tensile strength, a situation as this one could potentially result in a tensile outburst failure, also known as spalling. In case of a lower wellbore fluid temperature, the effective radial stresses are compressive in nature. Again the compressive magnitude is higher for the transversely isotropic case. Figure 4.3 shows the effective tangential stress as a function of the radial distance along the $\theta = 0°$ direction. The $\theta = 0°$ direction represents the direction of maximum in-plane principal stress where the effective tangential stress would attain its minimum value around the wellbore. As seen from Fig 4.3, higher effective tangential stresses are observed when the wellbore fluid has a higher temperature. With a lower

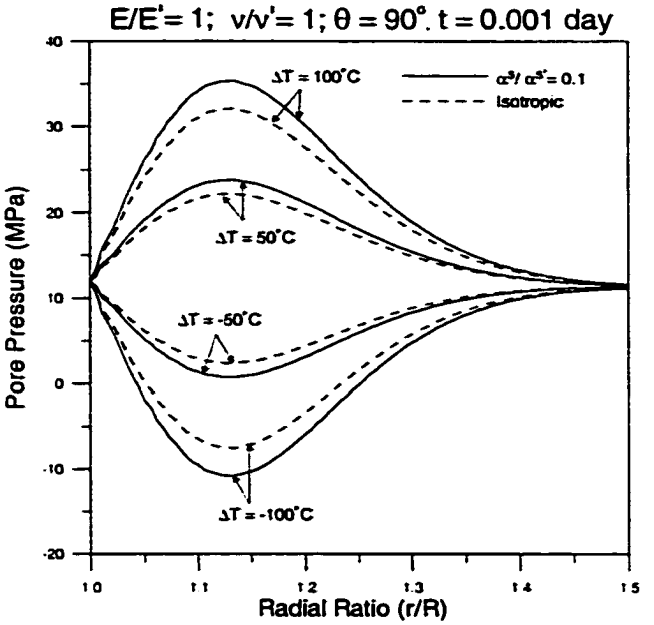


Figure 4.1: Pore pressure varying with $r/R$ along $\theta = 90°$ at $t = 0.001$ day for different values of $\Delta T$

wellbore fluid temperature, the effective tangential stresses are reduced. In general, increase/reduction in the pore pressure and stress distributions due to the temperature difference, is more prevailing for the transversely isotropic case.

### 4.6.2 Effect of Anisotropy of Thermic Coefficients

To evaluate effect of the anisotropic nature of the thermic coefficients on the stress and pore pressure distributions, we fix the ratios for $E/E' = 1$ and $\nu/\nu' = 1$ and vary $\alpha^s/\alpha^{s'}$. In other words, we assume that material anisotropy is only because of a different $\alpha^{s'}$ value in the transverse direction. Notice that the above choice results only in the variation of values for the thermic coefficients $\beta^s$, $\beta^{s'}$ and $\beta^{sf}$ with all other material coefficients ($M_{ijkl}$'s, $\alpha$ and $\alpha'$) assuming their values as in the isotropic case. Data given in Table 1 is used for the analysis. The temperature difference between the wellbore fluid and the formation is assumed to be $\Delta T = 50°C$. Again, results are shown for a short time

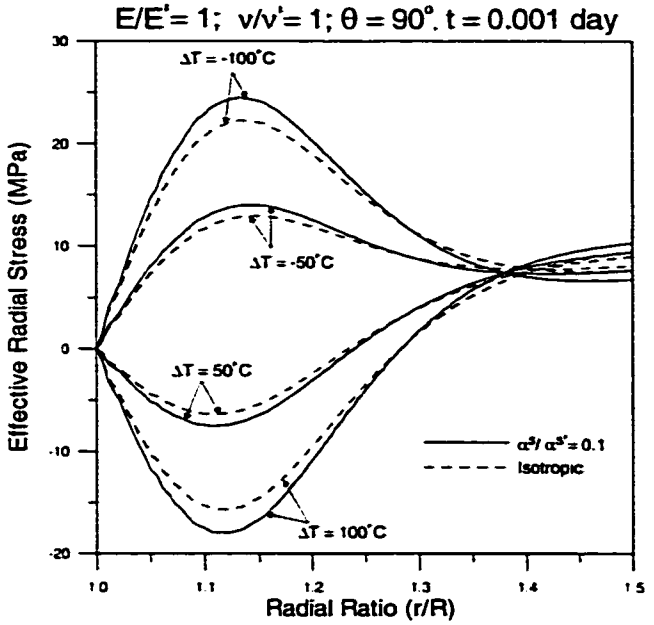


Figure 4.2: Effective radial stress varying with $r/R$ along $\theta = 90°$ at $t = 0.001$ day for different values of $\Delta T$

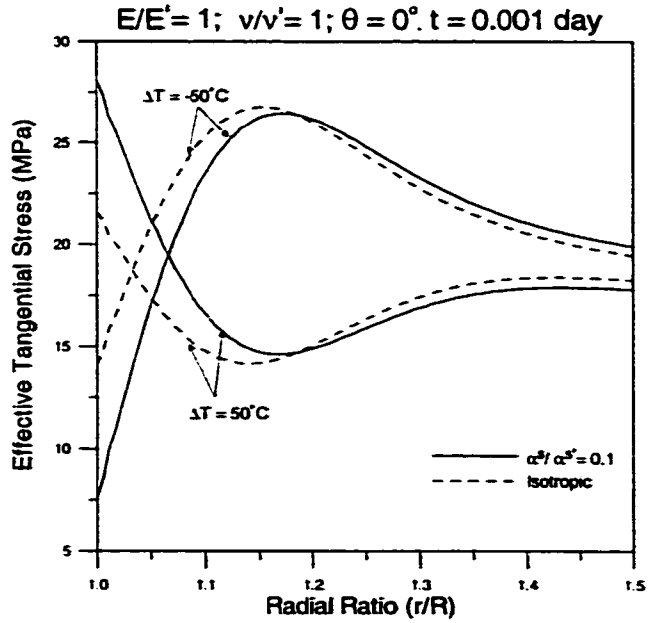


Figure 4.3: Effective tangential stress varying with $r/R$ along $\theta = 90°$ at $t = 0.001$ day for different values of $\Delta T$

interval, i.e., $t = 0.001$ day.

Figures 4.4 and 4.5 show the pore pressure profile as a function of the radial distance along the $\theta = 90°$ direction. In Fig 4.4 results are shown for lower thermic coefficient ratios $\alpha^s/\alpha^{sf} = 0.1, 0.5$ along with the corresponding isotropic porothermoelastic and poroelastic cases. On the other hand, Fig 4.5 show results corresponding for higher values of thermic coefficient ratios i.e., $\alpha^s/\alpha^{sf} = 2.0, 5.0$. Firstly, the pore pressure profile in the poroelastic case exhibits the well known Mandel-Cryer effect. In addition, all the porothermoelastic cases, show an increased value of the pore pressure close to the region near the borehole wall. As discussed earlier, this increase is a direct consequence of the temperature perturbation resulting in an induced pore pressure. As seen from Fig 4.4, the magnitude of this increase is higher for lower values of the $\alpha^s/\alpha^{sf}$ ratio indicating that for higher thermal expansion coefficients in the transverse direction the induced pore pressure would be larger. In contrast, the magnitude of the increase is much lower for the higher $\alpha^s/\alpha^{sf}$ ratios as can be seen from Fig 4.5.

Figures 4.6 and 4.7 show, respectively, the effective radial and tangential stress profiles for the two lower values of the thermic coefficient ratios i.e., $\alpha^s/\alpha^{sf} = 0.1, 0.5$. Tensile effective radial stresses are observed in vicinity of the borehole which is a natural consequence of the high induced pore pressure as discussed above. Again as observed in the earlier cases, the tensile magnitude of the stress is more predominant for the case with lower $\alpha^s/\alpha^{sf}$ ratio. In contrast, lower $\alpha^s/\alpha^{sf}$ ratios result in more compressive tangential stresses as can be seen from Fig 4.7. However, at a short distance inside the formation, the effective tangential stresses are lowered which may be again attributed to the effect of the induced pore pressure. The aforementioned observations can be directly linked to the effect of the $\alpha^s/\alpha^{sf}$ ratios on values of $\beta^s$, $\beta^{sf}$ and $\beta^{sf}$. A simple calculation shows that, for lower values of the $\alpha^s/\alpha^{sf}$ ratio ($\alpha^s/\alpha^{sf} < 1.0$), the thermic coefficients $\beta^s$, $\beta^{sf}$ and $\beta^{sf}$ assume higher values. As a result, a higher magnitude of the pore pressure is

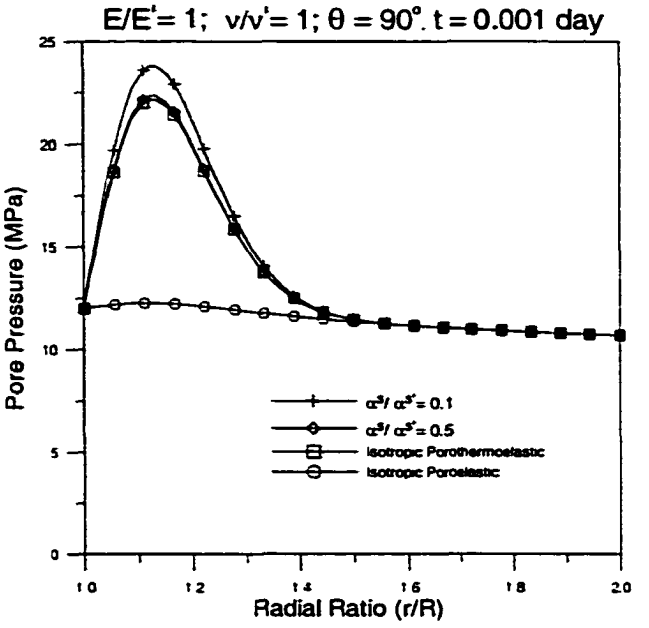


Figure 4.4: Pore pressure varying with $r/R$ along $\theta = 90°$ for $\alpha^s/\alpha^{s\prime} = 0.1, 0.5$ at $t = 0.001$ day

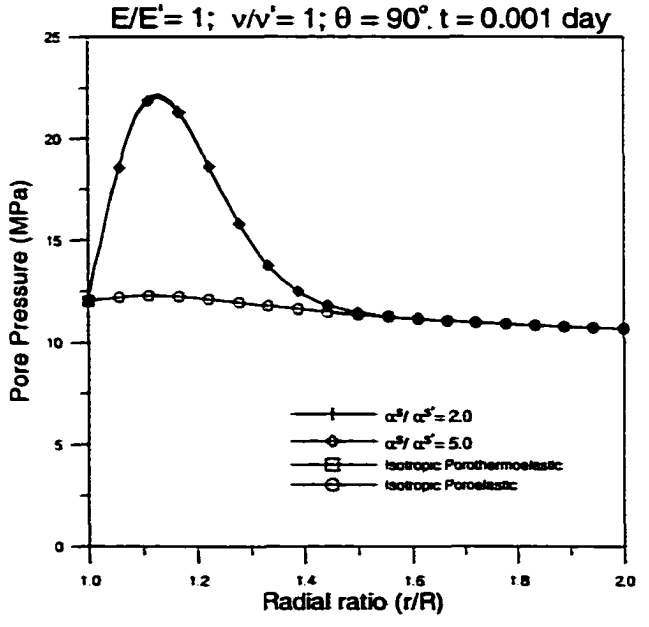


Figure 4.5: Pore pressure varying with $r/R$ along $\theta = 90°$ for $\alpha^s/\alpha^{s\prime} = 2.0, 5.0$ at $t = 0.001$ day

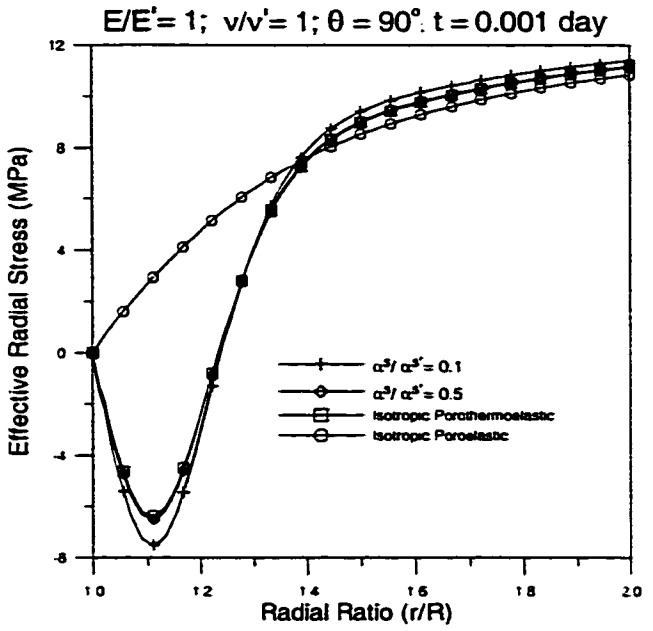


Figure 4.6: Effective radial stress varyings with $r/R$ along $\theta = 90°$ and at $t = 0.001$ day

induced and the total stresses are more compressive. On the other hand, higher values of the $\alpha^s/\alpha^{s\prime}$ ratios ($\alpha^s/\alpha^{s\prime} > 1.0$) have little effect on the thermic coefficient values resulting in a near-isotropic behavior.Next we present results in the form of stress clouds to illustrate the shear failure potential. The 'stress clouds' represent the amalgamation of the effective radial, tangential and shear stresses presented in the $\sqrt{J_2} - S_p$ space where, $S_p$ and$\sqrt{J_2}$ are given by equations (3.70) and (3.71) respectively. The stress cloud is obtained by evaluating pairs of ($S_p$, $\sqrt{J_2}$) by varying the angle around the borehole, $\theta$ for a fixed radial distance and time (*Cui et al.*, 1997). The stress cloud concept is used in conjunction with the Drucker-Prager criterion for a shear failure analysis. The Drucker-Prager criterion given by equation (3.69). Values of $A = 0.1$ and $D = 14$ MPa are chosen to represent the failure envelope.

Figure 4.9 shows the stress clouds at the borehole wall, i.e. $r/R = 1.0$. It is seen that, for a lower $\alpha^s/\alpha^{s\prime}$ ratio the stress cloud moves to the right and higher pushing it

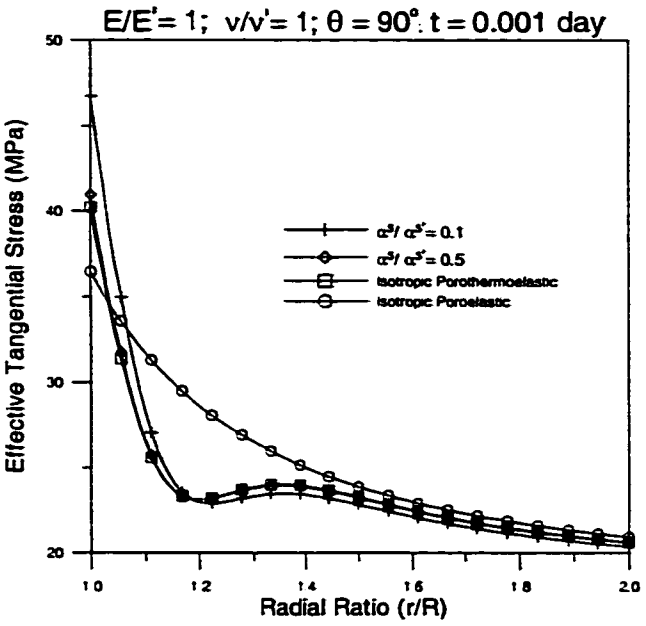


Figure 4.7: Effective tangential stress varying with $r/R$ along $\theta = 90°$ and at $t = 0.001$ day

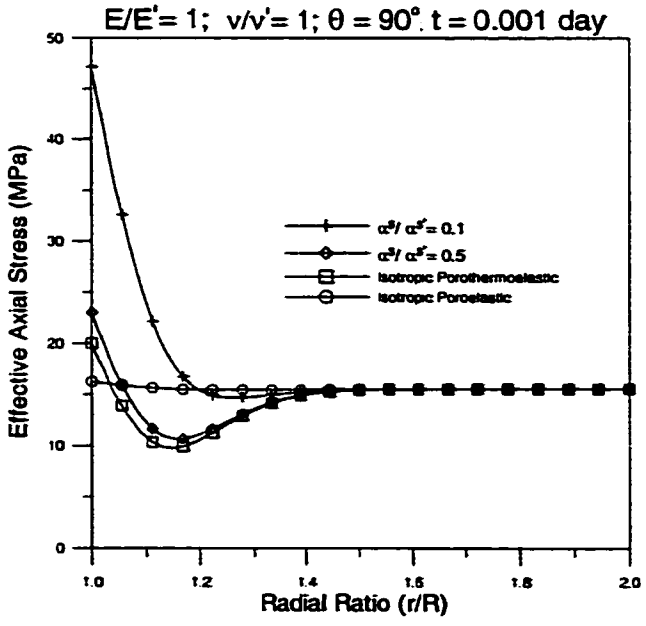


Figure 4.8: Effective axial stress varying with $r/R$ along $\theta = 90°$ and at $t = 0.001$ day

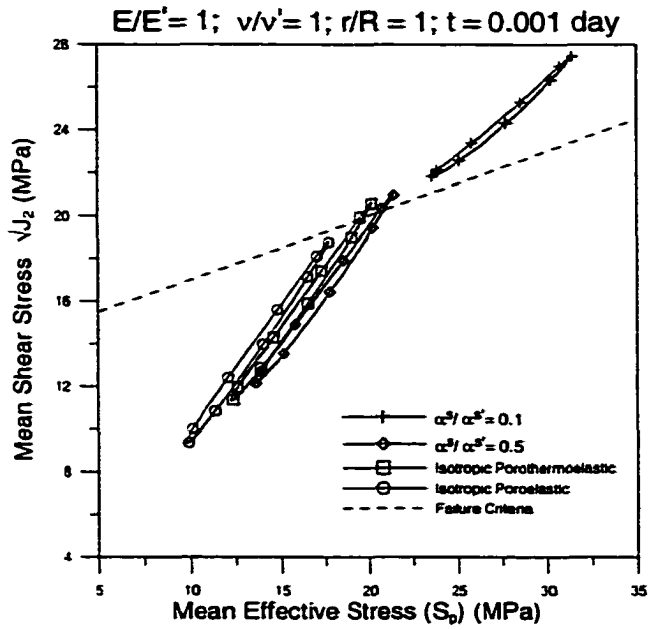


Figure 4.9: Stress clouds at $r/R = 1$ and $t = 0.001$ day

outside the failure envelope. At the borehole wall, the effective radial stresses are always zero. However there is an increase in the effective tangential stress and the effective axial stress for the lower $\alpha^s/\alpha^{s\prime}$ ratio. This results in a higher difference between the stresses which causes the mean shear stress, $\sqrt{J_2}$, to increase. With higher effective tangential and axial stresses, the mean effective stress, $S_p$, is naturally higher. Hence the stress cloud moves higher and to the right for the lower $\alpha^s/\alpha^{s\prime}$ ratio. Figure 4.10 shows the stress clouds at a fractional distance inside the formation given by. $r/R = 1.1$. At this location, the effective radial stresses are tensile (Fig 4.6), whereas, a reduction in the effective tangential and axial stresses (Figs 4.7 and 4.8) is seen due to effect of the induced pore pressure as explained earlier. However, the relative magnitudes of the stresses are still quite different for the lower $\alpha^s/\alpha^{s\prime}$ ratio resulting in a cloud which is partially outside the failure envelope. Again, Figs 4.9 and 4.10 show that higher thermal expansion coefficients in the transverse direction lead to a higher shear failure potential.

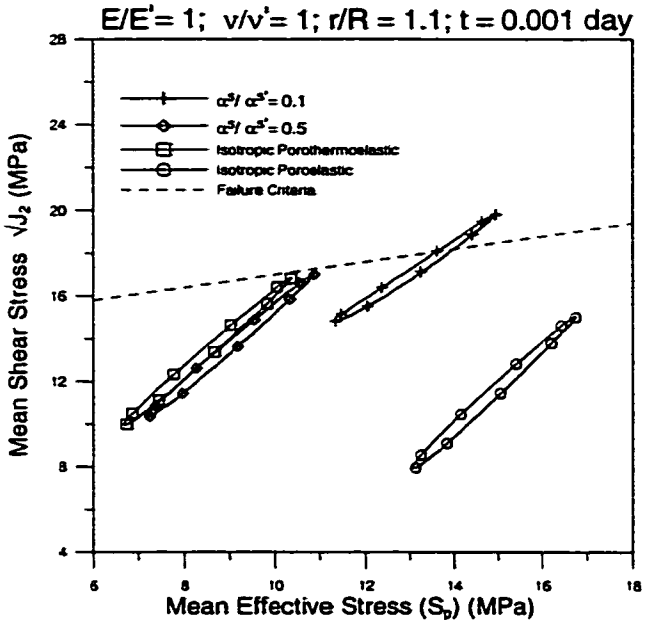


Figure 4.10: Stress clouds at $r/R = 1.1$ and $t = 0.001$ day

In addition to the spalling and shear failures, the borehole can also fail under the fracturing mode which is governed by the minimum effective tangential stress. As the wellbore pressure is increased progressively, the effective tangential stress reduces until a threshold wellbore pressure is reached where some part of the tangential stress goes into the tensile zone causing the borehole to fracture. Figure 4.11 shows the variation of the effective tangential stress as a function of the angle around the borehole, $\theta$, at the borehole wall. The tangential stress is more compressive for lower values of the $\alpha^s/\alpha^{s\prime}$ ratio. A higher wellbore pressure would thus be required to produce tensile zones indicating that a higher thermal coefficient in the transverse direction results in decreasing the fracturing failure potential.

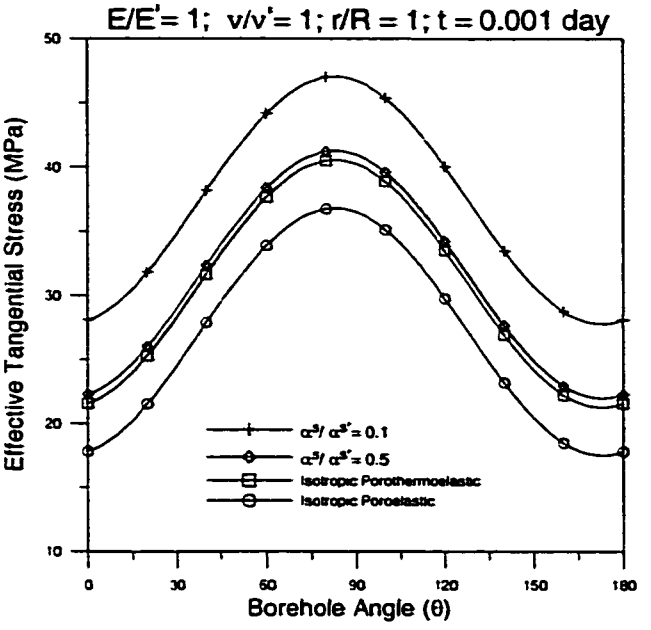


Figure 4.11: Effective tangential stress varying with $\theta$ at $r/R = 1$ and $t = 0.001$ day

### 4.6.3 Time-dependent Effects

It is interesting to show the behavior of stresses and pore pressure as time progresses. In Figs 4.12 - 4.14 we show their variation with radial distance, along the $\theta = 90°$ direction for three time intervals, $t = 0.001$, 0.01 and 0.1 day. Also results are shown for two values of the thermal expansion coefficient ratios, i.e., $\alpha^s/\alpha^{s'} = 0.1$ and 1.0. It is seen from Fig 4.12 that the magnitude of the induced pore pressure progressively decreases with time. In addition, the location of the maximum pore pressure gradually moves into the formation and away from the borehole wall. The magnitude of the pore pressure for the lower $\alpha^s/\alpha^{s'}$ is, however, always higher. It is seen from Fig 4.13 that with the passage of time effective radial stresses in the vicinity of the borehole change from tensile to compressive in nature as a result of the diffusion process. Correspondingly, as time progresses the effective tangential stresses become more compressive as can be seen from Fig 4.14. It may be expected that as the induced pore pressure front progresses into

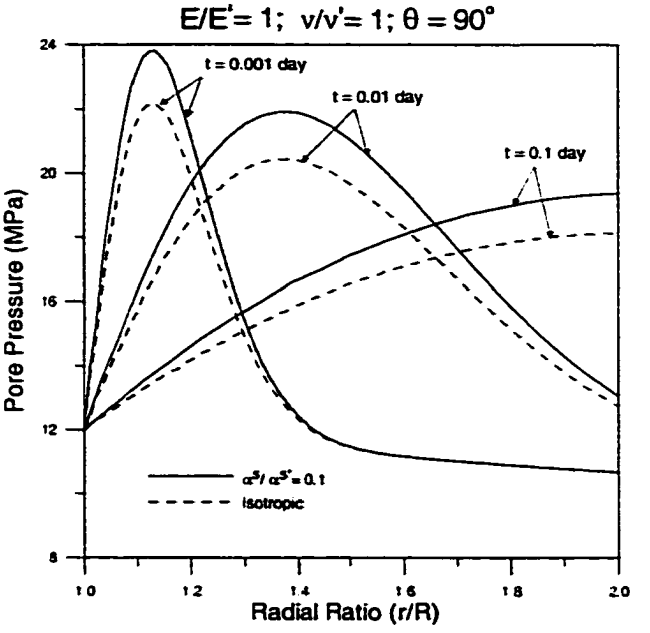


Figure 4.12: Pore pressure varying with $r/R$ for $\alpha_m/\alpha_m^{'} = 0.1, 1.0$ for $t = 0.001$, 0.01 and 0.1 day

the formation, it results in lowering the effective stresses indicating that the potential shear failure zone gradually shifts into the formation. However, this zone is restricted to the small neighborhood around the wellbore wall due to the increase in the compressive magnitudes of the stresses with time.

### 4.6.4 Combined Anisotropic Effects

The combined effect of the anisotropy of elastic parameters and the thermal expansion coefficient ratios is analyzed in Figs 4.15 - 4.17. The pore pressure profiles for four sets of values of the $E/E'$, $\nu/\nu'$ and $\alpha^s/\alpha^{s'}$ ratios are shown in Fig 4.15. It can be seen that for the two curves where $E/E' = 2$, $\nu/\nu' = 2$, the pore pressure induced is higher for the case when $\alpha^s/\alpha^{s'} = 0.1$ as compared to that for the $\alpha^s/\alpha^{s'} = 0.5$. In contrast, when $E/E' = 0.5$, $\nu/\nu' = 0.5$, the pore pressure is lower for the case where $\alpha^s/\alpha^{s'} = 0.1$ than for $\alpha^s/\alpha^{s'} = 0.5$. A similar observation is made about the tensile nature of the effective

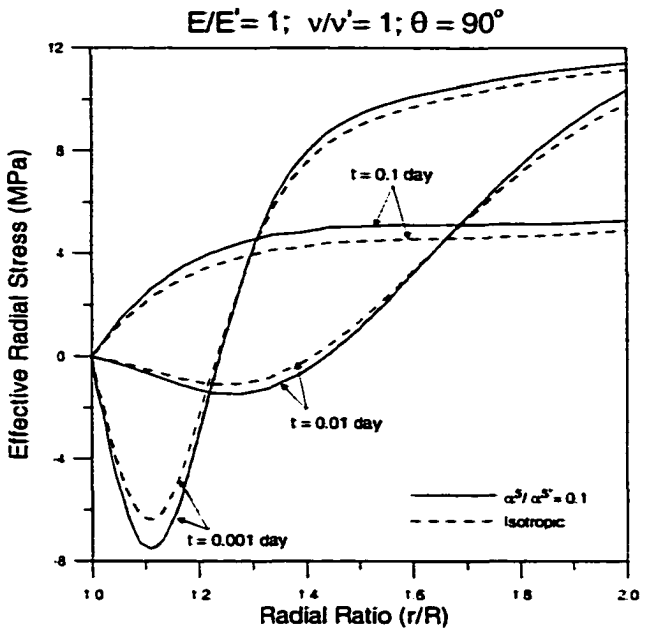


Figure 4.13: Effective radial stress varying with $r/R$ for $\alpha_m/\alpha_m^{'} = 0.1, 1.0$ for $t = 0.001$, 0.01 and 0.1 day

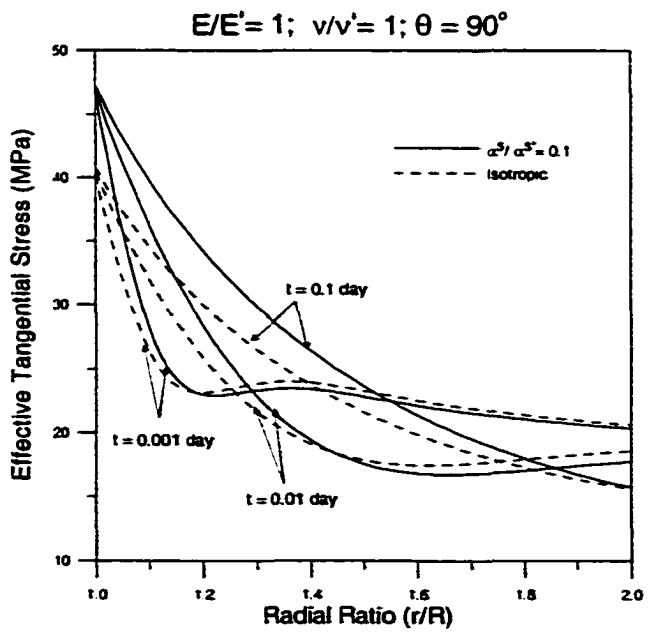


Figure 4.14: Effective tangential stress varying with $r/R$ for $\alpha_m/\alpha_m^{'} = 0.1, 1.0$ for $t =$ 0.001, 0.01 and 0.1 day

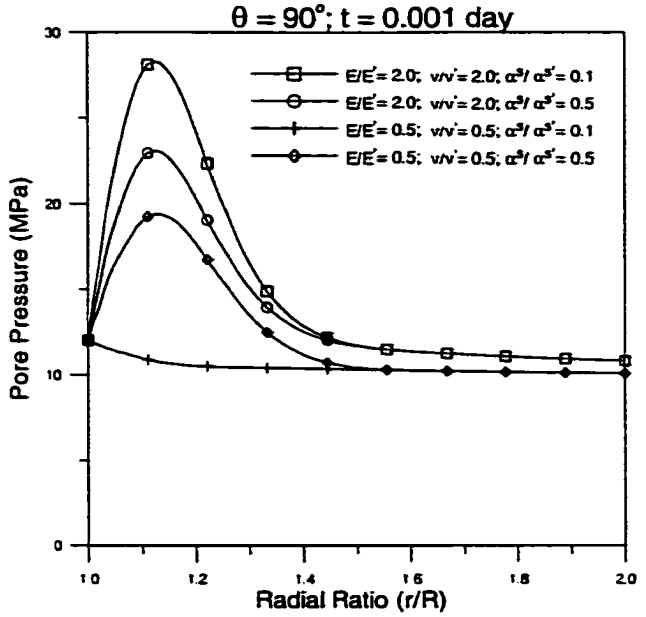


Figure 4.15: Pore pressure varying with $r/R$ at $t = 0.001$ day for different combinations of $E/E'$, $\nu/\nu'$ and $\alpha_m/\alpha_m'$

radial stresses, shown in Fig 4.16. On the other hand, the effective tangential stress shown in Fig 4.17 is most compressive for lower ratios of $E/E'$, $\nu/\nu'$ and $\alpha^s/\alpha^{s'}$. The combined effect of the anisotropy of both the material and thermal expansion coefficients results in complex behavior patterns. A consistent inference may be difficult to draw which relates the change in values for these ratios to behavior of the stresses and pore pressure. However, noting that a change in these ratios results in a corresponding modification of the values for $\beta^s$, $\beta^{s'}$and $\beta^{sf}$ a fair prediction is plausible.

## 4.7 Summary

A porothermoelastic formulation for general anisotropy and specialized for transversely isotropic media along with the solution for the inclined borehole problem has been presented in this chapter. Borehole solutions assuming permeable as well as impermeable

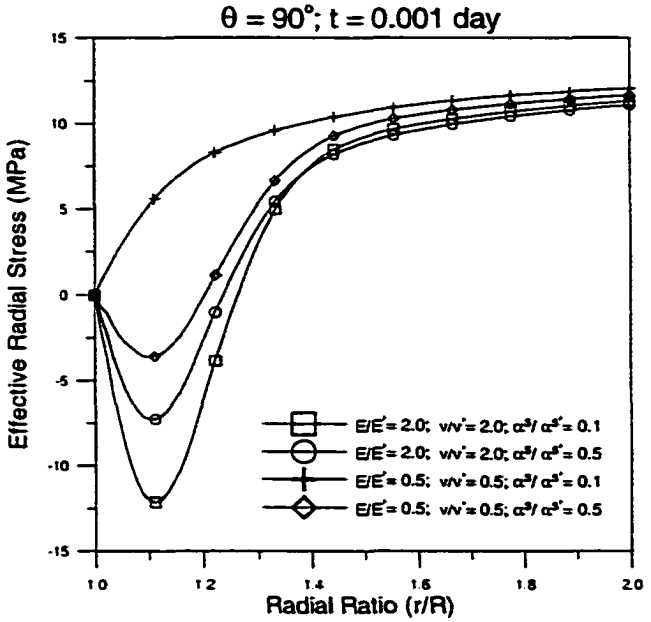


Figure 4.16: Effective radial stress varying with $r/R$ at $t = 0.001$ day for different combinations of $E/E'$, $\nu/\nu'$ and $\alpha_m/\alpha_m'$

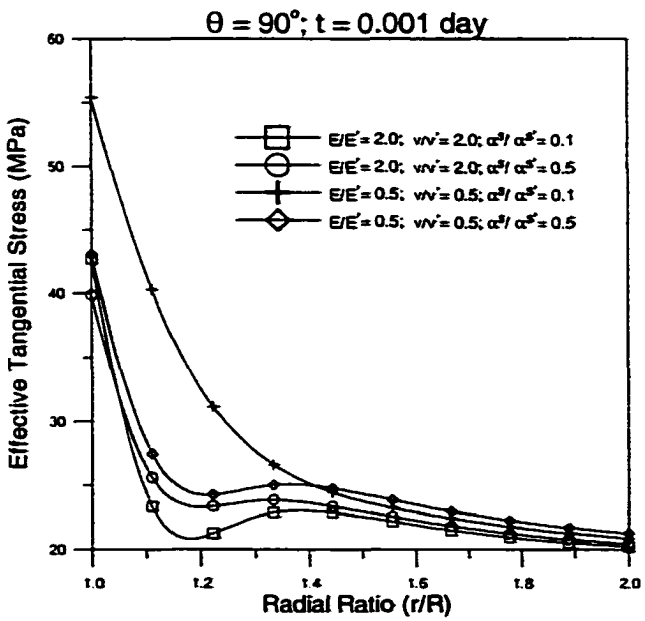


Figure 4.17: Effective tangential stress varying with $r/R$ at $t = 0.001$ day for different combinations of $E/E'$, $\nu/\nu'$ and $\alpha_m/\alpha_m'$

boundary conditions at the borehole wall have been presented. A superposition scheme, involving decomposition of the complex problem along with its boundary conditions into simpler problems which can be solved easily, has been used to arrive upon the solution. A parametric analysis has been presented to study the material anisotropy effect on the stress and pore pressure profiles.

The temperature difference leads to a modification of both, the pore pressure and stress distributions. A higher wellbore fluid temperature results in a higher induced pore pressure whereas a lower temperature of the wellbore fluid results in the opposite. Modification of the pore pressure response has a direct effect on the effective stress distributions in the vicinity of the borehole. The effect of the anisotropy of thermic coefficients has been studied varying the thermal expansion coefficients in the isotropic and transverse directions while keeping the mechanical parameters isotropic. It was found that the effects on the pore pressure and stress profiles are more pronounced when the material has a higher thermal expansion coefficient in the transverse direction. In contrast, the stress and pore pressure responses are more or less comparable to the isotropic case when the thermal expansion coefficients are lower in the transverse direction. The time-dependent variation of the induced pore pressure is characterized by a front which moves into the formation as time progress. In addition, the peak of the induced pore pressure also subsides with the passage of time. The effect of anisotropy of mechanical parameters has been studied varying $E/E'$ and $\nu/\nu'$. It is interesting to note that for ratios of $E/E', \nu/\nu' > 1$, the ratios of the thermal expansion coefficients affect the stress and pore pressure distributions in a manner similar to the case when the mechanical parameters are isotropic. On the other hand, when $E/E', \nu/\nu' < 1$, trend of these results (i.e., effect of $\alpha^s/\alpha^{s'}$) is reversed.

Again, it must be noted that applicability of the analytical solution may seem limited for the case where the isotropic plane is perpendicular to the borehole axis. Neverthe-

less, it serves as a unique tool in both, understanding the underlying phenomena, and validation of numerical analyses in which some of the assumptions may be relaxed subsequently (*Nair et al.*, 2002).

# Chapter 5

# Anisotropic Porochemoelasticity

## 5.1 Introduction

Understanding the nature of physicochemical interactions in porous media and quantifying these effects on their mechanical response has invoked the interest of researchers over the past few years. Indeed, in a chemically active porous system, the interactions that occur at the microscale, result in a modification of flow patterns, pressure distributions and stresses. Such interactions are specifically known to exist in sedimentary and argillaceous rocks such as shales (*Mitchell*, 1993; *Yeung and Mitchell*, 1993). Typically, shales are composed of clay compacted over geological time scales wherein the relative incompressibility of the solid grains and pore fluid along with charged surfaces on the clay constituents make them excellent candidates for exhibiting a fully coupled physicochemical response to technogenic activities. An improper assessment of the magnitude of these effects can result in a design failure of the associated engineering problem.

Of particular interest is the chemical effect on the stress and pore pressure distributions around wellbores in deep drilling projects. The chemical interactions between the formation pore fluid and the wellbore drilling fluid result in an alteration of the pore pressure distribution. Naturally, effective stress distributions are modified with adverse consequences to the stability of boreholes drilled in such formations (*Mody and Hale*, 1993; *van Oort*, 1997).

Shales are highly water-sensitive and swell when brought in contact with aqueous drilling fluids (*Sherwood and Bailey*, 1994). The swelling may also result in a structural weakening followed by a complete disintegration thereby resulting in borehole closure (*Sherwood and Bailey*, 1994). Differences in chemical potentials of the species in the formation pore fluid and wellbore drilling fluid result in the development of a non-equilibrium state which causes the flux of water and ions (*Sherwood*, 1994a, 1994b; *Lomba et al.*, 2000b). Moreover, the low permeability of shales and presence of charged surfaces on the constituent clays contribute to add complexity to the phenomenon. These problems associated with water/shale interaction were averted in the past by use of an oil-based drilling fluid which somewhat simplifies the situation with the oil acting as a barrier to the movement of ions. However, the use of oil-based drilling fluids has raised significant environmental concerns (*Mody and Hale*, 1993).

A wide variety of models have been presented which attempt to quantify the chemical interactions in porous media. In the simplest approximation, the modified pore pressure is evaluated using the concept of a chemical potential and used in estimation of effective stresses following a linear elastic analysis (*Mody and Hale*, 1993). The chemical effects are woven into Biot's theory (*Biot*, 1941) to account for the transient evolution of the hydraulic, chemical and mechanical processes (*Sherwood*, 1993). Sherwood (1993) used the concept of a chemical potential to incorporate the chemical effects within the framework of Biot's theory. This approach, in conjunction with the concept of membrane efficiency, has been applied to evaluate the swelling effects on pore pressure magnitudes around wellbores (*Sherwood and Bailey*, 1994; *Abousleiman et al.*, 2001).

The aforementioned formulation has been extended to be a porous system saturated with several species of pore fluid and has been specialized for an ideal solution comprising of two species, a solute and a solvent (*Sherwood*, 1994a, 1994b, 1995). The chemical effects are due to the interaction between the matrix and constituents within the pore

fluid. Other models based on the mixture theory (*Huyghe and Janssen*, 1999; *Li and Li*, 1992) and non-linear poroelastic analysis (*Coussy et al.*, 1999; *Dormieux et al.*, 1995) have also been introduced. Experimental efforts have focused on quantifying swelling behavior of shale when brought into contact with aqueous and oil-based fluids having varying salt concentrations (*Bailey et al.*, 1994; *Lomba et al.*, 2000a).

Anisotropy of rock formations, where drilling activities are carried out, adds an additional degree of complexity. The anisotropic nature is attributed to deposition of sedimentary rocks such as shales over geological time scales. In the absence of any chemical interactions, the coupling between the hydraulic and mechanical processes in response to perturbations has been addressed within a generalized anisotropic poroelastic formulation (*Abousleiman and Cui*, 2000). Analytical solutions for a wide variety of fundamental problems have been developed (*Abousleiman et al.*, 1995, 1996a; *Abousleiman and Cui*, 1998). Subsequently, the anisotropic poroelastic formulation has been extended to incorporate thermal effects (*Abousleiman and Ekbote*, 2002).

In this chapter, the focus is on the development of a generalized linear anisotropic formulation for chemically active porous media under the framework of Biot's theory. The model, termed as porochemoelastic, fully-couples the perturbations in the stress, pore pressure and solute molar fractions in a consistent form. The anisotropic porochemoelastic formulation is first specialized for a transversely isotropic material and next for an isotropic material. Field equations for both the transversely isotropic and the isotropic cases are developed. These are applied to present a solution for an inclined borehole in transversely isotropic media. Corresponding isotropic solution is included in Appendix D. The chemical effects on the stress and pore pressure distribution around a borehole are discussed using a simplified problem which nullifies all other effects except the ones generated by the chemical interactions. A numerical example of an inclined borehole problem is presented to assess the nature of the chemical effects on wellbore stability.

## 5.2 General Formulation

The porochemoelastic model is formulated as an extension of Biot's linear poroelastic model and accounts for the chemical interaction between the porous formation and the fluid saturating it (*Sherwood*, 1993). The porous medium is assumed to comprise of a solid matrix with interconnected pore space. The pore space is completely saturated with a fluid containing $n$ chemical species. A perturbed state, introduced by application of stress, results in a change in the strain of the solid matrix and changes in chemical potential of each of the pore fluid species. These are related by (*Sherwood*, 1993)

$$\epsilon_{ij} = C_{ijkl}\sigma_{kl} + \sum_{p} Q^{p}_{ij}\mu^{p} \tag{5.1}$$

$$M^{p} = Q^{p}_{ij}\sigma_{ij} + \sum_{q} B^{pq}\mu^{q} \tag{5.2}$$

where $\epsilon_{ij}$ is the strain tensor, $\sigma_{kl}$ is the stress tensor, $C_{ijkl}$ is the drained compliance tensor, $\mu^{i}$ is the chemical potential of the $i^{th}$ species, $M^{i}$ is the mass per unit reference volume of the $i^{th}$ species, $Q_{ij}$ is a material coefficient tensor with the symmetry $Q_{ij} = Q_{ji}$. For simplicity, we assume that the pore fluid comprises of two chemical species; a solute and a solvent denoted by a superscripts $s$ and $w$, respectively. The solute and solvent mole fractions are denoted by $\bar{m}^{s}$ and $\bar{m}^{w}$, respectively, such that

$$V_{sol} = V_{s}\bar{m}^{s} + V_{w}\bar{m}^{w} \tag{5.3}$$

where $V_s$ and $V_w$ are the partial molar volumes of the solute and solvent respectively, $V_{sol}$ is the molar volume of the solution and $\bar{m}^{w} = 1 - \bar{m}^{s}$. The chemical potentials are given by (*Sherwood*, 1993)

$$\mu^{s} = pV_{s} + RT\ln(\varrho^{s}\bar{m}^{s}) \tag{5.4}$$

$$\mu^{w} = pV_{w} + RT\ln(\varrho^{w}\bar{m}^{w}) \tag{5.5}$$

where $\mu^{s}$ is the chemical potential of the solute, $\mu^{w}$ is the chemical potential of the solvent, $p$ is the thermodynamic pore pressure, $R$ is the universal gas constant, $T$ is the

temperature and $\varrho^s$, $\varrho^w$ are the activity coefficients of the solute and solvent respectively. The solution is assumed to be ideal with $\varrho^s = \varrho^w = 1$.

*Constitutive Equations*

The constitutive equations relate the changes in the dynamic variables (stress, pore pressure) to changes in the kinematic variables (strain, variation in content of each of the pore fluid species). For the porochemoelastic model, the constitutive equations comprise of the stress-strain relations and equations for variation in content for each of the species effected due to perturbation. The term '*variation in content of the $i^{th}$ species*' is analogous to the term '*variation of fluid content*' used in poroelastic model in which the porous matrix is saturated by a single species chemically inert pore fluid. In the porochemoelastic model, a change in the solute concentration affects the stresses, solute content and the solvent content. The constitutive equations for a chemically active porous matrix with a pore fluid consisting of two species are given by

$$\sigma_{ij} = M_{ijkl}\epsilon_{kl} - \alpha_{ij}p + \gamma^s_{ij}m^s \tag{5.6}$$

$$\zeta^s = \bar{m}^s\left[\frac{p}{M} + \alpha_{ij}\epsilon_{ij}\right] + \bar{\beta}^c\frac{V_{sol}}{V_s}m^s \tag{5.7}$$

$$\zeta^w = (1-\bar{m}^s)\left[\frac{p}{M} + \alpha_{ij}\epsilon_{ij}\right] - \bar{\beta}^c\frac{V_{sol}}{V_w}m^s \tag{5.8}$$

where $\sigma_{ij}$ is the total stress tensor, $\epsilon_{ij}$ is the strain tensor, $p$ is the pore pressure, $m^s$ is the variation in the solute mole fraction, $\bar{m}^s$ is the initial mole fraction, $\zeta^s$ is the variation in the solute content, $\zeta^w$ is the variation in the solvent content, $M_{ijkl}$ is the drained elastic modulus tensor, $M$ is Biot's modulus, $\alpha_{ij}$ is the Biot's effective stress coefficient tensor, $\gamma^s_{ij}$ is the chemo-mechanical coupling coefficient tensor, and $\bar{\beta}^c$ is the hydro-chemical coupling constant. The chemo-mechanical coupling coefficient tensor $\gamma^s_{ij}$ has the dimensions of stress and gives the change in stress due to a change in the solute molar fractions. Equations (5.6) - (5.8) form the quasi-static constitutive equations for the porochemoelastic model. A non-equilibrium state is introduced by a difference in the

potentials across the porous medium which are handled appropriately by the transport equations.

*Transport Equations*

A generalized form of the transport equations as given by Onsager's relation is (*De Groot*, 1952)

$$J_i = \sum_{k=1}^{n} L_{ik} X_k \tag{5.9}$$

where $J_i$ is the flux of the $i^{th}$ species, $X_k$ are the gradients in the potentials causing the fluxes and $L_{ik}$ are the phenomenological constants which are related by Onsager's principle as $L_{ik} = L_{ki}$. A difference in the chemical potentials of the solute and solvent results in a flux. The chemical potential differences can either be caused by a difference in the pore pressure or a difference in the solute molar fraction. Accordingly, transport equations for the solute flux and solvent flux are given by

$$q_i^s = -(1-\chi)\left[\bar{m}^s \kappa_{ij} p_{,j} + D_{ij} m^s_{,j}\right] \tag{5.10}$$

$$q_i^w = -(1-\bar{m}^s)\kappa_{ij} p_{,j} + \frac{1}{V_w}\left[\chi RT \kappa_{ij} + (1-\chi) V_s D_{ij}\right] m^s_{,j} \tag{5.11}$$

where $q_i^s$ is the solute flux vector, $q_i^w$ is the solvent flux vector. $\kappa_{ij}$ is the mobility coefficient tensor, $D_{ij}$ is the solute diffusivity tensor and $\chi$ is the reflection coefficient. The anisotropic mobility coefficient tensor, $\kappa_{ij}$, is related to the intrinsic permeability tensor, $k_{ij}$, and the pore fluid viscosity, $\mu$, by $\kappa_{ij} = k_{ij}/\mu$.

*Conservation laws*

The system is subject to balance laws for mass and momentum. Momentum balance yields the equilibrium equations which are given by

$$\sigma_{ij,j} = 0 \tag{5.12}$$

where equation (5.12) has been written ignoring any body forces. Mass balance is applied

individually for the solute and the solvent and the equations for the same are given as

$$\frac{\partial \zeta^s}{\partial t} + \nabla \cdot q_i^s = 0 \tag{5.13}$$

$$\frac{\partial \zeta^w}{\partial t} + \nabla \cdot q_i^w = 0 \tag{5.14}$$

In writing equations (5.13) and (5.14) it has been assumed that the system is devoid of any sources or sinks.

The above set of equations (5.1) - (5.14) represent the most general form anisotropic of the porochemoelastic model of a porous media saturated with a pore fluid consisting of two species. These equations are specialized for the transversely isotropic case in the next section.

## 5.3 Transversely Isotropic Porochemoelasticity

For a transversely isotropic material, it is assumed that the $z$-axis coincides with the axis of material rotational symmetry. Consequently, the transversely isotropic material is characterized by an isotropic plane, in which material properties are independent of the direction, and a transverse direction along which the material properties are different. The transversely isotropic poroelastic material is characterized by 8 material parameters which have been related to the drained elastic parameters for the transversely isotropic material (*Cheng*, 1997; *Abousleiman and Cui*, 2000). For a transversely isotropic material the constitutive relations for porochemoelasticity are given as

$$\sigma_{xx} = M_{11}\epsilon_{xx} + M_{12}\epsilon_{yy} + M_{13}\epsilon_{zz} - \alpha p + \gamma^s m^s \tag{5.15}$$

$$\sigma_{yy} = M_{12}\epsilon_{xx} + M_{11}\epsilon_{yy} + M_{13}\epsilon_{zz} - \alpha p + \gamma^s m^s \tag{5.16}$$

$$\sigma_{zz} = M_{13}\epsilon_{xx} + M_{13}\epsilon_{yy} + M_{33}\epsilon_{zz} - \alpha' p + \gamma^{s'} m^s \tag{5.17}$$

$$\tau_{xy} = G\gamma_{xy}; \qquad \tau_{yz} = G'\gamma_{yz}; \qquad \tau_{zx} = G'\gamma_{zx}$$

$$\zeta^s = \bar{m}^s \left[\frac{p}{M} + \alpha(\epsilon_{xx} + \epsilon_{yy}) + \alpha'(\epsilon_{zz})\right] + \bar{\beta}^c \frac{V_{sol}}{V_s} m^s \tag{5.18}$$

$$\zeta^w = (1 - \bar{m}^s) \left[\frac{p}{M} + \alpha(\epsilon_{xx} + \epsilon_{yy}) + \alpha'(\epsilon_{zz})\right] - \bar{\beta}^c \frac{V_{sol}}{V_w} m^s \tag{5.19}$$

where the unprimed variables are material properties in the isotropic plane and the primed variables are material properties in the transverse direction. The constitutive equations for transverse isotropy given above are specialized for the plane $x-y$ case which will be utilized in obtaining analytical solutions under the assumption of a generalized plane strain condition. Consequently, the constitutive equations for a plane $x - y$ case are written as

$$\sigma_{xx} = M_{11}\epsilon_{xx} + M_{12}\epsilon_{yy} - \alpha p + \gamma^s m^s \tag{5.20}$$

$$\sigma_{yy} = M_{12}\epsilon_{xx} + M_{11}\epsilon_{yy} - \alpha p + \gamma^s m^s \tag{5.21}$$

where $\alpha$ is the Biot's effective stress coefficient in the isotropic plane and $\gamma^s$ is the chemo-mechanical coupling coefficient also in the isotropic plane. From equations (5.18) and (5.19), the equations for variation of solute content and solvent content for the transversely isotropic case are given by

$$\zeta^s = \frac{\alpha \bar{m}^s}{(M_{11} + M_{12})} \left[\sigma_{kk} + \frac{(M_{11} + M_{12} + 2\alpha^2 M)}{\alpha M} p\right] + \beta^c \frac{V_{sol}}{V_s} m^s \tag{5.22}$$

$$\zeta^w = \frac{\alpha(1 - \bar{m}^s)}{(M_{11} + M_{12})} \left[\sigma_{kk} + \frac{(M_{11} + M_{12} + 2\alpha^2 M)}{\alpha M} p\right] - \beta^c \frac{V_{sol}}{V_w} m^s \tag{5.23}$$

Combining the above equations with the mass and momentum balance equations yields the field equations. Substituting equations (5.20) and 5.21) in equation (5.12) gives the Navier-type equations given by

$$\frac{1}{2}(M_{11} - M_{12})u_{i,jj} + \frac{1}{2}(M_{11} + M_{12})u_{j,ji} = \alpha p_{,i} - \gamma^s m^s_{,i} \quad (i, j = 1, 2) \tag{5.24}$$

where $u_i$ is the solid displacement vector. The equilibrium equations can also be expressed in terms of stresses yielding the Beltrami-Michell compatibility equations. For

the plane $x-y$ case these are given by

$$\left(C_{11}-\frac{C_{13}^2}{C_{33}}\right)\nabla^2\left(\sigma_{xx}+\sigma_{xy}\right)+\alpha\left(C_{11}+C_{12}-\frac{2C_{13}^2}{C_{33}}\right)\nabla^2 p$$
$$-\gamma^s\left(C_{11}+C_{12}-\frac{2C_{13}^2}{C_{33}}\right)\nabla^2 m^s=0 \tag{5.25}$$

where $C_{11}$, $C_{12}$, $C_{13}$ and $C_{33}$ are elements of the compliance matrix for the transversely isotropic case. Equation (5.25) can also be written in terms of the drained elastic coefficients as follows

$$\nabla^2\left(\sigma_{xx}+\sigma_{xy}+\alpha\left(1-\frac{M_{12}}{M_{11}}\right)p-\gamma^s\left(1-\frac{M_{12}}{M_{11}}\right)m^s\right)=0 \tag{5.26}$$

The transport equations for the plane $x-y$ case are specialized as follows

$$q_i^s=-(1-\chi)\left[\bar{m}^s\kappa p_{,i}+Dm_{,i}^s\right] \tag{5.27}$$

$$q^w=-(1-\bar{m}^s)\kappa p_{,i}+\frac{1}{V_w}\left[\chi RT\kappa+(1-\chi)V_sD\right]m_{,i}^s \tag{5.28}$$

where the index $i=1,2$, and $\kappa$, $D$ are the mobility coefficient and solute diffusivity, respectively in the isotropic $x-y$ plane. Substituting equations (5.22) and (5.27) in the solute mass conservation equation (5.13) yields

$$\frac{\alpha\bar{m}^s}{(M_{11}+M_{12})}\left[\frac{\partial\sigma_{kk}}{\partial t}+\frac{(M_{11}+M_{12}+2\alpha^2M)}{\alpha M}\frac{\partial p}{\partial t}\right]+\beta^c\frac{V_{sol}}{V_s}\frac{\partial m^s}{\partial t}$$
$$=(1-\chi)\left[\kappa\nabla^2p+D\nabla^2m^s\right] \tag{5.29}$$

Again substituting equations (5.23) and (5.28) in the solvent mass conservation equation (5.14) yields

$$\frac{\alpha(1-\bar{m}^s)}{(M_{11}+M_{12})}\left[\frac{\partial\sigma_{kk}}{\partial t}+\frac{(M_{11}+M_{12}+2\alpha^2M)}{\alpha M}\frac{\partial p}{\partial t}\right]-\beta^c\frac{V_{sol}}{V_w}\frac{\partial m^s}{\partial t}$$
$$=(1-\bar{m}^s)\kappa\nabla^2p-\frac{1}{V_w}\left[\chi RT+(1-\chi)V_sD\right]\nabla^2m^s \tag{5.30}$$

Using the relation given by equation (5.26) in equations (5.29) and (5.30) yields

$$\frac{\alpha}{(M_{11}+M_{12})}\frac{\partial\Theta}{\partial t}+\frac{\beta^cV_{sol}}{\bar{m}^sV_s}\frac{\partial m^s}{\partial t}=\left[\frac{(1-\chi)\kappa\alpha MM_{11}}{(\alpha^2M+M_{11})(M_{11}+M_{12})}\right]\nabla^2\Theta$$
$$+\left[\gamma^s\left(1-\frac{M_{12}}{M_{11}}\right)\frac{(1-\chi)\kappa\alpha MM_{11}}{(\alpha^2M+M_{11})(M_{11}+M_{12})}+\frac{(1-\chi)D}{\bar{m}^s}\right]\nabla^2m^s \tag{5.31}$$

$$\frac{\alpha}{(M_{11}+M_{12})}\frac{\partial\Theta}{\partial t}-\frac{\beta^c V_{sol}}{\bar{m}^s V_w}\frac{\partial m^s}{\partial t}=\left[\frac{\kappa\alpha M M_{11}}{(\alpha^2 M+M_{11})(M_{11}+M_{12})}\right]\nabla^2\Theta$$
$$+\left[\gamma^s\left(1-\frac{M_{12}}{M_{11}}\right)\frac{\kappa\alpha M M_{11}}{(\alpha^2 M+M_{11})(M_{11}+M_{12})}-\frac{[\chi RT\kappa+(1-\chi)V_s D]}{(1-\bar{m}^s)V_w}\right]\nabla^2 m^s \tag{5.32}$$

where $\Theta$ is given by

$$\Theta=\sigma_{kk}+\frac{(M_{11}+M_{12}+2\alpha^2 M)}{\alpha M}p \tag{5.33}$$

Equations (5.31) and (5.32) can be modified to yield

$$\frac{\partial\Theta}{\partial t}=Y_1\nabla^2\Theta+Y_2\nabla^2 m^s \tag{5.34}$$
$$\frac{\partial m^s}{\partial t}=Z_1\nabla^2\Theta+Z_2\nabla^2 m^s \tag{5.35}$$

where the coefficients $Y_1$, $Y_2$, $Z_1$ and $Z_2$ are given by

$$Y_1=\frac{\kappa M M_{11}}{(\alpha^2 M+M_{11})V_{sol}}[V_{sol}-\chi\bar{m}^s V_s] \tag{5.36}$$
$$Y_2=\gamma^s\left(1-\frac{M_{12}}{M_{11}}\right)\frac{\kappa M M_{11}}{(\alpha^2 M+M_{11})V_{sol}}[V_{sol}-\chi\bar{m}^s V_s]-\frac{(M_{11}+M_{12})\chi RT\kappa}{\alpha V_{sol}} \tag{5.37}$$
$$Z_1=-\frac{\chi\kappa\alpha M M_{11}}{(\alpha^2 M+M_{11})(M_{11}+M_{12})}\frac{\bar{m}^s(1-\bar{m}^s)V_s V_w}{\beta^c V_{sol}^2} \tag{5.38}$$
$$Z_2=\frac{V_s}{\beta^c V_{sol}^2}[(1-\chi)DV_{sol}+\chi RT\kappa\bar{m}^s] \tag{5.39}$$

We define $n_1$, $n_2$, $c_1$ and $c_2$, as follows

$$n_{1,2}=\frac{(Z_2-Y_1)\pm\sqrt{(Z_2-Y_1)^2+4Y_2Z_1}}{2Z_1} \tag{5.40}$$
$$c_{1,2}=\frac{\left[(Z_2+Y_1)\pm\sqrt{(Z_2-Y_1)^2+4Y_2Z_1}\right]}{2} \tag{5.41}$$

Using equations (5.40) and (5.41) the coupled diffusion equations (5.34) and (5.35) can be combined to give

$$\frac{\partial}{\partial t}(\Pi_i)-c_i\nabla^2(\Pi_i)=0;\quad i=1,2 \tag{5.42}$$

Equation (5.42) gives a set of coupled homogeneous diffusion equations in which

$$\Pi_i = \Theta + n_i m^s \tag{5.43}$$

Due to the relatively different magnitudes of the constants appearing in the expressions for coefficients $n_1$, $n_2$, $c_1$, and $c_2$, they can be simplified by introducing some approximations. Following Sherwood (1994a) the expressions for $n_1$, $n_2$, $c_1$, and $c_2$ simplify as follows

$$n_1 \approx \frac{(M_{11} + M_{12})}{\alpha} \frac{\beta^c V_{sol}^2}{\chi \bar{m}^s V_s V_w} \tag{5.44}$$

$$n_2 \approx -\frac{(\alpha^2 M + M_{11})(M_{11} + M_{12})}{\alpha M M_{11}} \frac{\chi RT}{V_{sol}} \tag{5.45}$$

$$c_1 \approx \frac{V_s}{\beta^c V_{sol}^2} [(1-\chi) D V_{sol} + \chi RT \kappa \bar{m}^s] \tag{5.46}$$

$$c_2 \approx \frac{\kappa M M_{11}}{(\alpha^2 M + M_{11})} \tag{5.47}$$

The field equations for transversely isotropic porochemoelasticity can therefore be summarized as follows; Navier-type equation (5.24), coupled diffusion equations (5.34) and (5.35).

## 5.4 Isotropic Porochemoelasticity

For an isotropic material the constitutive equations for porochemoelasticity reduce to

$$\sigma_{ij} = 2G\epsilon_{ij} + \frac{2G\nu}{1-2\nu}\epsilon\delta_{ij} - \alpha p \delta_{ij} + \gamma^s m^s \delta_{ij} \tag{5.48}$$

$$\zeta^s = \frac{\alpha(1-2\nu)\bar{m}^s}{2G(1+\nu)} \left[\sigma_{kk} + \frac{3p}{B}\right] + \beta^c \frac{V_{sol}}{V_s} m^s \tag{5.49}$$

$$\zeta^w = \frac{\alpha(1-2\nu)(1-\bar{m}^s)}{2G(1+\nu)} \left[\sigma_{kk} + \frac{3p}{B}\right] - \beta^c \frac{V_{sol}}{V_w} m^s \tag{5.50}$$

where $G$ is the shear modulus, $\nu$ is the Poisson's ratio, $\alpha$ is the Biot's effective stress coefficient, $B$ is the Skempton's coefficient. Field equations for the isotropic material

are obtained by combining the balance equations with the constitutive and transport equations.

Following the approach outlined in the previous section, the governing equations for isotropic porochemoelasticity are given as

$$G\nabla^2 u_i + \frac{G}{1-2\nu} u_{k,ki} = \alpha p_{,i} - \gamma^s m^s_{,i} \tag{5.51}$$

$$\frac{\partial}{\partial t}(\Pi_i) - c_i \nabla^2 (\Pi_i) = 0; \quad i = 1,2 \tag{5.52}$$

in which

$$\Pi_i = \Theta + n_i m^s \tag{5.53}$$

where $n_1$, $n_2$, $c_1$, and $c_2$ for the isotropic case are as follows

$$n_1 \approx \frac{2G(1+\nu)}{\alpha(1-2\nu)} \frac{\beta^c V_{sol}^2}{\chi \bar{m}^s V_s V_w} \tag{5.54}$$

$$n_2 \approx -\frac{2\eta(1+\nu)(1-\nu_u)}{(\nu_u - \nu)} \frac{\chi RT}{V_{sol}} \tag{5.55}$$

$$c_1 \approx \frac{V_s}{\beta^c V_{sol}^2} [(1-\chi) D V_{sol} + \chi RT \kappa \bar{m}^s] \tag{5.56}$$

$$c_2 \approx \frac{G\kappa(\nu_u - \nu)}{\alpha\eta(1-2\nu)(1-\nu_u)} \tag{5.57}$$

## 5.5 Inclined Borehole Problem

The solution for the inclined borehole problem for transversely isotropic porochemoelasticity under permeable and impermeable boundary conditions are presented in this section. Corresponding isotropic solutions are included in the Appendix D.

It is assumed that an infinitely long borehole is drilled in a chemically active transversely isotropic formation with its axis perpendicular to the plane of isotropy. A schematic of the inclined borehole is shown in Figure 3.1. The formation is characterized

by in-situ stresses $S_{x'}$, $S_{y'}$, and $S_{z'}$, virgin pore pressure $p_o$. The formation pore fluid has a solute molar fraction $m_o^s$. The inclination and azimuth for the inclined borehole are given by $\varphi_z$ and $\varphi_y$ respectively. Following a transformation to a local coordinate system, the borehole is subject to normal as well as shear stresses (*Cui et al.*, 1997).

The boundary conditions for the inclined borehole problem, discussed in Chapter 3, are specialized for the porochemoelastic problem. The boundary conditions of the problem at the far field, $r \rightarrow \infty$, are as follows

$$\sigma_{xx} = -S_x; \quad \sigma_{yy} = -S_y; \quad \sigma_{zz} = -S_z; \tag{5.58}$$

$$\tau_{xy} = -S_{xy}; \quad \tau_{yz} = -S_{yz}; \quad \tau_{xz} = -S_{xz}; \tag{5.59}$$

$$p = p_o; \quad m^s = m_o^s \tag{5.60}$$

and at the borehole wall, $r = R$,

$$\sigma_{rr} = -p_w H(t); \quad \tau_{r\theta} = \tau_{rz} = 0; \tag{5.61}$$

$$L_1 p + L_2 q_r = L_1 p_w H(t) + L_2 q_i H(t) \tag{5.62}$$

$$m^s = m_w^s H(t) \tag{5.63}$$

where $p_w$ is the wellbore fluid pressure, $m_w^s$ is the solute molar fraction in the wellbore fluid, and $H(t)$ is the Heaviside unit step function. $L_1$ and $L_2$ are coefficients which determine the borehole wall idealization under consideration. With $L_1 = 1$ and $L_2 = 0$, the boundary conditions reduce to the permeable boundary condition model, and with $L_1 = 0$ and $L_2 = 1, q_r = q_i = 0$ yields boundary conditions for the impermeable boundary condition model.

As discussed in Chapter 3, the decomposition scheme results in three sub-problems (*Cui et al.*, 1997). For the porochemoelastic model, Problem I (modified plane strain problem) accounts for the in-plane normal and shear stresses and the pore pressure and solute mole fraction perturbations. Problems II and III are time-independent since they do not trigger any diffusion phenomena.

The boundary conditions in the decomposition scheme are given as follows:

**Problem 1:** At far field ( $r \to \infty$)

$$\sigma_{xx} = -S_x; \quad \sigma_{yy} = -S_y; \quad \tau_{xy} = -S_{xy} \tag{5.64}$$

$$\sigma_{zz} = -\nu^{'}(S_x + S_y) - (\alpha^{'} - 2\nu^{'}\alpha)p_o + (\gamma^{s'} - 2\nu^{'}\gamma^{s})m_o^s \tag{5.65}$$

$$\tau_{yz} = \tau_{xz} = 0; \qquad p = p_o; \quad m^s = m_o^s \tag{5.66}$$

At the borehole wall ($r = R$)

$$\sigma_{rr} = -p_w H(t); \qquad m^s = m_o^s H(t) \tag{5.67}$$

$$L_1 p + L_2 q_r = L_1 p_w H(t) + L_2 q_i H(t) \tag{5.68}$$

**Problem 2:** At far field ( $r \to \infty$)

$$\sigma_{zz} = -S_z + [\nu^{'}(S_x + S_y) + (\alpha^{'} - 2\nu^{'}\alpha)p_o - (\gamma^{s'} - 2\nu^{'}\gamma^{s})m_o^s] \tag{5.69}$$

$$\sigma_{xx} = \sigma_{yy} = \tau_{xy} = \tau_{yz} = \tau_{xz} = p = m^s = 0 \tag{5.70}$$

At borehole wall ($r = R$)

$$\sigma_{rr} = \tau_{r\theta} = \tau_{rz} = p = m^s = 0 \tag{5.71}$$

**Problem 3:** At far field ( $r \to \infty$)

$$\sigma_{xx} = \sigma_{yy} = \sigma_{zz} = \tau_{xy} = p = m^s = 0 \tag{5.72}$$

$$\tau_{xy} = -S_{xy}; \quad \tau_{yz} = -S_{yz} \tag{5.73}$$

At the borehole wall ($r = R$)

$$\sigma_{rr} = \tau_{r\theta} = \tau_{rz} = p = m^s = 0 \tag{5.74}$$

The complete solution for the inclined borehole problem in a transversely isotropic medium is given by equations (3.54) - (3.61) setting $\varpi_1 = 1, \varpi_2 = 0, \varpi_3 = 1$.

### 5.5.1 Permeable Boundary Condition Model

The boundary conditions at the borehole wall for the permeable model are as follows:

*Case 1:*

$$\sigma_{rr}^{(1)} = P_o - p_w \tag{5.75}$$

$$\sigma_{r\theta}^{(1)} = p^{(1)} = m^{s(1)} = 0 \tag{5.76}$$

*Case 2:*

$$\sigma_{rr}^{(2)} = \sigma_{r\theta}^{(2)} = 0 \tag{5.77}$$

$$p^{(2)} = (p_w - p_o); \qquad m^{s(2)} = (m_w^s - m_o^s) \tag{5.78}$$

*Case 3:*

$$\sigma_{rr}^{(3)} = -S_o \cos 2(\theta - \theta_r) \tag{5.79}$$

$$\sigma_{r\theta}^{(3)} = S_o \sin 2(\theta - \theta_r) \tag{5.80}$$

$$p^{(3)} = m^{s(3)} = 0 \tag{5.81}$$

Solutions for the stresses, pore pressure, and mole fraction for the three cases described above are presented.

**Solutions for Case 1:**

Case1 is characterized by a hydrostatic state of stress with no effect on the pore pressure and solute molar fractions. The solution for $\sigma_{rr}^{(1)}$ and $\sigma_{\theta\theta}^{(1)}$ is purely elastic and is given by equations (B.1) - (B.2) in Appendix B.

**Solutions for Case 2:**

Case 2 is characterized by a perturbation of the pore pressure and solute mole fraction. Solution for this case is obtained by solving the coupled diffusion equations (5.42). Expressions for pore pressure, stress and solute mole fraction are obtained in the Laplace

domain and inverted to the time domain using the Stehfest algorithm (*Stehfest*, 1970; *Davies and Martin*, 1970). Solution for equation (5.42) is given by

$$\bar{\Theta} + n_i \bar{m}^s = D_i \mathrm{K}_0(\xi_i r) \quad i = 1, 2 \tag{5.82}$$

where $\bar{}$ denotes the Laplace transform and $\mathrm{K}_n$ is the modified Bessel function of the second kind of order n, $\xi_i = \sqrt{s/c_i}$ and $s$ is the Laplace transform parameters. The expressions for $\bar{m}^s$, $\bar{p}$ and $\bar{\Theta}$ are obtained as

$$\bar{m}^s = \frac{D_1 \mathrm{K}_0(\xi_1 r) - D_2 \mathrm{K}_0(\xi_2 r)}{(n_1 - n_2)} \tag{5.83}$$

$$\bar{\Theta} = \frac{n_2 D_1 \mathrm{K}_0(\xi_1 r) - n_1 D_2 \mathrm{K}_0(\xi_2 r)}{(n_2 - n_1)} \tag{5.84}$$

$$\bar{p} = \frac{\alpha M M_{11}}{(\alpha^2 M + M_{11})(M_{11} + M_{12})} \left[ \frac{n_2 D_1 \mathrm{K}_0(\xi_1 r) - n_1 D_2 \mathrm{K}_0(\xi_2 r)}{(n_2 - n_1)} \right] \tag{5.85}$$

Substituting boundary conditions in equation (5.82) yields the constants $D_1$ and $D_2$ as follows

$$D_i = \frac{1}{s \mathrm{K}_0(\xi_i R)} \left[ \frac{(\alpha^2 M + M_{11})(M_{11} + M_{12})}{\alpha M M_{11}} (p_w - p_o) + n_i (m_w^s - m_o^s) \right]; \quad i = 1, 2 \tag{5.86}$$

Generalized solutions for the solute mole fraction $\bar{m}^s$ and pore pressure $\bar{p}$ are obtained substituting expressions for $D_1$ and $D_2$. Following approximations are applied $n_1 >> n_2$ and $n_1 m^s >> p_w$ the solutions for $\bar{m}^s$ and $\bar{p}$ are obtained as

$$s\bar{m}^s = [(m_w^s - m_o^s)]\, \Phi(\xi_1) \tag{5.87}$$

$$s\bar{p} = F_4 \Phi(\xi_1) + F_5 \Phi(\xi_2) \tag{5.88}$$

where $\Phi(x)$ is given by equation (B.8) in Appendix B and $F_4$, $F_5$ are given by

$$F_4 = \left( \frac{\chi RT}{V_w} \right) (m_w^s - m_o^s) \tag{5.89}$$

$$F_5 = \left[ (p_w - p_o) - \left( \frac{\chi RT}{V_w} \right) (m_w^s - m_o^s) \right] \tag{5.90}$$

The expressions for the radial and tangential stress are obtained as

$$s\tilde{\sigma}_{rr}^{(2)} = \alpha\left(1 - \frac{M_{12}}{M_{11}}\right)\{F_4\Psi(\xi_1) + F_5\Psi(\xi_2)\}$$
$$-\gamma^s\left(1 - \frac{M_{12}}{M_{11}}\right)\{(m_w^s - m_o^s)\,\Psi(\xi_1)\} \tag{5.91}$$

$$s\tilde{\sigma}_{\theta\theta}^{(2)} = -\alpha\left(1 - \frac{M_{12}}{M_{11}}\right)\{F_4\Omega(\xi_1) + F_5\Omega(\xi_2)\}$$
$$+\gamma^s\left(1 - \frac{M_{12}}{M_{11}}\right)\{(m_w^s - m_o^s)\,\Omega(\xi_1)\} \tag{5.92}$$

where $\Psi(x)$ and $\Omega(x)$ are given by equations (B.9) and (B.10) in Appendix B respectively.

**Solutions for Case 3:**

Case 3 is characterized by an asymmetric state of stress. Excess pore pressure is induced due to the Skempton effect. However, there is no variation is the solute mole fractions as a result of which the solutions for this case are the same as its poroelastic counterpart and given by (*Cui et al.*, 1997; *Abousleiman and Cui*, 1998). Solutions for $\sigma_{rr}^{(3)}$, $\sigma_{\theta\theta}^{(3)}$, $\sigma_{r\theta}^{(3)}$, $p^{(3)}$ are the same as that for the transversely isotropic permeable poroelastic case and are given by equations (B.11) - (B.22) in Appendix B where $\xi_f = \xi_2$.

### 5.5.2 Impermeable Boundary ConditionModel

Assuming an impermeable boundary condition at the borehole wall, the boundary conditions for the three contributing loading cases at the borehole wall ($r = R$) are given as follows:

**Case1:**

$$\sigma_{rr}^{(1)} = P_o - p_w \tag{5.93}$$

$$\sigma_{r\theta}^{(1)} = q^{(1)} = m^{s(1)} = 0 \tag{5.94}$$

**Case 2:**

$$\sigma_{rr}^{(2)} = \sigma_{r\theta}^{(2)} = q^{(2)} = 0 \tag{5.95}$$

$$m^{s(2)} = (m_w^s - m_o^s) \tag{5.96}$$

**Case 3:**

$$\sigma_{rr}^{(3)} = -S_o \cos 2(\theta - \theta_r) \tag{5.97}$$

$$\sigma_{r\theta}^{(3)} = S_o \sin 2(\theta - \theta_r) \tag{5.98}$$

$$q^{(3)} = m^{s(3)} = 0 \tag{5.99}$$

Solutions for the stresses, pore pressure, and mole fraction for the three cases described above are presented.

**Solutions for Case 1:**

Case1 is characterized by a hydrostatic state of stress with no effect on the pore pressure and solute molar fractions. The solution for $\sigma_{rr}^{(1)}$ and $\sigma_{\theta\theta}^{(1)}$ is purely elastic and is given by equations (B.1) - (B.2) in Appendix B.

**Solutions for Case 2:**

The solution is time-dependent and is obtained in the Laplace domain and inverted to the time-domain using the Stehfest algorithm (*Stehfest*, 1970; *Davies and Martin*, 1979). Generalized solutions for the solute mole fraction $\bar{m}^s$ and pore pressure $\bar{p}$ under the impermeable boundary condition are obtained as follows

$$s\bar{m}^s = \left[(m_w^s - m_o^s)\right] \Phi(\xi_1) \tag{5.100}$$

$$s\bar{p} = F_4 \left\{ \Phi(\xi_2) - \frac{\xi_1}{\xi_2} \left[ \frac{\mathrm{K}_1(\xi_1 R)}{\mathrm{K}_0(\xi_1 R)} \right] \left[ \frac{\mathrm{K}_0(\xi_2 r)}{\mathrm{K}_1(\xi_2 R)} \right] \right\} \tag{5.101}$$

The expressions for the radial and tangential stress are obtained as

$$\begin{aligned} s\bar{\sigma}_{rr}^{(2)} = \alpha \left(1 - \frac{M_{12}}{M_{11}}\right) F_4 \left\{ \left[ \frac{\xi_1}{\xi_2} \frac{1}{\xi_2 r} \frac{\mathrm{K}_1(\xi_1 R)}{\mathrm{K}_0(\xi_1 R)} \right] \left[ \frac{R}{r} - \frac{\mathrm{K}_1(\xi_2 r)}{\mathrm{K}_1(\xi_2 R)} \right] \right. \\ \left. + \left[ \frac{1}{\xi_1 r} \frac{\mathrm{K}_1(\xi_1 R)}{\mathrm{K}_0(\xi_1 R)} \left(1 - \frac{R}{r}\right) \right] \right\} \\ -\gamma^s \left(1 - \frac{M_{12}}{M_{11}}\right) (m_w^s - m_o^s) \left\{ \frac{1}{\xi_1 r} \frac{\mathrm{K}_1(\xi_1 R)}{\mathrm{K}_0(\xi_1 R)} \left(1 - \frac{R}{r}\right) \right\} \end{aligned} \tag{5.102}$$

$$s\bar{\sigma}_{\theta\theta}^{(2)} = -\alpha\left(1-\frac{M_{12}}{M_{11}}\right)F_4\left\{\left[\frac{\xi_1}{\xi_2}\frac{\mathrm{K}_1(\xi_1 R)}{\mathrm{K}_0(\xi_1 R)}\right]\left[\frac{1}{\xi_2 r}\frac{R}{r}-\frac{1}{\xi_2 r}\frac{\mathrm{K}_1(\xi_2 r)}{\mathrm{K}_1(\xi_2 R)}-\frac{\mathrm{K}_0(\xi_2 r)}{\mathrm{K}_1(\xi_2 R)}\right]\right.$$
$$\left.+\left[\frac{1}{\xi_1 r}\frac{\mathrm{K}_1(\xi_1 r)}{\mathrm{K}_0(\xi_1 R)}-\frac{R}{r}\frac{1}{\xi_1 r}\frac{\mathrm{K}_1(\xi_1 R)}{\mathrm{K}_0(\xi_1 R)}+\Phi(\xi_1)\right]\right\}$$
$$+\gamma^s\left(1-\frac{M_{12}}{M_{11}}\right)(m_w^s-m_o^s)\left\{\frac{1}{\xi_1 r}\frac{\mathrm{K}_1(\xi_1 r)}{\mathrm{K}_0(\xi_1 R)}\right.$$
$$\left.-\frac{R}{r}\frac{1}{\xi_1 r}\frac{\mathrm{K}_1(\xi_1 R)}{\mathrm{K}_0(\xi_1 R)}+\Phi(\xi_1)\right\} \qquad (5.103)$$

where $\Phi(x)$ is given by equation (B.8) in Appendix B and $F_4$ is as defined in equations (5.89).

**Solutions for Case 3:**

Again solution for Case 3 is the same as in the poroelastic permeable model since the boundary conditions indicate no variation in the solute molar fraction field.. Solutions for $\sigma_{rr}^{(3)}$, $\sigma_{\theta\theta}^{(3)}$, $\sigma_{r\theta}^{(3)}$, $p^{(3)}$ are the same as that for the transversely isotropic impermeable poroelastic case and are given by equations (B.9) - (B.12) and (B.23) - (B.30) in Appendix B where $\xi_f = \xi_2$.

## 5.6 Numerical Examples

The solutions developed in the previous section are applied to assess the chemical effect on the stress and pore pressure distribution in the vicinity of the borehole. The observations are extended to evaluate the implications of the same on borehole stability. A borehole is assumed to be drilled in a formation saturated by a pore fluid which can be described as comprising of two species, i.e., a solute fraction and a solvent fraction. Similarly, the borehole is filled with a borehole fluid comprising of two species. A difference in the solute concentrations in the formation pore fluid and the borehole fluid generates a chemical potential gradient which affects the stress and pore pressure distributions.

For the presentation of results, the borehole radius is assumed to be 0.1 m and a section at a depth of 1000 m is analyzed. The formation material properties are those

of a Gulf of Mexico shale (*Cui et al.*, 1999a). For simplicity, the material is assumed to be isotropic. The material properties, pore fluid properties and wellbore fluid properties are as given in Table 5.1. Note that for the presentation of results compressive stresses are denoted positive to comply with the traditional rock mechanics convention.

Table 5.1: Material Parameters for Porochemoelastic Analysis .

| Parameter | Units | Value |
|---|---|---|
| Elastic Modulus ($E$) | MPa | 1853.0 |
| Poisson's Ratio ($\nu$) | - | 0.22 |
| Undrained Poisson's Ratio ($\nu_u$) | - | 0.46 |
| Skempton's Coefficient ($B$) | - | 0.92 |
| Permeability ($k$) | md | $1.0 \times 10^{-4}$ |
| Fluid Viscosity ($\mu$) | MPa.s | $10^{-9}$ |
| Solute Diffusivity.($c_2$) | $m^2$/day | $8.64 \times 10^{-5}$ |
| Temperature ($T$) | °K | 300 |
| Reflection Coefficient ($\chi$) | - | 0.9 |
| Porosity ($\phi$) | - | 0.14 |

### 5.6.1 Chemical effect on stresses and pore pressure

The chemical effect on the stresses and pore pressure is examined by considering a simplified example. The borehole is assumed to be vertical i.e.. $\varphi_y = \varphi_z = 0°$. The insitu stress gradients $S_{x'}$, $S_{y'}$ and $S_{z'}$ are assumed to be trivial such that $S_{x'} = S_{y'} = S_{z'} = 0$ kPa/m. The formation pore pressure and wellbore fluid pressure gradient are assumed to be $p_o = p_w = 9.8$ kPa/m. The solvent species of both, the formation pore fluid and the wellbore fluid, is assumed to be water. The chemical effect is demonstrated by varying the solute concentration gradient between the formation pore fluid and the wellbore fluid.

Under the aforementioned conditions, the changes in the stress and pore pressure distributions are purely because of the difference in solute concentrations. Two cases are considered. In the first case, the formation pore fluid is assumed to have a higher

solute concentration than the wellbore fluid. In other words, $m_w^s < m_o^s$. The difference in solute molar fractions is assumed to be $1.8 \times 10^{-2}$ such that $m_w^s - m_o^s = -1.8 \times 10^{-2}$ which is equivalent of a solute concentration difference of 1 mol/kg in a solvent (water). In the second case, $m_w^s > m_o^s$ with $m_w^s - m_o^s = 1.8 \times 10^{-2}$.

Figure 5.1 shows the pore pressure variation along the radial distance. As seen from the figure, a higher solute concentration of the formation pore fluid results in an increased pore pressure in regions close to the borehole wall. Results are shown for the porochemoelastic case for $t = 0.001, 0.01, 0.1$ and 0.5 day. The magnitude of the chemically-induced pore pressure assumes its highest peak close to the borehole wall for smaller time intervals. This reduces with the passage of time and the peak moves into the formation and away from the borehole wall for larger time intervals.Since the solute concentration is higher in the formation pore fluid, the chemical potential of the solvent i.e., water is higher in the wellbore fluid. As a result an increase in the pore pressure close to the wellbore wall is observed. Figures 5.2 and 5.3 shows the total radial and tangential stress distributions, respectively, generated by the chemical effect. Compressive radial and tangential stresses are generated for this case. As in the case of the pore pressure, the front of the 'induced-stress' progresses gradually into the formation for both the radial and tangential stress.

For the second case, we examine the effect on the stress and pore pressure distributions when the solute concentration in the borehole fluid is more than that of the formation pore fluid, i.e., $m_w^s > m_o^s$. As before we assume the difference in the solute mole fractions to be $1.8 \times 10^{-2}$ such that $m_w^s - m_o^s = 1.8 \times 10^{-2}$. Figure 5.4 shows the pore pressure distribution for this case. In contrast to the previous case, there is a reduction in the pore pressure in regions close to the borehole wall. The solute concentration in the wellbore fluid is more than that in the formation pore fluid and hence the chemical potential of the water in the formation pore fluid is higher and a reduction in the pore

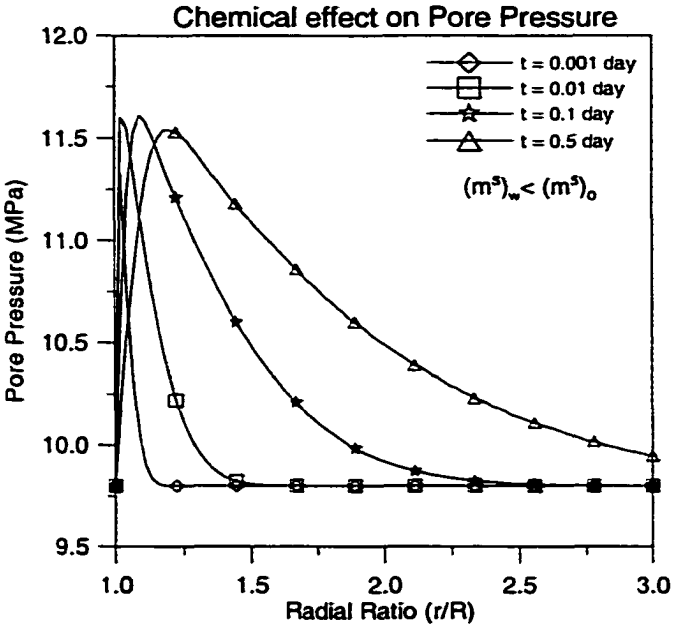


Figure 5.1: The chemical effect on the pore pressure for $m_w^s < m_o^s$.

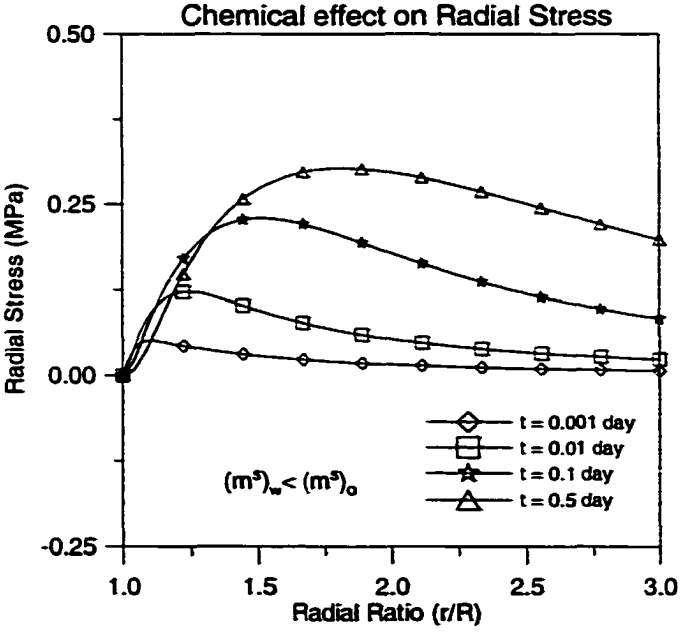


Figure 5.2: The chemical effect on the radial stress for $m_w^s < m_o^s$.

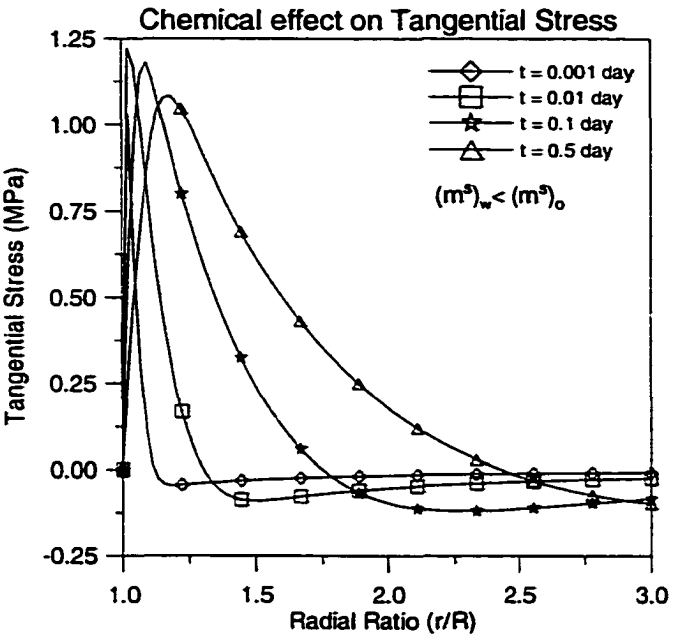


Figure 5.3: The chemical effect on the tangential stress for $m_w^s < m_o^s$.

pressure is observed. Figures 5.5 and 5.6 show the radial and tangential stresses induced by the chemical effect for this case. Again, contrary to the previous case. tensile stresses are induced by the chemical effect when $m_w^s > m_o^s$.

### 5.6.2 Implications on borehole stability

To examine the chemical effect on wellbore stability, we consider the stress and pore pressure distributions around an inclined borehole in a three-dimensional *in-situ* stress field. The borehole orientation is given by two angles as shown in Fig 3.1 which are the azimuth, $\varphi_y = 30°$, and the inclination $\varphi_z = 60°$. The formation in-situ stress and pore pressure gradients given as : $S_{x'} = 25$ kPa/m, $S_{y'} = 22$ kPa/m, $S_{z'} = 29$ kPa/m, $p_o = 9.8$ kPa/m. The borehole fluid pressure is maintained at $p_w = 12.0$ MPa . The difference in the solute molar fractions of the pore fluid and the wellbore fluid is equivalent of 1 mol/kg with $m_w^s < m_o^s$. Material properties given in Table 5.1 are used

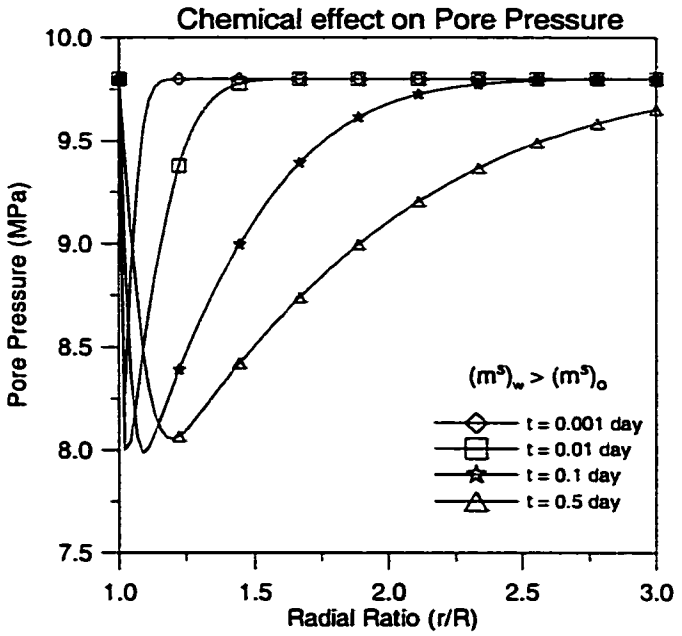


Figure 5.4: The chemical effect on the pore pressure for $m_w^s > m_o^s$.

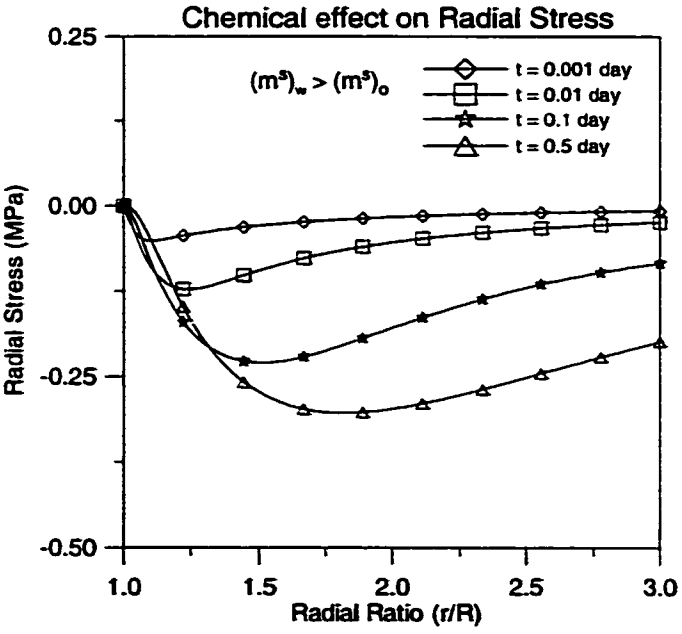


Figure 5.5: The chemical effect on the radial stress for $m_w^s > m_o^s$.

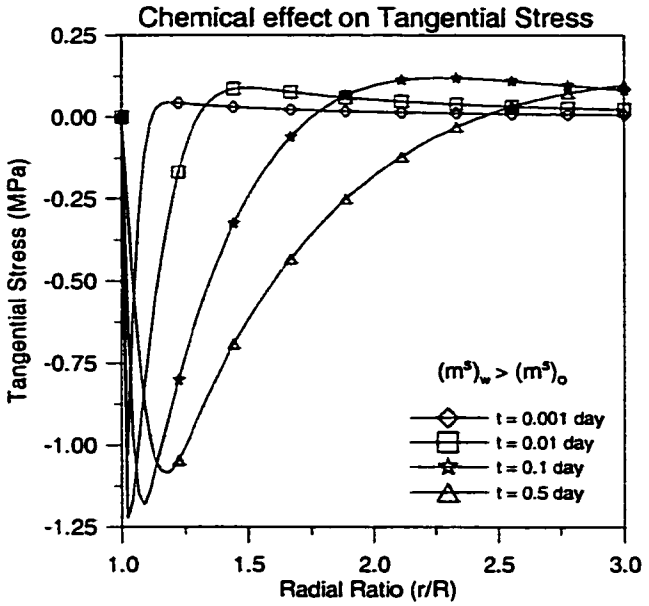


Figure 5.6: The chemical effect on the tangential stress for $m_w^s > m_o^s$.

in the computations.

As discussed earlier, a higher chemical potential of water in the wellbore fluid results in a chemically-induced pore pressure close to the borehole wall. For the present case, the wellbore fluid pressure is $p_w = 12.0$ MPa and the formation pore pressure is $p_w = 9.8$ MPa. The time-dependent variation of pore pressure along the $\theta = 90°$ direction is shown in figure 5.7. The $\theta = 90°$ direction corresponds to direction of the minimum in-plane principal stress. As seen from the figure, the peak of the induced pore pressure occurs close to the borehole wall. The magnitude of this induced pore pressure reduces with the passage of time and the peak gradually progresses into the formation. The peak of the pore pressure occurs approximately at a normalized radial distance $r/R = 1.05$ and at short time. Figures 5.8 and 5.9 show the effective radial and tangential stresses along the $\theta = 90°$ direction. Corresponding to the peak in the chemically induced pore pressure, tensile effective radial stresses are observed close to the borehole wall. The tensile magnitude, however, reduces as time progresses. Similarly, the effective tangential

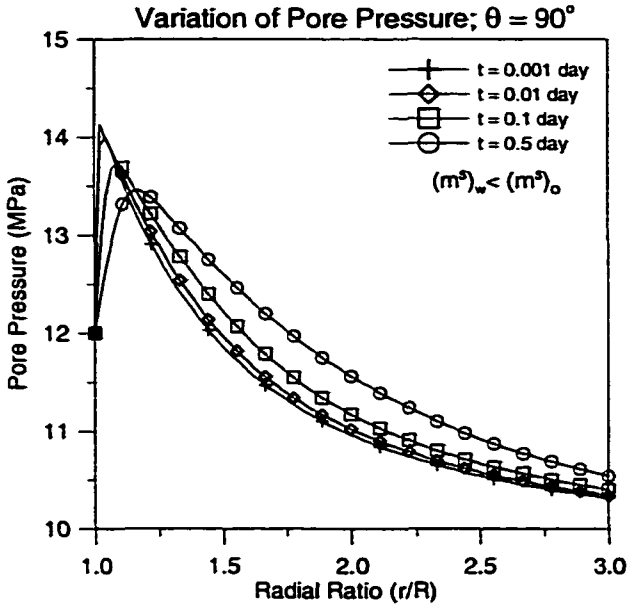


Figure 5.7: Pore pressure variation along $\theta = 90°$ ($m_w^s < m_o^s$) for $t = 0.001$, 0.01, 0.1 and 0.5 day

stress becomes more compressive with the passage of time.Figure 5.10 shows the effective tangential stress distribution varying the angle around the borehole at a radial distance $r/R = 1.05$. As seen from the figure, the minimum effective tangential stress, reduces with time indicating that the chemical effects introduce a delayed potential for fracturing.

Figures 5.11 shows the stress clouds for the case where $m_w^s < m_o^s$ for $t = 0.2$, 0.5 day at $r/R = 1.1$. Curves for both the poroelastic and porochemoelastic cases are shown. As seen from the figure, the cloud for the porochemoelastic case at $t = 0.2$ day is most critical curve with respect to shear failure. The reduction in the effective stresses due to the chemical effect results in a higher shear failure potential. However, with the passage of time, the porochemoelastic curves approach the corresponding poroelastic ones. Figure 5.12 shows the stress clouds at $r/R = 1.1$ for the case where $m_w^s > m_o^s$. As seen from the figure a higher solute concentration in the wellbore fluid has an initial stabilizing effect with reference to shear failure.

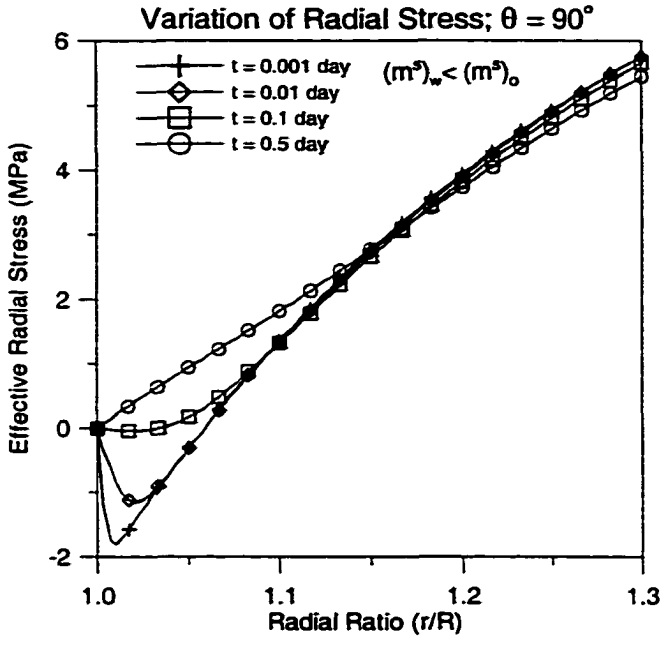


Figure 5.8: Effective radial stress variation along $\theta = 90°$ ($m_w^s < m_o^s$) for $t = 0.001$, 0.01, 0.1 and 0.5 day

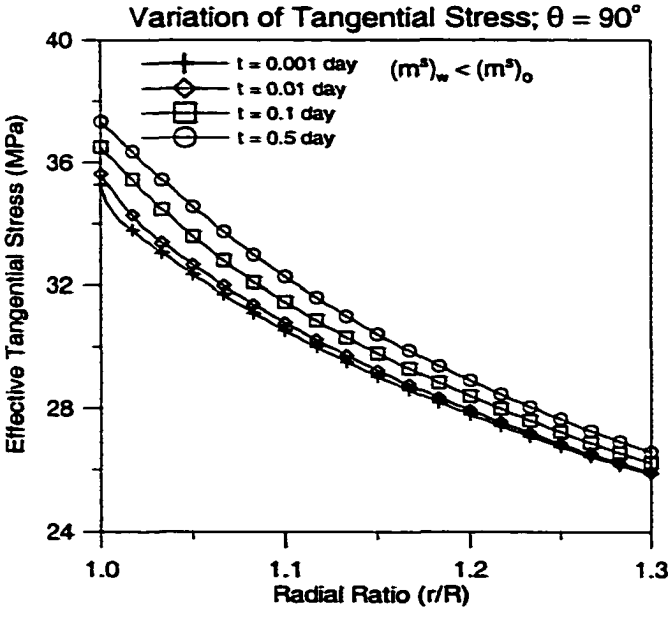


Figure 5.9: Effective tangential stress variation along $\theta = 90°$ ($m_w^s < m_o^s$) for $t = 0.001$, 0.01, 0.1 and 0.5 day

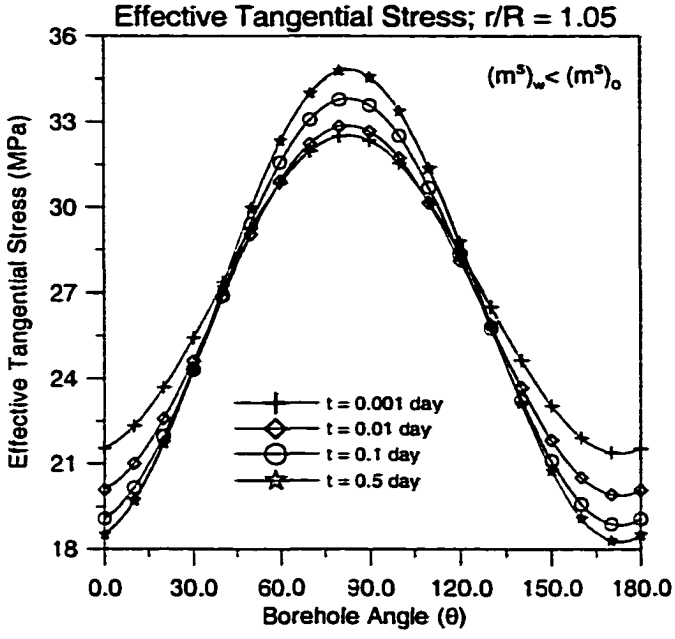


Figure 5.10: Effective tangential stress varying with angle around the borehole for $r/R = 1.05$

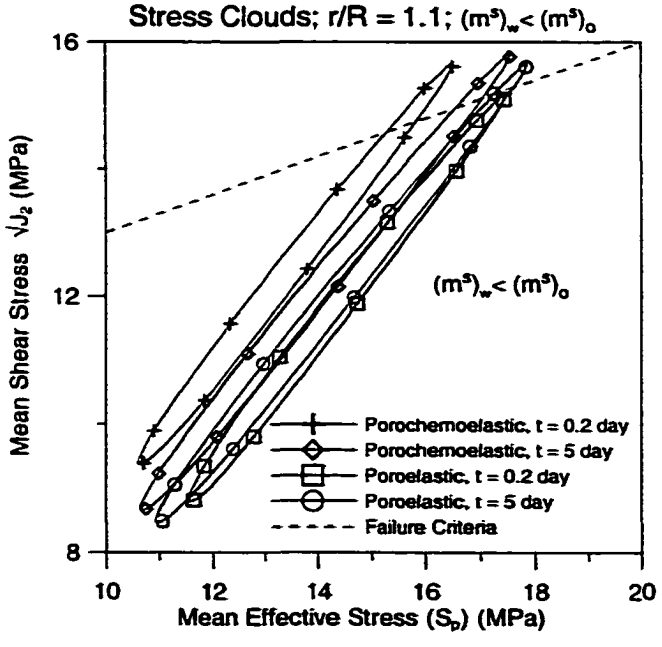


Figure 5.11: Stress clouds at $r/R = 1.1$ for $t = 0.2$, 0.5 day for the porochemoelastic model ($m_w^s < m_o^s$) compared with the poroelastic model

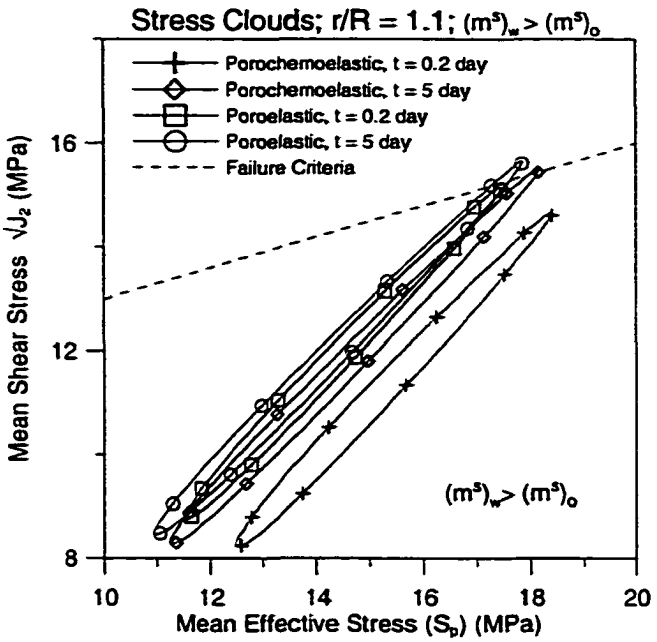


Figure 5.12: Stress clouds at $r/R = 1.1$ for $t = 0.2$, 0.5 day for the porochemoelastic model ($m_w^s > m_o^s$) compared with the poroelastic model

## 5.7 Summary

A generalized anisotropic porochemoelastic formulation has been presented in this chapter. The porochemoelastic model is formulated as an extension of Biot's poroelastic model to account for the chemically active nature of rock formations. The anisotropic equations were specialized for transversely isotropic and isotropic materials. Field equations (Navier-type equations, and a set of coupled diffusion equations) were developed for both cases. The solution for an inclined borehole problem under the framework of the porochemoelastic model has been presented.

The chemical effect on stress and pore pressure distributions in the vicinity of a borehole has been examined. An axisymmetric simplified problem has been presented wherein conditions imposed were such that results show a modification in the stress and pore pressure profiles purely due to a chemical effect. A higher chemical potential of

water in the wellbore fluid results in an increase in the pore pressure close to the wellbore wall. In addition, the model has been applied to the problem of an inclined borehole. In this case, the chemically induced pore pressure results in tensile effective radial stresses close to the borehole wall. This implies an increased potential for failure by spalling at early time. The minimum effective tangential stress, on the other hand, reduces with time indicating a delayed potential for fracturing. The stress clouds indicate a higher potential for shear failure that progressively reduces when the solute concentration in the wellbore fluid is lower. On the other hand, increasing solute concentration in the wellbore fluid has an initial stabilizing effect on the borehole.

# Chapter 6

# Anisotropic Porochemothermoelasticity

## 6.1 Introduction

Over the past few years, research efforts in understanding the mechanics of fluid saturated porous media have culminated in the identification of various driving forces that contribute in affecting behavior patterns (*Yeung and Mitchell*, 1993). Broadly termed as the physicochemical processes, each has a unique effect and, at the same time, the effects of cross-interactions (between various driving forces), result in a coupled response (*Yeung and Mitchell*, 1993; *Huyghe and Janssen*, 1999; *Li and Li*, 1992; *Yuan and Abousleiman*, 1995). In fact, the mathematical complexities involved in representing these complex coupled mechanisms, restrict their assessment, even though they may be known to exist. For example, over 90% drilling projects associated with oil and gas exploration, are usually carried out in shale formations which can be broadly classified as chemically active (*Mody and Hale*, 1993). Shales are host to a variety of chemical effects primarily attributed to their swelling behavior (*Mitchell*, 1993; *Heidug and Wong*, 1996). In addition, shales are clay-rich bearing a low permeability and diffusivity thereby naturally exhibiting coupling between the mechanical and hydraulic processes and appropriately addressed by Biot's theory of poroelasticity (*Biot*, 1941; *Coussy*, 1991, 1995). At the same time, drilling activities are often carried out under non-isothermal

conditions and the effect of thermal gradients comes into play. In fact, all of the aforementioned processes interact in a coupled manner affecting stress distributions, pore pressure profiles and flow patterns and ultimately affecting the stability of the drilled wells. Despite its significance from a practical viewpoint, a comprehensive formulation which addresses the coupled interplay between the mechanical, hydraulic, chemical and thermal processes, has not been pursued.

The thermo-hydro-mechanical effects on the response of porous media have been successfully studied under the porothermoelastic model (*Bear and Corapcioglu*, 1981; *McTigue*, 1986, 1990; *Coussy*, 1989, 1995; *Abousleiman and Ekbote*, 2002). When viewed at the microscale, thermal gradients result in differential expansion or contraction of the constituents within a fluid saturated porous medium. The volume changes associated with the expansion/contraction lead to a modification of the stress and pore pressure distributions. On the other hand, as a first approximation, the chemical effects are woven into a poromechanics formulation using the concept of a chemical potential and membrane efficiency (*Sherwood*, 1993, *Abousleiman et al.*, 2001). This approach has been successfully applied in estimating the swelling effects on stress and pore pressure distributions in the vicinity of deep wellbores (*Sherwood and Bailey*, 1994; *Abousleiman et al.*, 2001, 2002).

In a more rigorous approach, the chemical effects are addressed by considering a pore fluid comprised of two constituents i.e., the solute and solvent, and appropriately accounting for the interaction between the two-component pore fluid and porous matrix (*Sherwood*, 1994a). The chemical effects are due to the interaction between the matrix and constituents within the pore fluid. The presence of both thermal and chemical gradients would affect the engineering design estimates of mudweights and salt concentrations relevant to deep drilling projects carried out in shale formations.

In addition, the anisotropic nature of rock formations, where these activities are

carried out, presents an additional challenge in predicting appropriate behavior. Comprehensive formulations for anisotropic poroelasticity and porothermoelasticity have been addressed and the material characterizations introduced by the anisotropy, have been linked to well understood engineering constants (*Abousleiman and Cui*, 2000; *Abousleiman and Ekbote*, 2002). Subsequently analytical solutions for a variety of fundamental problems have been developed in anisotropic poroelasticity (*Abousleiman et al.*, 1995, 1996a; *Abousleiman and Cui*, 1998) and anisotropic porothermoelasticity (*Abousleiman and Ekbote* 1999, 2002). Indeed, the anisotropic nature of rock formations, their chemically active nature, presence of non-isothermal drilling conditions and the interplay between the aforementioned factors, have a bearing upon the stability assessment of wellbores drilled in such formations.

In this chapter, the focus is on the development of a poromechanics model which addresses the chemical effects within the framework of the anisotropic porothermoelastic model (*Abousleiman and Ekbote*, 2002). The resulting model, termed as porochemothermoelastic, accounts for fully coupled hydro-thermo-chemo-mechanical response of a chemically active formation saturated with a pore fluid comprising of '$n$' species under non-isothermal conditions. Figure 6.1 shows the resulting physicochemical processes and the interactions between them addressed in this work. The general anisotropic equations are first presented which are specialized for the transversely isotropic and isotropic cases. Governing equations are developed for the transversely isotropic and isotropic cases. The solution for an inclined borehole in a transversely isotropic chemically active porous formation subjected to non-isothermal conditions is presented. The corresponding isotropic solution presented in the Appendix. Numerical examples included demonstrate the thermo-chemical effect on the stress and pore pressure distributions in the vicinity of a borehole and its eventual impact on borehole stability.

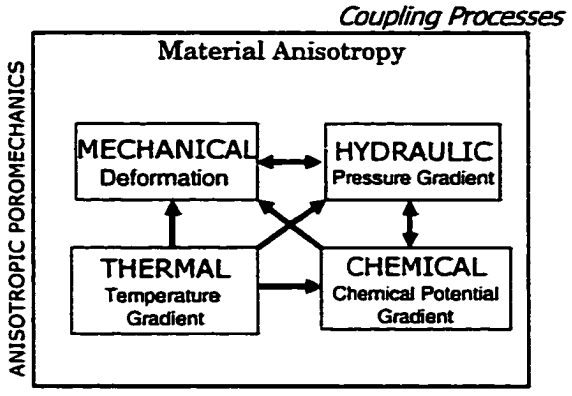


Figure 6.1: The physicochemical coupling processes

## 6.2 General Formulation

The porochemothermoelastic model is formulated by extending the porochemoelastic model to incorporate thermal effects. With the introduction of boundary temperatures, i.e., a non-isothermal state, both the pore fluid and pore volume are subject to differential expansion or contraction resulting in additional coupling associated with the temperature change. Here we consider a porous system saturated by a pore fluid containing two chemical species; a solute and a solvent with mole fractions $\bar{m}^s$ and $\bar{m}^w$, respectively. A temperature perturbation affects both the strain of the solid matrix as well as the mass fraction of each of the chemical species in the pore fluid due to differential expansion or contraction rates. The thermal gradient introduces an additional flux component associated with heat flow. In addition, the solvent flux is also modified due to the presence of a thermal gradient (thermo-osmosis). The system is subject to conservation laws of mass, momentum and energy balance. The chemical potentials of the two species are given by (*Sherwood*, 1993)

$$\mu^s = pV_s + R\bar{T}\ln(\varrho^s\bar{m}^s) \tag{6.1}$$

$$\mu^w = pV_w + R\bar{T}\ln(\varrho^w\bar{m}^w) \tag{6.2}$$

where $\mu^s$ and $\mu^w$ are the chemical potentials for the solute and solvent, $V_s$ and $V_w$ are the partial molar volumes of the solute and solvent, $p$ is the thermodynamic pore pressure, $R$ is the universal gas constant, $\bar{T}$ is the average temperature, $\varrho^s$ and $\varrho^w$ are the activity coefficients of the solute and the solvent, and $\bar{m}^w = 1 - \bar{m}^s$. The solution is assumed to be ideal with $\varrho^s = \varrho^w = 1$. In the following sections we develop a full set of governing equations for the porochemothermoelastic model.

*Constitutive Equations*

The constitutive equations, as in the porochemoelastic model, comprise of the stress-strain relations and equations for variation in content for each species due to perturbation. The constitutive equations for the anisotropic porochemothermoelastic model are given by

$$\sigma_{ij} = M_{ijkl}\epsilon_{kl} - \alpha_{ij}p - \beta^s_{ij}T + \gamma^s_{ij}m^s \tag{6.3}$$

$$\zeta^s = \bar{m}^s\left[\frac{p}{M} + \alpha_{ij}\epsilon_{ij} - \beta^{sf}T\right] + \bar{\beta}^c\frac{V_{sol}}{V_s}m^s \tag{6.4}$$

$$\zeta^w = (1 - \bar{m}^s)\left[\frac{p}{M} + \alpha_{ij}\epsilon_{ij} - \beta^{sf}T\right] - \bar{\beta}^c\frac{V_{sol}}{V_w}m^s \tag{6.5}$$

where $\sigma_{ij}$ is the total stress tensor, $\epsilon_{ij}$ is the solid strain tensor, $\zeta^s$ is the variation of solute content, $\zeta^w$ is the variation of the solvent content, $p$ is the pore pressure, $T$ is the temperature, $m^s$ is the variation of the solute mole fraction, $\bar{m}^s$ is the initial solute molar fraction, $M_{ijkl}$ is the drained elastic modulus tensor, $M$ is Biot's modulus, $\alpha_{ij}$ is the Biot's effective stress coefficient tensor, $\gamma^s_{ij}$ is the chemo-mechanical coupling coefficient tensor, $\bar{\beta}^c$ is hydro-mechanical coupling coefficient, $\beta^s_{ij}$ is the thermic coefficient tensor related to the solid skeleton, $\beta^{sf}$ is the thermic coefficient tensor related to the fluid constituent and $\delta_{ij}$ is the Kronecker delta. $\beta^s_{ij}$ is related to the expansion coefficients of the solid matrix $\alpha^s_{ij}$ and the relation is given by (*Abousleiman and Ekbote*, 2002)

$$\beta^s_{ij} = M_{ijkl}\alpha^s_{kl} \tag{6.6}$$

$\beta^{sf}$ is also related to the thermal expansion coefficients as follows (*Abousleiman and Ekbote*, 2002)

$$\beta^{sf} = \alpha_{ij}\alpha^{s}_{ij} + (\alpha^{f} - \alpha^{s}_{kk})\phi \tag{6.7}$$

where $\alpha^f$ is the volumetric expansion coefficient of the fluid and $\phi$ is the porosity.

*Transport Equations*

Transport equations are written for the fluxes of the solute, solvent and heat. The solute, solvent and heat flux can be caused by gradients in pressure, temperature and solute molar fraction. The solvent flux, herein, is assumed to be caused due to gradients in all the aforementioned driving forces. Thermo-osmosis effects are thus appropriately addressed. The solute flux, on the other hand, is assumed to be generated by gradients in pressure and the solute molar fraction. Finally, the heat flux is assumed to be generated only by a temperature gradient. Accordingly, transport equations for the solute flux, solvent flux and heat flux are given by

$$q^{s}_{i} = -(1-\chi)\left[\bar{m}^{s}\kappa_{ij}p_{,j} + D_{ij}m^{s}_{,j}\right] \tag{6.8}$$

$$q^{w}_{i} = -(1-\bar{m}^{s})\kappa_{ij}p_{,j} + \frac{1}{V_w}\left[\chi R\bar{T}\kappa_{ij} + (1-\chi)V_s D_{ij}\right]m^{s}_{,j} + D^{T}_{ij}T_{,j} \tag{6.9}$$

$$q^{h}_{i} = -\lambda_{ij}T_{,j} \tag{6.10}$$

where $q^s_i$ is the solute flux, $q^w_i$ is the solvent flux, $q^h_i$ is the heat flux, $\kappa_{ij}$ is the mobility coefficient tensor, $D_{ij}$ is the solute diffusivity tensor, $D^T$ is a phenomenological coefficient tensor associated with thermo-osmosis, $\chi$ is the reflection coefficient and $\lambda_{ij}$ is the thermal conductivity tensor.

*Conservation Laws*

The system is subject to balance laws for mass, momentum and energy. Momentum balance yields the equilibrium equations which are given by

$$\sigma_{ij,j} = 0 \tag{6.11}$$

Mass balance is applied individually for the solute and the solvent and the equations for the same are given as

$$\frac{\partial \zeta^s}{\partial t} + \nabla \cdot q_i^s = 0 \tag{6.12}$$

$$\frac{\partial \zeta^w}{\partial t} + \nabla \cdot q_i^w = 0 \tag{6.13}$$

Equations (6.11) - (6.13) are written ignoring any body forces, sources or sinks. It is assumed that the heat transport between the matrix and the pore fluid at the local level is much faster than the overall heat diffusion process. In other words, it is assumed that a local equilibrium of temperatures within various components of the pore fluid and the matrix is instantaneously established. The energy balance equation is given as (*Bird et al.*, 1960; *Bear and Corapcioglu*, 1981)

$$\rho C_v \frac{\partial T}{\partial t} = -\nabla \cdot q_i^h - \left(\rho C_v \left(q_i^s + q_i^w\right)\right) \cdot \nabla T \tag{6.14}$$

where $\rho C_v$ is the heat capacity of the matrix-pore fluid mixture. In addition, we assume that the porous material bears a low fluid diffusivity and that the heat diffusion occurs much faster than the fluid diffusion. Under these circumstances, the term corresponding to convection can be dropped from equation (6.14) resulting in a linearized form of the energy balance given by:

$$\rho C_v \frac{\partial T}{\partial t} + \nabla \cdot q_i^h = 0 \tag{6.15}$$

The 'bulk heat capacity', $\rho C_v$, and thermal conductivity, $\lambda$, are related to individual heat capacities of the matrix, solute and solvent

$$\rho C_v = (1-\phi)\rho^m C_v^m + \phi\left[(1-\bar{m}^s)\rho^f C_v^f + \bar{m}^s \rho^s C_v^s\right] \tag{6.16}$$

$$\lambda_{ij} = (1-\phi)\lambda_{ij}^m + \phi\left[(1-\bar{m}^s)\lambda^f + \bar{m}^s \lambda^s\right]\delta_{ij} \tag{6.17}$$

in which the superscripts $m$, $s$ and $f$ refer to the matrix, solute and solvent, respectively and $\delta_{ij}$ is the Kronecker delta.

The above set of equations (6.1) - (6.17) represent the anisotropic porochemothermoelastic model applicable to a porous media saturated with a pore fluid consisting of two species. These equations are specialized for the transversely isotropic case in the next section

## 6.3 Transversely Isotropic Porochemothermoelasticity

It is assumed that the $z$-axis coincides with the axis of material rotational symmetry of a transversely isotropic material. The transversely isotropic material bears an isotropic plane $(x-y)$ and a transverse direction ($z$-axis) along which the material properties are different. The constitutive relations given by equations (6.3) - (6.5) are specialized for transversely isotropic media as follows

$$\sigma_{xx} = M_{11}\epsilon_{xx} + M_{12}\epsilon_{yy} + M_{13}\epsilon_{zz} - \alpha p - \beta^s T + \gamma^s m^s \tag{6.18}$$

$$\sigma_{yy} = M_{12}\epsilon_{xx} + M_{11}\epsilon_{yy} + M_{13}\epsilon_{zz} - \alpha p - \beta^s T + \gamma^s m^s \tag{6.19}$$

$$\sigma_{zz} = M_{13}\epsilon_{xx} + M_{13}\epsilon_{yy} + M_{33}\epsilon_{zz} - \alpha' p - \beta^{s'} T + \gamma^{s'} m^s \tag{6.20}$$

$$\tau_{xy} = G\gamma_{xy}; \qquad \tau_{yz} = G'\gamma_{yz}; \qquad \tau_{zx} = G'\gamma_{zx} \tag{6.21}$$

$$\zeta^s = \bar{m}^s \left[\frac{p}{M} + \alpha(\epsilon_{xx} + \epsilon_{yy}) + \alpha'(\epsilon_{zz}) - \beta^{sf} T\right] + \bar{\beta}^c \frac{V_{sol}}{V_s} m^s \tag{6.22}$$

$$\zeta^w = (1 - \bar{m}^s) \left[\frac{p}{M} + \alpha(\epsilon_{xx} + \epsilon_{yy}) + \alpha'(\epsilon_{zz}) - \beta^{sf} T\right] - \bar{\beta}^c \frac{V_{sol}}{V_w} m^s \tag{6.23}$$

The two-dimensional $(x-y)$ plane form of these equations will be used in obtaining solutions based on the generalized plane strain conditions. For a plane $(x-y)$ case, the constitutive equations are written as

$$\sigma_{xx} = M_{11}\epsilon_{xx} + M_{12}\epsilon_{yy} - \alpha p - \beta^s T + \gamma^s m^s \tag{6.24}$$

$$\sigma_{xy} = M_{12}\epsilon_{xx} + M_{11}\epsilon_{yy} - \alpha p - \beta^s T + \gamma^s m^s \tag{6.25}$$

where $\alpha$ is the Biot's effective stress coefficient, $\beta^s$ is the thermic coefficient related to the solid matrix, and $\gamma^s$ is the chemo-mechanical coupling coefficient, all of which are properties in the isotropic plane. The equations for variation of solute content and solvent content are given by

$$\zeta^s = \frac{\alpha \bar{m}^s}{(M_{11}+M_{12})}\left[\sigma_{kk} + \frac{(M_{11}+M_{12}+2\alpha^2 M)}{\alpha M}p\right] - \beta^{sm}T + \beta^c \frac{V_{sol}}{V_s}m^s \tag{6.26}$$

$$\zeta^w = \frac{\alpha(1-\bar{m}^s)}{(M_{11}+M_{12})}\left[\sigma_{kk} + \frac{(M_{11}+M_{12}+2\alpha^2 M)}{\alpha M}p\right] - \beta^{fm}T - \beta^c \frac{V_{sol}}{V_w}m^s \tag{6.27}$$

where $\beta^{sm}$, $\beta^{fm}$ are thermic coefficients given by

$$\beta^{sm} = (\alpha^p - \alpha^s_{kk})\phi \tag{6.28}$$

$$\beta^{fm} = (\alpha^f - \alpha^s_{kk})\phi \tag{6.29}$$

where $\alpha^p$ is the volumetric expansion coefficient for the solute, $\alpha^f$ is the volumetric expansion coefficient for the solvent and $\alpha^s_{ij}$ is the linear expansion coefficient of solid matrix. Equations (6.24) and (6.25) are combined the equilibrium equations to give the Navier-type equations. These are expressed as

$$\frac{1}{2}(M_{11}-M_{12})u_{i,jj} + \frac{1}{2}(M_{11}+M_{12})u_{j,ji} = \alpha p_{,i} + \beta^s T_{,i} - \gamma^s m^s_{,i} \quad (i,j=1,2) \tag{6.30}$$

Following Rice and Cleary (1976), the Beltrami-Michell compatibility equations are given as

$$\nabla^2\left(\sigma_{xx}+\sigma_{xy} + \alpha\left(1-\frac{M_{12}}{M_{11}}\right)p + \beta^s\left(1-\frac{M_{12}}{M_{11}}\right)T - \gamma^s\left(1-\frac{M_{12}}{M_{11}}\right)m^s\right) = 0 \tag{6.31}$$

The transport equations are written for the plane $(x-y)$ case as follows

$$q^s_i = -(1-\chi)\left[\bar{m}^s \kappa p_{,i} + D m^s_{,i}\right] \tag{6.32}$$

$$q^w = -(1-\bar{m}^s)\kappa p_{,i} + \frac{1}{V_w}\left[\chi R\bar{T}\kappa + (1-\chi)V_s D\right] m^s_{,i} + D^T T_{,i} \tag{6.33}$$

$$q^h = \lambda T_{,i} \tag{6.34}$$

where $\kappa$, $\lambda$, $D$, and $D^T$are the mobility coefficient, thermal conductivity, solute diffusivity and thermo-osmotic coefficient respectively in the isotropic $x-y$ plane. Energy conservation yields the heat diffusion equation given as follows

$$\frac{\partial T}{\partial t} - c_h \nabla^2 T = 0 \tag{6.35}$$

where $c_h$ is the heat diffusivity in the isotropic plane and is given by

$$c_h = \frac{\lambda}{\rho C_v} \tag{6.36}$$

Mass conservation for the solute yields

$$\frac{\alpha \bar{m}^s}{(M_{11}+M_{12})}\left[\frac{\partial \sigma_{kk}}{\partial t} + \frac{(M_{11}+M_{12}+2\alpha^2 M)}{\alpha M}\frac{\partial p}{\partial t}\right] - \beta^{fm}\frac{\partial T}{\partial t} + \beta^c \frac{V_{sol}}{V_s}\frac{\partial m^s}{\partial t}$$
$$= (1-\chi)\left[\bar{m}^s \kappa \nabla^2 p + D\nabla^2 m^s\right] \tag{6.37}$$

Similarly solvent mass conservation yields

$$\frac{\alpha(1-\bar{m}^s)}{(M_{11}+M_{12})}\left[\frac{\partial \sigma_{kk}}{\partial t} + \frac{(M_{11}+M_{12}+2\alpha^2 M)}{\alpha M}\frac{\partial p}{\partial t}\right] - (1-\bar{m}^s)\beta^{fm}\frac{\partial T}{\partial t}$$
$$-\beta^c \frac{V_{sol}}{V_w}\frac{\partial m^s}{\partial t} = (1-\bar{m}^s)\kappa\nabla^2 p - \frac{1}{V_w}\left[\chi R\bar{T} + (1-\chi)V_s D\right]\nabla^2 m^s - D^T\nabla^2 T \tag{6.38}$$

Utilizing equation (6.31) in equations (6.37) and (6.38)

$$\frac{\alpha}{(M_{11}+M_{12})}\frac{\partial \Theta}{\partial t} + \frac{\beta^c V_{sol}}{\bar{m}^s V_s}\frac{\partial m^s}{\partial t} = \left[\frac{(1-\chi)\kappa\alpha M M_{11}}{(\alpha^2 M + M_{11})(M_{11}+M_{12})}\right]\nabla^2\Theta$$
$$+\left[\gamma^s\left(1-\frac{M_{12}}{M_{11}}\right)\frac{(1-\chi)\kappa\alpha M M_{11}}{(\alpha^2 M + M_{11})(M_{11}+M_{12})} + \frac{(1-\chi)D}{\bar{m}^s}\right]\nabla^2 m^s + Q_1\frac{\partial T}{\partial t} \tag{6.39}$$

$$\frac{\alpha}{(M_{11}+M_{12})}\frac{\partial \Theta}{\partial t} - \frac{\beta^c V_{sol}}{\bar{m}^s V_w}\frac{\partial m^s}{\partial t} = \left[\frac{\kappa\alpha M M_{11}}{(\alpha^2 M + M_{11})(M_{11}+M_{12})}\right]\nabla^2\Theta$$
$$+\left[\gamma^s\left(1-\frac{M_{12}}{M_{11}}\right)\frac{\kappa\alpha M M_{11}}{(\alpha^2 M + M_{11})(M_{11}+M_{12})} - \frac{\left[\chi R\bar{T}\kappa + (1-\chi)V_s D\right]}{(1-\bar{m}^s)V_w}\right]\nabla^2 m^s$$
$$+Q_2\frac{\partial T}{\partial t} \tag{6.40}$$

where $\Theta$ is given by

$$\Theta = \sigma_{kk} + \frac{(M_{11} + M_{12} + 2\alpha^2 M)}{\alpha M} p \tag{6.41}$$

and $Q_1$ and $Q_2$ are given by

$$Q_1 = \left[ (1-\chi) \frac{4G\kappa(\nu_u - \nu)}{3\alpha(1-2\nu)(1-\nu_u)} \frac{\alpha^m}{c_h} + \beta^{sm} \right] \tag{6.42}$$

$$Q_2 = \left[ \frac{4G\kappa(\nu_u - \nu)}{3\alpha(1-2\nu)(1-\nu_u)} \frac{\alpha^m}{c_h} - \frac{D^T}{c_h} + \beta^{fm} \right] \tag{6.43}$$

With some manipulation equations (6.39) and (6.40) are modified to give a set of coupled non-homogeneous diffusion equations given by

$$\frac{\partial \Theta}{\partial t} = Y_1 \nabla^2 \Theta + Y_2 \nabla^2 m^s + Y_3 \frac{\partial T}{\partial t} \tag{6.44}$$

$$\frac{\partial m^s}{\partial t} = Z_1 \nabla^2 \Theta + Z_2 \nabla^2 m^s + Z_3 \frac{\partial T}{\partial t} \tag{6.45}$$

where the coefficients $Y_1$, $Y_2$, $Y_3$, $Z_1$, $Z_2$ and $Z_3$ are given by

$$Y_1 = \frac{\kappa M M_{11}}{(\alpha^2 M + M_{11}) V_{sol}} \left[ V_{sol} - \chi \bar{m}^s V_s \right] \tag{6.46}$$

$$Y_2 = \gamma^s \left( 1 - \frac{M_{12}}{M_{11}} \right) \frac{\kappa M M_{11}}{(\alpha^2 M + M_{11}) V_{sol}} \left[ V_{sol} - \chi \bar{m}^s V_s \right] - \frac{(M_{11} + M_{12}) \chi R \bar{T} \kappa}{\alpha V_{sol}} \tag{6.47}$$

$$Y_3 = \frac{(M_{11} + M_{12})}{\alpha} \left[ \frac{Q_1 \bar{m}^s V_s + Q_2 (1 - \bar{m}^s) V_w}{V_{sol}} \right] \tag{6.48}$$

$$Z_1 = -\frac{\chi \kappa \alpha M M_{11}}{(\alpha^2 M + M_{11})(M_{11} + M_{12})} \frac{\bar{m}^s (1 - \bar{m}^s) V_s V_w}{\beta^c V_{sol}^2} \tag{6.49}$$

$$Z_2 = \frac{V_s}{\beta^c V_{sol}^2} \left[ (1-\chi) D V_{sol} + \chi R \bar{T} \kappa \bar{m}^s \right] \tag{6.50}$$

$$Z_3 = [Q_1 - Q_2] \left[ \frac{\bar{m}^s (1 - \bar{m}^s) V_s V_w}{\beta^c V_{sol}^2} \right] \tag{6.51}$$

We define $n_1$, $n_2$, $c_1$, $c_2$, $l_1$, $l_2$ as follows

$$n_{1,2} = \frac{(Z_2 - Y_1) \pm \sqrt{(Z_2 - Y_1)^2 + 4 Y_2 Z_1}}{2 Z_1} \tag{6.52}$$

$$c_{1,2} = \frac{\left[ (Z_2 + Y_1) \pm \sqrt{(Z_2 - Y_1)^2 + 4 Y_2 Z_1} \right]}{2} \tag{6.53}$$

$$l_{1,2} = Y_3 + n_{1,2} Z_3 \tag{6.54}$$

Using equations (6.52) - (6.54) the coupled diffusion equations (6.44) and (6.45) can be combined to give

$$\frac{\partial}{\partial t}(\Pi_i) - c_i \nabla^2 (\Pi_i) = l_i \frac{\partial T}{\partial t}; \quad i = 1, 2 \tag{6.55}$$

where $\Pi_i = \Theta + n_i m^s$. Equation (6.55) gives a set of coupled non-homogeneous diffusion equations where $n_1$, $n_2$, $c_1$, and $c_2$ are given by

$$n_1 \approx \frac{(M_{11} + M_{12})}{\alpha} \frac{\beta^c V_{sol}^2}{\chi \bar{m}^s V_s V_w} \tag{6.56}$$

$$n_2 \approx -\frac{(\alpha^2 M + M_{11})(M_{11} + M_{12})}{\alpha M M_{11}} \frac{\chi R \bar{T}}{V_{sol}} \tag{6.57}$$

$$c_1 \approx \frac{V_s}{\beta^c V_{sol}^2} \left[ (1 - \chi) D V_{sol} + \chi R \bar{T} \kappa \bar{m}^s \right] \tag{6.58}$$

$$c_2 \approx \frac{\kappa M M_{11}}{(\alpha^2 M + M_{11})} \tag{6.59}$$

The Navier-type equations (6.30), the heat diffusion equation (6.35) and the coupled diffusion equations (6.55) constitute a set of field equations.

## 6.4 Isotropic Porochemothermoelasticity

For an isotropic material, the constitutive equations for porochemothermoelasticity are given as

$$\sigma_{ij} = 2G\epsilon_{ij} + \frac{2G\nu}{1 - 2\nu} \epsilon \delta_{ij} - \alpha p \delta_{ij} - \beta^s T \delta_{ij} + \gamma m^s \delta_{ij} \tag{6.60}$$

$$\zeta^s = \frac{\alpha(1 - 2\nu)\bar{m}^s}{2G(1 + \nu)} \left[ \sigma_{kk} + \frac{3p}{B} \right] - \beta^{sm} T + \beta^c \frac{V_{sol}}{V_s} m^s \tag{6.61}$$

$$\zeta^w = \frac{\alpha(1 - 2\nu)(1 - \bar{m}^s)}{2G(1 + \nu)} \left[ \sigma_{kk} + \frac{3p}{B} \right] - \beta^{fm} T - \beta^c \frac{V_{sol}}{V_w} m^s \tag{6.62}$$

where $G$ is the shear modulus, $\nu$ is the Poisson's ratio, $\alpha$ is the Biot's effective stress coefficient, $B$ is the Skempton's coefficient.

Following the approach outlined in the previous section, the governing equations for isotropic porochemothermoelasticity are given as

$$G\nabla^2 u_i + \frac{G}{1-2\nu} u_{k,ki} = \alpha p_{,i} + \beta^s T_{,i} - \gamma^s m^s_{,i} \tag{6.63}$$

$$\frac{\partial T}{\partial t} - c_h \nabla^2 T = 0 \tag{6.64}$$

$$\frac{\partial}{\partial t}(\Pi_i) - c_i \nabla^2 (\Pi_i) = l_i \frac{\partial T}{\partial t}; \quad i = 1, 2 \tag{6.65}$$

where $n_1$, $n_2$, $c_1$, and $c_2$ for the isotropic case are as follows

$$n_1 \approx \frac{2G(1+\nu)}{\alpha(1-2\nu)} \frac{\beta^c V_{sol}^2}{\chi \bar{m}^s V_s V_w} \tag{6.66}$$

$$n_2 \approx -\frac{2\eta(1+\nu)(1-\nu_u)}{(\nu_u - \nu)} \frac{\chi R\bar{T}}{V_{sol}} \tag{6.67}$$

$$c_1 \approx \frac{V_s}{\beta^c V_{sol}^2} \left[(1-\chi) D V_{sol} + \chi R\bar{T}\kappa\bar{m}^s\right] \tag{6.68}$$

$$c_2 \approx \frac{G\kappa(\nu_u - \nu)}{\alpha\eta(1-2\nu)(1-\nu_u)} \tag{6.69}$$

We consider the application of the porochemothermoelastic model to the inclined borehole problem.

## 6.5 Inclined Borehole Problem

Solution for the inclined borehole problem under transversely isotropic porochemothermoelasticity is presented in this section. Corresponding isotropic solutions are included in the Appendix E. The borehole is assumed to be infinitely long and inclined with respect to the in-situ three-dimensional state of stress. The axis of the borehole is assumed to be perpendicular to the plane of isotropy of the transversely isotropic formation. As

explained in Chapter 3, a transformation of the far-field in-situ stress to a local borehole coordinate system is carried out, and in the local coordinate system the borehole is subjected to normal as well as shear components of stress.

The boundary conditions for the inclined borehole problem, discussed in Chapter 3, are specialized for the porochemothermoelastic problem. The boundary conditions of the problem at the far field, $r \rightarrow \infty$, are as follows

$$\sigma_{xx} = -S_x; \quad \sigma_{yy} = -S_y; \quad \sigma_{zz} = -S_z; \tag{6.70}$$

$$\tau_{xy} = -S_{xy}; \quad \tau_{yz} = -S_{yz}; \quad \tau_{xz} = -S_{xz}; \tag{6.71}$$

$$p = p_o; \quad m^s = m^s_o; \quad T = T_o \tag{6.72}$$

and at the borehole wall, $r = R$,

$$\sigma_{rr} = -p_w H(t); \quad \tau_{r\theta} = \tau_{rz} = 0; \tag{6.73}$$

$$p = p_w H(t); \quad m^s = m^s_w H(t); \quad T = T_w H(t); \tag{6.74}$$

where $p_w$ is the wellbore fluid pressure, $m^s_w$ is the solute molar fraction in the wellbore fluid, $T_w$ is the wellbore fluid temperature and $H(t)$ is the Heaviside unit step function.

*Problem Decomposition*

Following the decomposition scheme discussed in Chapter 3, the inclined borehole problem is sub-divided into three sub-problems.

The boundary conditions in the decomposition scheme are given as follows:

**Problem 1:**

At far field ( $r \rightarrow \infty$)

$$\sigma_{xx} = -S_x; \quad \sigma_{yy} = -S_y; \quad \tau_{xy} = -S_{xy}; \quad \tau_{yz} = \tau_{xz} = 0 \tag{6.75}$$

$$\sigma_{zz} = -\nu'(S_x + S_y) - (\alpha' - 2\nu'\alpha)p_o - (\beta^{s'} - 2\nu'\beta^s)T_o + (\gamma^{s'} - 2\nu'\gamma^s)m^s_o \tag{6.76}$$

$$p = p_o; \quad m^s = m^s_o; \quad T = T_o \tag{6.77}$$

At the borehole wall ($r = R$)

$$\sigma_{rr} = -p_w H(t); \qquad p = p_w H(t) \tag{6.78}$$

$$m^s = m_o^s H(t); \qquad T = T_w H(t) \tag{6.79}$$

**Problem 2:**

At far field ( $r \rightarrow \infty$)

$$\sigma_{zz} = -S_z + [\nu'(S_x + S_y) + (\alpha' - 2\nu'\alpha)p_o + (\beta^{s'} - 2\nu'\beta^s)T_o - (\gamma^{s'} - 2\nu'\gamma^s)m_o^s] \tag{6.80}$$

$$\sigma_{xx} = \sigma_{yy} = \tau_{xy} = \tau_{yz} = \tau_{xz} = p = m^s = T = 0 \tag{6.81}$$

At borehole wall ($r = R$)

$$\sigma_{rr} = \tau_{r\theta} = \tau_{rz} = p = m^s = T = 0 \tag{6.82}$$

**Problem 3:**

At far field ( $r \rightarrow \infty$)

$$\sigma_{xx} = \sigma_{yy} = \sigma_{zz} = \tau_{xy} = p = m^s = T = 0 \tag{6.83}$$

$$\tau_{xy} = -S_{xy}; \quad \tau_{yz} = -S_{yz} \tag{6.84}$$

At the borehole wall ($r = R$)

$$\sigma_{rr} = \tau_{r\theta} = \tau_{rz} = p = m^s = T = 0 \tag{6.85}$$

The complete solution for the inclined borehole problem in a transversely isotropic medium is given by equations (3.54) - (3.61) setting $\varpi_1 = 1, \varpi_2 = 1, \varpi_3 = 1$.

### 6.5.1 Permeable Boundary Condition Model

The boundary conditions at the borehole wall for the permeable boundary condition model are as follows:

*Case 1:*

$$\sigma_{rr}^{(1)} = P_o - p_w; \quad \sigma_{r\theta}^{(1)} = 0; \tag{6.86}$$

$$p^{(1)} = 0; \quad m^{s(1)} = 0; \quad T^{(1)} = 0 \tag{6.87}$$

*Case 2:*

$$\sigma_{rr}^{(2)} = 0; \quad \sigma_{r\theta}^{(2)} = 0; \tag{6.88}$$

$$p^{(2)} = (p_w - p_o); \quad m^{s(2)} = (m_w^s - m_o^s); \quad T^{(2)} = (T_w - T_o) \tag{6.89}$$

*Case 3:*

$$\sigma_{rr}^{(3)} = -S_o \cos 2(\theta - \theta_r) \tag{6.90}$$

$$\sigma_{r\theta}^{(3)} = S_o \sin 2(\theta - \theta_r) \tag{6.91}$$

$$p^{(3)} = 0; \quad m^{s(3)} = 0; \quad T^{(3)} = 0 \tag{6.92}$$

Solutions for the stresses, pore pressure, temperature and mole fraction for the three cases described above are presented.

**Solutions for Case 1:**

Case 1 is characterized by a hydrostatic state of stress with no effect on the pore pressure, temperature and solute mole fractions. The solution for $\sigma_{rr}^{(1)}$ and $\sigma_{\theta\theta}^{(1)}$ is purely elastic and is given by equations (B.1) - (B.2) in Appendix B.

**Solutions for Case 2:**

The perturbation in the pore pressure, temperature and the solute mole fraction are all incorporated into Case 2. Solutions are obtained by solving the heat diffusion equation (6.35) and the coupled non-homogeneous diffusion equations (6.55). The solution is time-dependent and is obtained in the Laplace domain and inverted to the time-domain using the Stehfest algorithm (*Stehfest*, 1970; *Davies and Martin*, 1979). Since the heat diffusion equation is uncoupled, solution for the temperature field is obtained as

$$s\bar{T}^{(2)} = (T_w - T_o)\Phi(\xi_3) \tag{6.93}$$

where ˜denotes the Laplace transform, $s$ is the Laplace transform parameter, $K_n$ is the modified Bessel function of the second kind of order n, $\xi_3 = \sqrt{s/c_h}$ and $\Phi$ is a function given by equation (B.8) in Appendix B. To obtain solutions for the stress and pore pressure fields we solve equation (6.55). Since equation (6.55) is non-homogeneous, the solution is written as a sum of the homogeneous and particular solutions. The homogeneous solution is given by for equation (6.55) is given by

$$\left(\tilde{\Theta} + n_i \tilde{m}^s\right)_h = D_i K_0(\xi_i r) \quad i = 1,2 \tag{6.94}$$

where $\xi_i = \sqrt{s/c_i}$ $(i = 1,2)$. The particular solution for equation (6.55) is given as

$$\left(\tilde{\Theta} + n_i \tilde{m}^s\right)_p = \frac{l_i}{1 - c_i/c_h} \tilde{T} \quad i = 1,2 \tag{6.95}$$

Hence from equations (6.94) and (6.95) we have

$$\tilde{\Theta} + n_i \tilde{m}^s = D_i K_0(\xi_i r) + \frac{l_i}{1 - c_i/c_h} \tilde{T} \quad i = 1,2 \tag{6.96}$$

Using equation (6.31) in equation (6.96) expressions for $\tilde{m}^s$, $\tilde{p}$ and $\tilde{\Theta}$ are obtained as

$$\begin{aligned} \tilde{m}^s = \frac{1}{(n_1 - n_2)} \{ & D_1 K_0(\xi_1 r) - D_2 K_0(\xi_2 r) \\ & \left[\frac{T_w - T_o}{s}\right] \left[\frac{l_1}{1 - c_1/c_h} - \frac{l_2}{1 - c_2/c_h}\right] \Phi(\xi_3) \Big\} \end{aligned} \tag{6.97}$$

$$\begin{aligned} \tilde{\Theta} = \frac{1}{(n_2 - n_1)} \{ & n_2 D_1 K_0(\xi_1 r) - n_1 D_2 K_0(\xi_2 r) \\ & + \left[\frac{T_w - T_o}{s}\right] \left[\frac{n_2 l_1}{1 - c_1/c_h} - \frac{n_1 l_2}{1 - c_2/c_h}\right] \Phi(\xi_3) \Big\} \end{aligned} \tag{6.98}$$

$$\begin{aligned} \tilde{p} = & \left[\frac{M M_{11}}{(\alpha^2 M + M_{11})}\right] \left[\frac{1}{(n_2 - n_1)}\right] \{ n_2 D_1 K_0(\xi_1 r) - n_1 D_2 K_0(\xi_2 r) \\ & + \left[\frac{T_w - T_o}{s}\right] \left[\frac{n_2 l_1}{1 - c_1/c_h} - \frac{n_1 l_2}{1 - c_2/c_h}\right. \\ & \left. + 2(n_2 - n_1) \beta^s \left(1 - \frac{M_{12}}{M_{11}}\right) + \Phi(\xi_3) \right\} \end{aligned} \tag{6.99}$$

Substituting boundary conditions yields the constants $D_1$ and $D_2$ as follows

$$D_i = \frac{1}{sK_0(\xi_i R)}\left[\frac{(\alpha^2 M + M_{11})}{M M_{11}}(p_w - p_o) + n_i(m_w^s - m_o^s)\right.$$
$$\left.\left(\frac{l_i}{1 - c_i/c_h} + 2\beta^s\left(1 - \frac{M_{12}}{M_{11}}\right)\right)(T_w - T_o)\right] \tag{6.100}$$

Generalized solutions for the solute mole fraction $\bar{m}^s$ and pore pressure $\bar{p}$ are obtained substituting expressions for $D_1$ and $D_2$ Following approximations are applied $n_1 >> n_2$ , $n_1 m^s >> p_w$ and $n_1 m^s >> T_w$ the solutions for $\bar{m}^s$ and $\bar{p}$ are obtained as

$$s\bar{m}^s = [(m_w^s - m_o^s)]\,\Phi(\xi_1) \tag{6.101}$$

$$\bar{p} = F_6\Phi(\xi_1) + F_7\Phi(\xi_2) + F_8\Phi(\xi_3) \tag{6.102}$$

where

$$F_6 = \left(\frac{\chi R\bar{T}}{V_w}\right)(m_w^s - m_o^s) \tag{6.103}$$

$$F_7 = \left[(p_w - p_o) - \left(\frac{\chi R\bar{T}}{V_w}\right)(m_w^s - m_o^s) - \left(\frac{c^{fT}}{1 - c_2/c_h}\right)(T_w - T_o)\right] \tag{6.104}$$

$$F_8 = \left(\frac{c^{fT}}{1 - c_2/c_h}\right)(T_w - T_o) \tag{6.105}$$

where $c^{fT}$ is given by

$$c^{fT} = \frac{c_2\alpha^m}{\kappa}\left[\frac{2\alpha}{3}\left(1 - \frac{M_{12}}{M_{11}}\right) + \left(\frac{\alpha^f}{\alpha^m} - 1\right)\phi - \frac{D^T}{c_h}\right] \tag{6.106}$$

The expressions for the radial and tangential stress are obtained as

$$s\bar{\sigma}_{rr}^{(2)} = \alpha\left(1 - \frac{M_{12}}{M_{11}}\right)\{F_6\Psi(\xi_1) + F_7\Psi(\xi_2) + F_8\Psi(\xi_3)\}$$
$$+\beta^s\left(1 - \frac{M_{12}}{M_{11}}\right)\{(T_w - T_o)\Psi(\xi_3)\}$$
$$-\gamma^s\left(1 - \frac{M_{12}}{M_{11}}\right)\{(m_w^s - m_o^s)\,\Psi(\xi_1)\} \tag{6.107}$$

$$s\bar{\sigma}_{\theta\theta}^{(2)} = -\alpha\left(1 - \frac{M_{12}}{M_{11}}\right)\{F_6\Omega(\xi_1) + F_7\Omega(\xi_2) + F_8\Omega(\xi_3)\}$$
$$-\beta^s\left(1 - \frac{M_{12}}{M_{11}}\right)\{(T_w - T_o)\Omega(\xi_3)\}$$
$$+\gamma^s\left(1 - \frac{M_{12}}{M_{11}}\right)\{(m_w^s - m_o^s)\,\Omega(\xi_1)\} \tag{6.108}$$

where $\Psi(x)$ and $\Omega(x)$ are given by equations (B.9) and (B.10) in Appendix B, respectively.

**Solutions for Case 3:**

Case 3 is characterized by an asymmetric state of stress. Excess pore pressure is induced due to the Skempton effect. However, there is no variation in the solute mole fraction or the temperature fields. Solutions for $\sigma_{rr}^{(3)}$, $\sigma_{\theta\theta}^{(3)}$, $\sigma_{r\theta}^{(3)}$, $p^{(3)}$ are the same as that for the transversely isotropic permeable poroelastic case (*Abousleiman and Cui* , 1998) and are given by equations (B.11) - (B.22) in Appendix B where $\xi_f = \xi_2$.

## 6.6 Numerical Examples

The porochemothermoelastic inclined borehole solution is applied in this section to assess the thermo-chemical effects on stresses and pore pressures and its eventual impact on borehole stability. As in Chapter 5, both the formation pore fluid and the wellbore fluid are assumed to comprise of two chemical species, i.e., a solute fraction and solvent fraction. The solvent species is assumed to be water. In addition to the difference in the solute concentrations, the formation and wellbore fluid temperatures are assumed to be different. A difference in the chemical potentials of the formation pore fluid and the wellbore fluid results in a modification of the stress and pore pressure distributions. The formation material properties are those of a Gulf of Mexico shale (*Cui et al.*, 1999a). The material properties and thermal properties are as given in Table 6.1. The borehole radius is assumed to be 0.1 m and a section at a depth of 1000 m is analyzed. Results are presented following a compression positive convention.

### 6.6.1 Thermo-chemical effect on stresses and pore pressure

As in the previous chapter, we consider a simplified example to demonstrate the thermo-chemical effects on stress and pore pressure distributions. The borehole is assumed to

Table 6.1: Material Parameters for Porochemothermoelastic Analysis .

| Parameter | Units | Value |
|---|---|---|
| Elastic Modulus ($E$) | MPa | 1853.0 |
| Poisson's Ratio ($\nu$) | - | 0.22 |
| Undrained Poisson's Ratio ($\nu_u$) | - | 0.46 |
| Skempton's Coefficient ($B$) | - | 0.92 |
| Permeability ($k$) | md | $1.0 \times 10^{-4}$ |
| Fluid Viscosity ($\mu$) | MPa.s | $10^{-9}$ |
| Solute Diffusivity.($c_2$) | $m^2$/day | $8.64 \times 10^{-5}$ |
| Reflection Coefficient ($\chi$) | - | 0.9 |
| Porosity ($\phi$) | - | 0.14 |
| Heat Diffusivity.($c_h$) | $m^2$/day | 0.13824 |
| Average Temperature ($T$) | °K | 300.0 |
| Thermo-osmotic diffusivity ($D^T$) | $m^2$/day | $-5.0 \times 10^{-5}$ |
| Linear Expansion Coefficient (solid skeleton, $\alpha^s$) | /°C | $6.0 \times 10^{-6}$ |
| Volumetric Expansion Coefficient (fluid, $\alpha^s$) | /°C | $3.0 \times 10^{-4}$ |

be vertical and the in-situ stress gradients $S_{x'}$, $S_{y'}$ and $S_{z'}$ are assumed to be trivial such that $S_{x'} = S_{y'} = S_{z'} = 0$ kPa/m. The pore pressure gradient of the formation fluid is assumed to be $p_o = 9.8$ kPa/m. At the same time, the wellbore fluid pressure gradient is assumed to be $p_w = 9.8$ kPa/m. The difference between the formation temperature and the wellbore fluid temperature is assumed to be 50°C. The solute concentration in the pore fluid is assumed to be more than that in the wellbore fluid such that $m_w^s < m_o^s$. The difference $m_w^s - m_o^s = -1.8 \times 10^{-2}$ which is equivalent of a solute concentration difference of 1 mol/kg.

Figure 6.2 shows the pore pressure variation along the radial distance. Results are shown for the porothermoelastic and the porochemothermoelastic analysis for $t = 0.001$, 0.01 day. A higher wellbore fluid temperature results in a temperature-induced pore pressure which is seen in the porothermoelastic curves. In the porochemothermoelastic case, the higher chemical potential of the water in the wellbore fluid induces an even higher pore pressure which is the thermo-chemical effect. As seen in figure 6.2, the magnitude of the pore pressure is higher for small time intervals and reduces as time

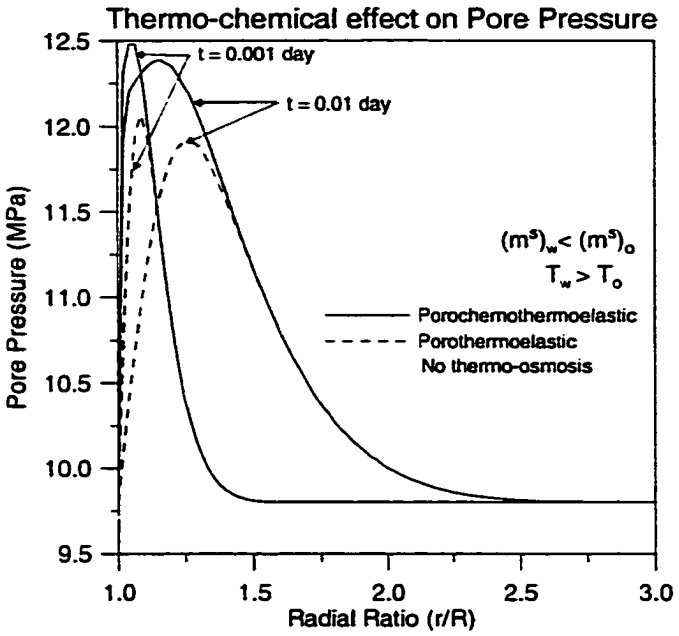


Figure 6.2: The thermo-chemical effect on the pore pressure distribution for $m_w^s < m_o^s$ with $T_w > T_o$ at $t = 0.001$, 0.01 day

increases. Figures 6.3 and 6.4 show the total radial and tangential stresses respectively generated by the thermo-chemical effect. These stresses are compressive in nature and higher for the porochemothermoelastic case. A variation of the pore pressure at larger values of time ($t = 0.1$, 0.5 day) is shown in Figure 6.5. With the passage of time, the peak of the induced pore pressure reduces and a pore pressure front progresses into the formation as is seen in figure 6.5.

Next we analyze the effect of thermo-osmosis on the pore pressure distribution. Figure 6.6 shows a comparison of the pore pressure curves for $t = 0.001$, 0.01 day considering the thermo-osmosis effect and ignoring them. The direction of osmotic flow has been assumed to be from the wellbore fluid into the formation. Higher pore pressures are induced when thermo-osmosis effects are taken into account. Again with the passage of time the peak of the induced pore pressure reduces and the pore pressure front progresses into the formation as is seen in figure 6.7.

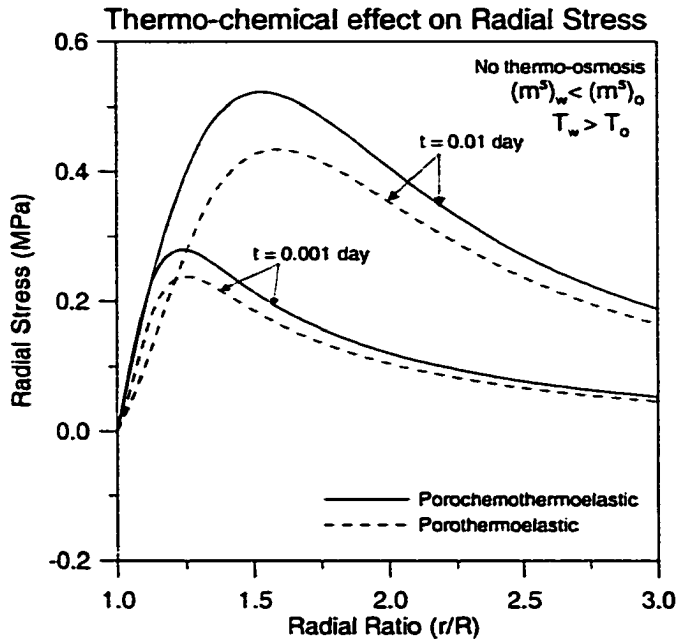


Figure 6.3: The thermo-chemical effect on the radial stress distribution for $m_w^s < m_o^s$ with $T_w > T_o$ at $t = 0.001$, 0.01 day

### 6.6.2 Implications on borehole stability

The thermo-chemical effect on wellbore stability is demonstrated by considering stress and pore pressure distributions around an inclined borehole in a three-dimensional *in-situ* stress field. The borehole orientation as shown in Fig 3.1 is given by the azimuth, $\varphi_y = 30°$, and the inclination $\varphi_z = 60°$. The formation in-situ stress and pore pressure gradients given as : $S_{x'} = 25$ kPa/m, $S_{y'} = 22$ kPa/m, $S_{z'} = 29$ kPa/m, $p_o = 9.8$ kPa/m. The borehole fluid pressure is by given by $p_w = 12.0$ MPa. A temperature difference between the formation and the borehole fluid is assumed to be $\Delta T = 50°$C with the borehole fluid at a higher temperature. The difference in the solute molar fractions between the formation pore fluid and the wellbore fluid is equivalent of 1 mol/kg with $m_w^s < m_o^s$. Material properties given in Table 6.1 are used in the computations.

Figure 6.8 shows the variation of pore pressure along the $\theta = 90°$ direction. As

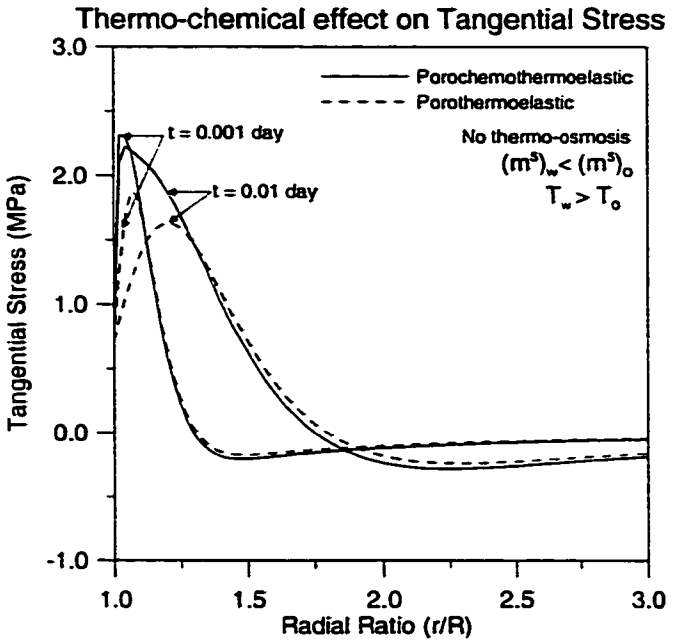


Figure 6.4: The thermo-chemical effect on the tangential stress distribution for $m_w^s < m_o^s$ with $T_w > T_o$ at $t = 0.001$, 0.01 day

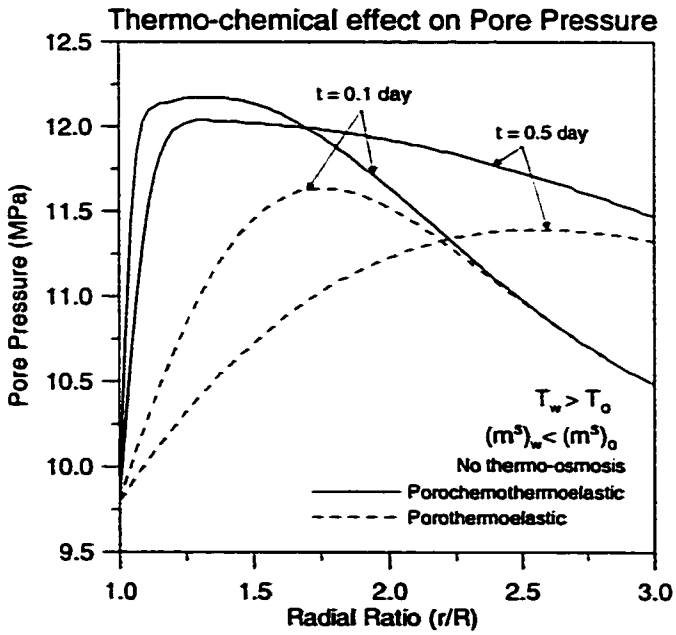


Figure 6.5: The thermo-chemical effect on the pore pressure distribution for $m_w^s < m_o^s$ with $T_w > T_o$ at $t = 0.1$, 0.5 day

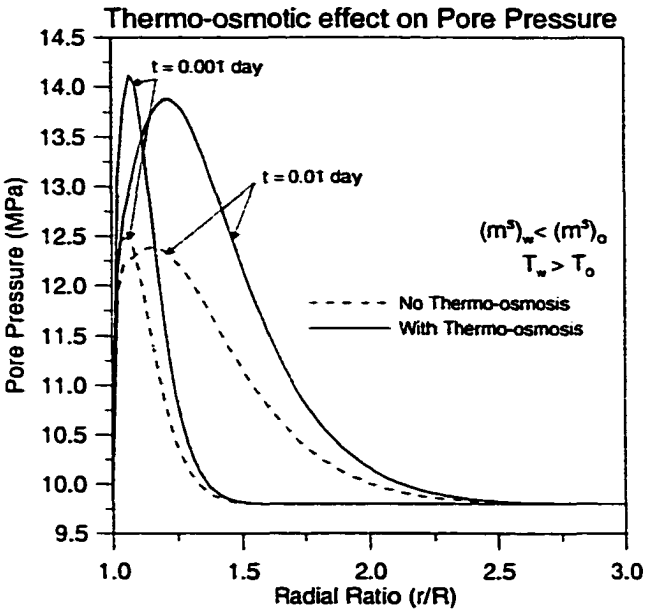


Figure 6.6: Pore pressure variation along $\theta = 90°$ from the porochemothermoelastic analysis ($m_w^s < m_o^s$) for $t = 0.2$, 0.5, 2.0 and 5.0 day

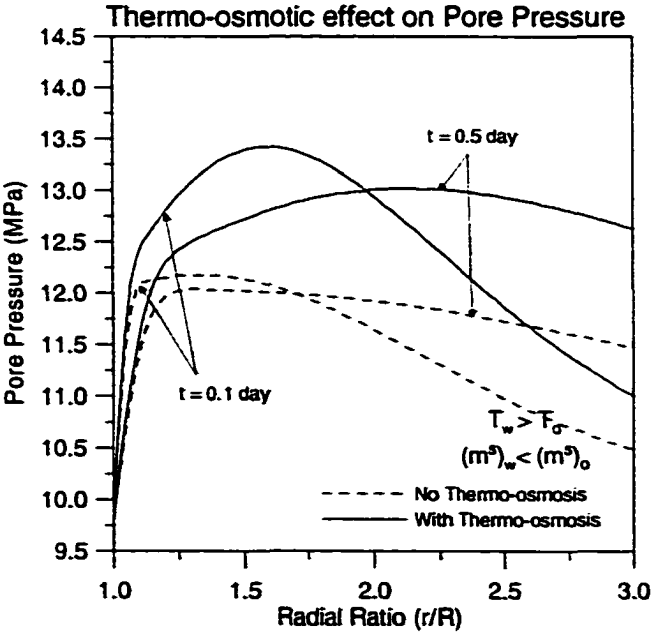


Figure 6.7: Pore pressure variation along $\theta = 90°$ at $t = 0.2$, 0.5 day obtained from the porothermoelastic and porochemothermoelastic ($m_w^s < m_o^s$) analysis.

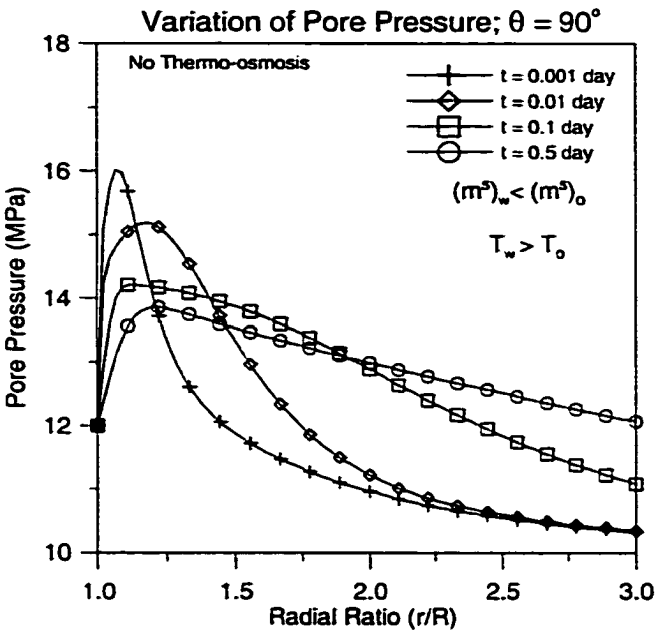


Figure 6.8: Pore pressure variation along $\theta = 90°$ for $t = 0.001$, 0.01, 0.1 and 0.5 day (Without thermo-osmosis)

seen from the figure, the thermo-chemical effect results in an increased pore pressure in regions close to the borehole wall. The peak of the induced pore pressure reduces with the passage of time and a pore pressure front progresses into the formation as discussed earlier. The corresponding effective radial and tangential stress distributions are shown in figures 6.9 and 6.10. Due to the high induced pore pressure, tensile effective radial stresses are observed in regions close to the borehole wall. Note that the thermo-osmosis effects are not included in figures 6.8 - 6.10. Figures 6.11 and 6.12 show the pore pressure and effective radial stress in which the thermo-osmosis effects have been included along the $\theta = 90°$ direction. The higher induced pore pressure in this case results in higher tensile effective radial stresses close to the borehole wall.

Figure 6.13 shows the variation of pore pressure around the borehole at a short distance into the formation ($r/R = 1.05$) for $t = 0.001$ day. The porochemothermoelastic

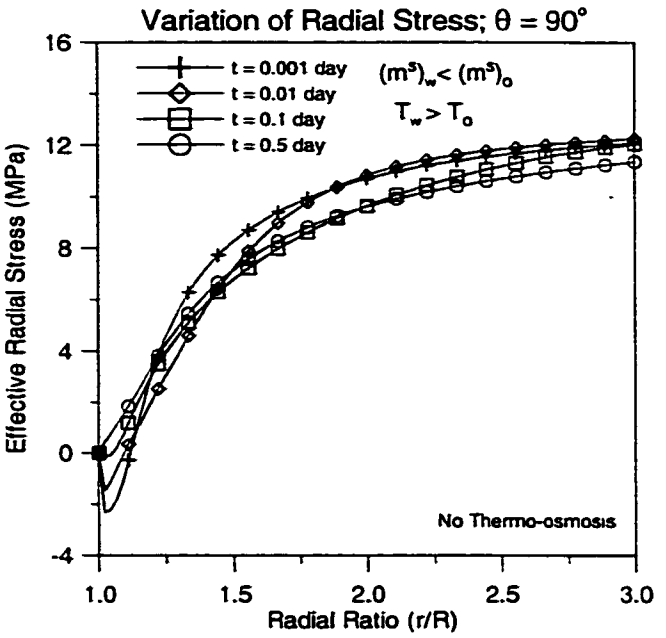


Figure 6.9: Effective radial stress along $\theta = 90°$ for $t = 0.001$, 0.01, 0.1 and 0.5 day (Without thermo-osmosis)

curves with and without thermo-osmosis effects are compared with the porothermoelastic curve. The magnitude of the pore pressure is highest for the case where thermo-osmosis effects are considered as was observed earlier. The higher pore pressure for this case would result in reducing the effective stresses. Figure 6.14 shows the pore pressure variation around the borehole for three time intervals with the thermo-osmosis effects considered. Figures 6.15 and 6.16 show the effective radial and tangential stresses respectively, around the borehole wall for this case. Tensile effective radial stresses are observed at smaller time intervals indicating that regions close to the borehole wall could potentially fail due to spalling. On the other hand, as seen from figure 6.16 the magnitude of the minimum effective tangential stress decreases with the passage of time. It must be noted that, curves obtained with the exclusion of the thermo-osmotic effects would be qualitatively similar with a lesser peak magnitude of the pore pressure, a lesser tensile magnitude of the effective radial stress and a more compressive effective

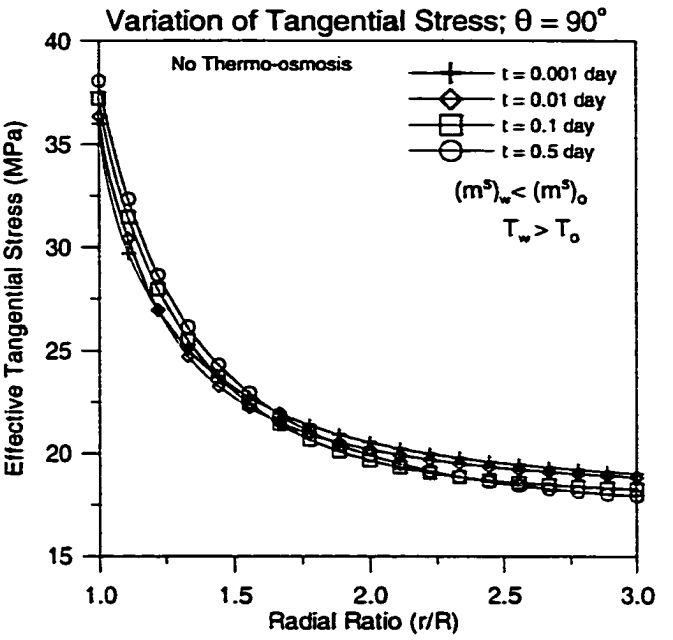


Figure 6.10: Effective tangential stress along $\theta = 90°$ for $t = 0.001$, 0.01, 0.1 and 0.5 day (Without thermo-osmosis)

tangential stress.Figure 6.17 shows the stress clouds at $r/R = 1.05$ and $t = 0.001$ day. Curves are shown for the porochemothermoelastic analysis with and without inclusion of the thermo-osmotic effects and compared to a porothermoelastic curve. It is seen that the porochemothermoelastic curve where the thermo-osmosis effects are considered is most critical with respect to shear failure. Figure 6.18 shows the stress clouds for the porochemothermoelastic case for different salt concentrations in the wellbore fluid. On comparison with the porochemoelastic case, it is seen that a higher salt concentration in the wellbore fluid is required to counteract the destabilizing thermal effects in the vicinity of the wellbore.

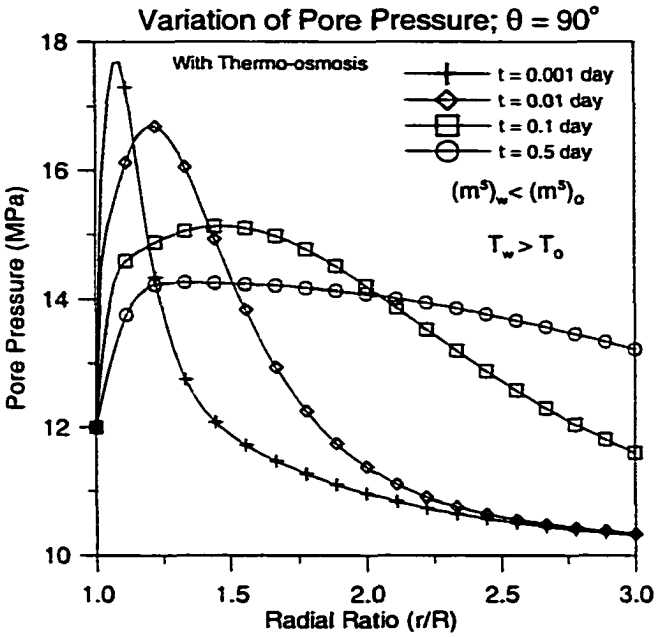


Figure 6.11: Pore pressure along $\theta = 90°$ for $t = 0.001$, 0.01, 0.1 and 0.5 day (With thermo-osmosis)

## 6.7 Summary

A generalized anisotropic porochemothermoelastic model has been presented in this chapter. The anisotropic equations have been specialized for the transversely isotropic and isotropic material. The field equations, in this case, comprise of the Navier-type equation, the heat diffusion equation, and a set of non-homogeneous coupled diffusion equations which account for the solute and fluid diffusion. The solution for the inclined borehole for the porochemothermoelastic model in a transversely isotropic material has been presented.

The thermo-chemical effects on stress and pore pressure distributions have been isolated in a simplified example. These effects are attributed to differential expansion/contraction rates of the solid and pore fluid constituents, presence of chemical gradients and thermo-osmosis. Results from the simplified example show that a higher

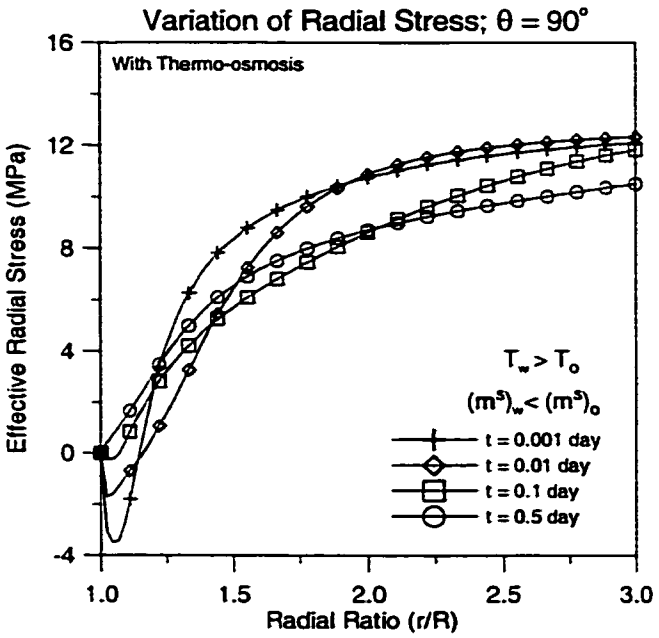


Figure 6.12: Effective radial stress along $\theta = 90°$ for $t = 0.001$, 0.01, 0.1 and 0.5 day (With thermo-osmosis)

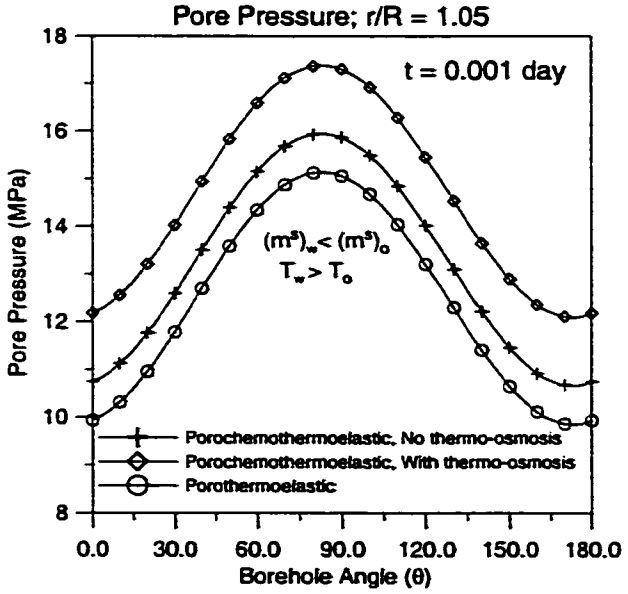


Figure 6.13: Pore pressure variation around the borehole at $r/R = 1.05$ to examine the thermo-osmotic and chemical effects

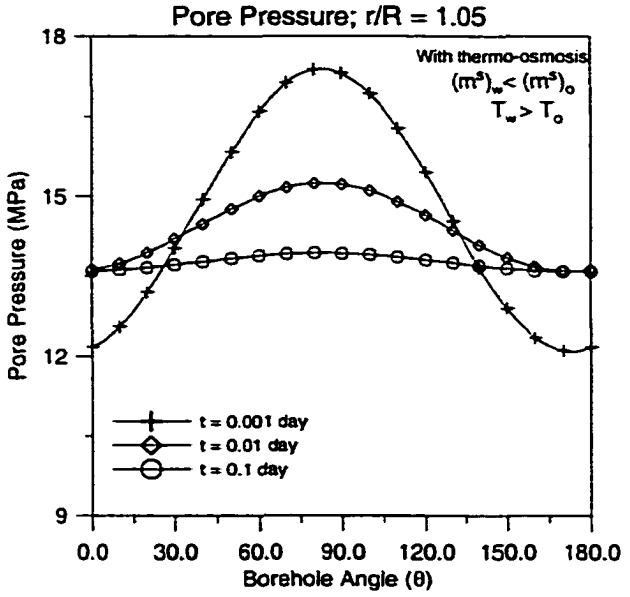


Figure 6.14: Pore pressure variation around the borehole at $r/R = 1.05$ from the porochemothermoelastic analysis with thermo-osmotic effects for $t = 0.001$, 0.01, 0.1 day

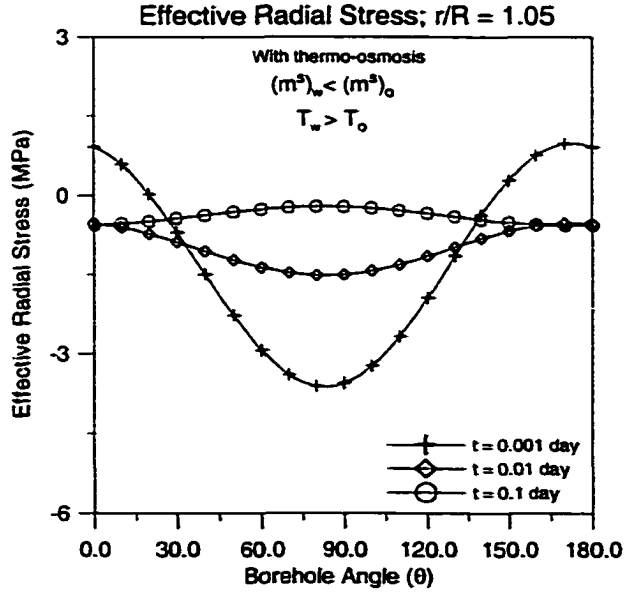


Figure 6.15: Effective radial stress variation around the borehole at $r/R = 1.05$ from the porochemothermoelastic analysis with thermo-osmotic effects for $t = 0.001$, 0.01, 0.1 day

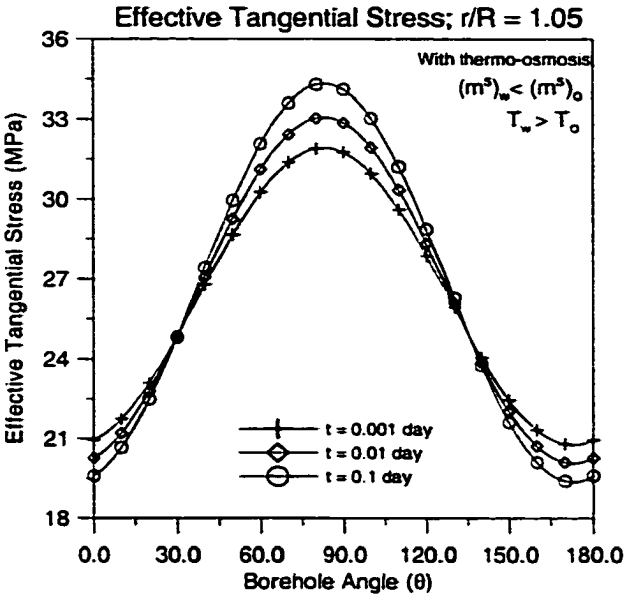


Figure 6.16: Effective tangential stress variation around the borehole at $r/R = 1.05$ from the porochemothermoelastic analysis with thermo-osmotic effects for $t = 0.001$, 0.01, 0.1 day

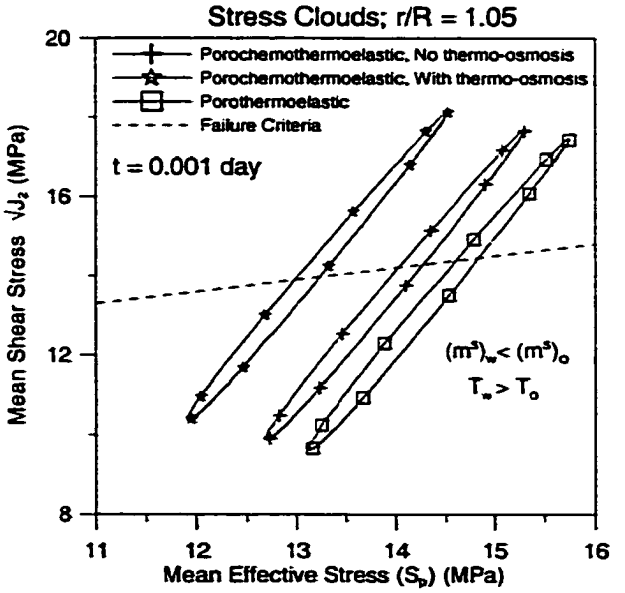


Figure 6.17: Stress clouds at $r/R = 1.05$ for $t = 0.001$ day for the porochemothermoelastic model with and without the thermo-osmotic effects compared with the porothermoelastic model

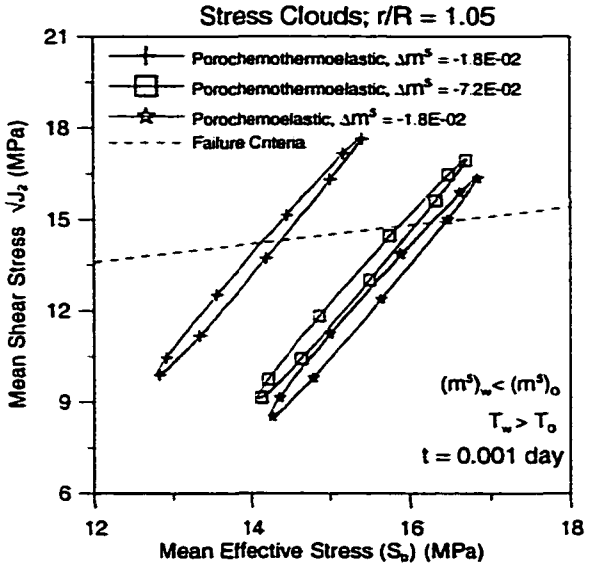


Figure 6.18: Stress clouds at $r/R = 1.05$ for $t = 0.001$ day for the porochemothermoelastic model with different salt concentrations in the wellbore fluid

temperature along with a lower solute concentration of the wellbore fluid results in increased magnitudes of the pore pressure near the wellbore. For the same case, incorporating thermo-osmotic effects results in even higher near wellbore pore pressures.

The model has been further applied to the problem of an inclined borehole. As in the case of the simplified example, higher pore pressures are observed in the vicinity of the wellbore. The effective radial stresses are more tensile at smaller time, when the temperature of the wellbore fluid is higher, its solute concentration is lower and when thermo-osmotic effects are considered. This implies an increased potential for failure by spalling at early time. On the other hand, the minimum effective tangential stress reduces with time indicating a delayed potential for fracturing. The stress clouds show that the porochemothermoelastic model wherein thermo-osmotic effects are considered is most critical with respect to shear failure. Consequently, a higher salt concentration in the wellbore fluid is required to stabilize wellbores drilled under non-isothermal conditions.

# Chapter 7

# Conclusions and Recommendations

## 7.1 Summary

The present work is an attempt to conduct a comprehensive study of the application of anisotropic poromechanics to the inclined borehole problem. The scope covers development of anisotropic poromechanics models accounting for coupling between the thermal, chemical, hydraulic and mechanical processes in fluid saturated porous media, evaluation of stress and pore pressure distributions around circular openings.

The basic concepts in poromechanics relevant to this work have been reviewed. The conservation equations for mass, momentum and energy have been presented. Constitutive equations and relations between the material constants for poroelasticity, porothermoelasticity, porochemoelasticity and porochemothermoelasticity have been presented in their isotropic and anisotropic forms.

A generalized solution strategy for the inclined borehole problem has been presented. The approach is essentially a superposition scheme which derives from the linearity of the stress-strain relations. The problem is sub-divided into simpler problems for which solutions are either known or can easily be obtained. The excavation of boreholes results in the development of stress concentrations which affect their stability. The tensile and shear modes of borehole failure and various failure criteria have been discussed.

A generalized anisotropic porothermoelastic formulation has been developed. The

formulation accounts for fully-coupled thermal, hydraulic and mechanical response of fluid saturated porous media. The governing equations have been tailored for transversely isotropic media and the solution for the inclined borehole problem has been developed. Solutions for permeable and impermeable boundary conditions have been presented. A parametric study has been carried out to analyze the effect of material anisotropy on stress and pore pressure profiles. It was found that a higher thermal expansion coefficient in the transverse direction has a more pronounced effect on the near-wellbore pressure and stresses. An interesting reversal in the trend of this effect is observed when the mechanical parameters in the transverse direction are higher.

A generalized anisotropic porochemoelastic formulation which accounts for fully-coupled hydraulic, chemical and mechanical processes, under isothermal conditions, has been presented. The porous media is assumed to be chemically active and saturated with a pore fluid consisting of two species - a solute and a solvent. Governing equations for the specialized cases of transverse isotropy and isotropy have been developed. Subsequently, the solution for the inclined borehole problem has been developed. Both the permeable and impermeable boundary conditions at the borehole wall have been considered. It was found that a higher chemical potential of the fluid in the wellbore increases the pore pressure in its vicinity. This 'chemically-induced' pore pressure thus results in a higher failure potential which may be reduced by increasing solute molar fraction in the wellbore fluid.

In the generalized anisotropic porochemothermoelastic formulation developed, the isothermal assumption in the porochemoelastic model has been relaxed. Field equations comprising of the Navier-type equation, heat diffusion equation, and a set of non-homogeneous coupled solute and fluid diffusion equations, have been developed for the transversely isotropic and isotropic case. The solution to the inclined borehole problem, under this scenario, has been developed. It was found that a higher wellbore fluid tem-

perature along with a higher chemical potential of the wellbore fluid results in induced pore pressures close to the borehole wall. The induced pore pressures are higher than the corresponding porochemoelastic cases. The magnitude of the induced pore pressure are higher when the thermo-osmotic effects are taken into account. Tensile effective radial stresses are observed at smaller time, when the temperature of the wellbore fluid is higher, its solute concentration is lower and when thermo-osmotic effects are considered. The stress clouds show that the porochemothermoelastic model wherein thermo-osmotic effects are considered is most critical with respect to shear failure. Consequently, a higher salt concentration in the wellbore fluid is required to stabilize wellbores drilled under non-isothermal conditions.

## 7.2 Recommendations for Future Work

Experimental studies are necessary to validate constitutive models. The material coefficient inherent in the anisotropic poromechanics models discussed in this work, need to be evaluated experimentally. The stress levels under which the assumption of linearity is valid needs to be assessed for individual rock types. The importance of measuring anisotropic parameters and the lack of experimental studies in this regard, warrant future research work in this area.

Fractured formations are an important class of subsurface flow systems. Drilling activities carried out in such formations require a clear understanding of matrix-fracture interaction in terms of fluid, heat and ion exchange. An accurate formulation of the physicochemical processes in such formations, need to be woven into numerical and possible analytical solutions.

Non-linear poromechanics has not been addressed in this work. However, it is not uncommon that rocks in practice are inelastic. Although limited theoretical work has been carried out in this area, a comprehensive analysis of the borehole problem accounting

for the various coupled processes addressed in this work, needs to be carried out.

Multiphase flow, coupled with thermal, chemical and mechanical processes, presents a level of complexity, which is yet to be addressed. It is envisaged that analytical solutions even for simple problems under such a scenario may be difficult to obtain. Interphase mass exchange triggered by pressure, temperature and chemical potential evolution and, the retroactive and simultaneous effect on the deformations, need to be considered under the framework of numerical techniques such as the finite element method.

# References


1. Abousleiman, Y., Personal Communication, 2002.

2. Abousleiman, Y., and Cheng, A.H-D., 'Anisotropic poroelasticity with applications,' Report Number RMC-93-19, *Rock Mechanics Consortium*, School of Petroleum and Geological Engineering, The University of Oklahoma, Norman, October, 1993.

3. Abousleiman, Y., Cheng, A.H-D., Cui, L., Detournay, E., & Roegiers, J.-C., 'Mandel's problem revisited.' *Géotechnique*, **46**(2), 187-195, 1996a.

4. Abousleiman, Y., Cheng, A.H-D., Jiang, C., and Roegiers, J.-C., 'A micromechanically consistent poroviscoelasticity theory for rock mechanics applications.' *Int. J. Rock Mech. Min. Sci. & Geomech. Abstr.*, **30**, 1177-1180, 1993.

5. Abousleiman, Y., Cheng, A.H-D., Jiang, C., and Roegiers, J.-C., 'Poroviscoelastic analysis of borehole and cylinder problems,' *Acta Mechanica*, **119**, 199-219, 1996b.

6. Abousleiman, Y., and Cui, L., 'Poroelastic solutions in transversely isotropic media for wellbore and cylinder,' *Int. J. Solids Structures*, **35**(34/35), 4905-4929, 1998.

7. Abousleiman, Y., and Cui, L., 'The theory of anisotropic poroelasticity with applications,' *Modeling and Applications in Geomechanics*, Eds. M. Zaman, J. Booker & G. Gioda, John Wiley & Sons, 2000.

8. Abousleiman, Y., Cui, L., Cheng, A.H-D. and Roegiers, J.-C., 'Poroelastic solution of an inclined borehole in a transversely isotropic medium,' In *Proc. 35th U.S. Symp. Rock Mech.*, Edited by J.J.K. Daemen and R.A. Schultz, Balkema, 313-318, 1995.

9. Abousleiman, Y., and Ekbote, S., 'Porothermoelasticity in transversely isotropic porous materials,' *The IUTAM Symposium on Theoretical and Numerical Methods in Continuum Mechanics of Porous Materials*, Ed. Wolfgang Ehlers, Stuttgart, Germany, Sep 5-10, 145-152, 1999.

10. Abousleiman, Y., and Ekbote, S., 'Porothermoelastic solution for an inclined borehole in transversely isotropic media,' submitted to *Journal of Applied Mechanics*, 2002.

11. Abousleiman, Y., Ekbote, S., and Kanj, M., 'Tools in poromechanics with laboratory and field validations,' *Proceedings of the 2nd Biot's Conference on Poromechanics*, Eds Aurialt et al., Grenoble, France, 85-92, 2002.

12. Abousleiman, Y., Ekbote, S., and Tare, U., 'Time-dependent wellbore stability predictions,' *J. Pet. Tech.*, February 2001, pp 29-30, 2001.

13. Abousleiman, Y., Ekbote, S., Cui, L., Mody, F.K., Roegiers, J.-C., and Zaman, M.M., 'Time-dependent coupled processes in wellbore design and stability: PBORE-3D, ' paper SPE 56759 presented at the 1999 *SPE Annual Technical Conference and Exhibition*, Houston, October 3-6, 1999.

14. Abousleiman, Y., and Kanj, M., 'The Generalized Lame Problem: Applications in Poromechanics,' submitted to *J. App Mech.*, 2002

15. Abramowitz, M., and Stegun, I.A., *Handbook of Mathematical Functions*, Appl. Math. Ser. 55. National Bureau of Standards, Washington, D.C., 1964.

16. Amadei, B., *Rock anisotropy and the theory of stress measurement*, Springer-Verlag, 1983.

17. Bailey, L., Denis, J.H., Goldsmith, G., Hall, P.L., and Sherwood, J.D., 'A wellbore simulator of mud-shale interaction studies,' *J. Pet. Sci. Engg.*, **11**, 195-211, 1994.

18. Bear, J., Dynamics of fluids in porous media, 3rd ed., American Elsevier, USA, 1972.

19. Bear, J., and Corapcioglu, M.Y., 'A Mathematical model for consolidation in a thermoelastic aquifer due to hot water injection or pumping,' *Water Resources Research*, **17**(3), 723-736, 1981.

20. Biot, M.A., 'General theory of three-dimensional consolidation,' *J. Appl. Phys.*, **12**, 155-164, 1941.

21. Biot, M.A., 'Theory of Elasticity and consolidation of a porous anisotropic solid,' *J. Appl. Phys.*, **26**, 182-185, 1955.

22. Biot, M.A., 'General solutions of the elasticity and consolidation for a porous material,' *J. Appl. Mech., Trans. Am. Soc. Mech. Engrs.*, **78**, 91-96, 1956a.

23. Biot, M.A., 'Theory of deformation of a porous viscoelastic anisotropic solid,' *J. Appl. Phys.*, **27**, 459-467, 1956b.

24. Biot, M.A., 'Theory of propagation of elastic waves in a fluid saturated porous solid. I Low frequency range,' *The Journal of the Acoustical Society of America*, **28**(2), 168-178, 1956c.

25. Biot, M.A., 'Theory of propagation of elastic waves in a fluid saturated porous solid. II Higher frequency range,' *The Journal of the Acoustical Society of America*, **28**(2), 179-191, 1956d.

26. Biot, M.A., 'Mechanics of deformation and acoustic propagation in porous media,' *J. Appl. Phys.*, **33**, 1482-1498, 1962a.

27. Biot, M.A., 'General theory of acoustic propagation in porous dissipative media,' *J. Acoustical Soc. Amer.*, **34**, 1254-1264, 1962b.

28. Biot, M.A., 'Theory of finite deformation of porous solids,' *Indiana University Mathematical Journal*, **21**, 597-620, 1972.

29. Biot, M.A., 'Nonlinear and semilinear rheology of porous solids,' *Journal of Geophysical Research*, **78**(23), 4924-4937, 1973.

30. Biot, M.A., and Willis, D.G., 'The elastic coefficients of the theory of consolidation,' *J. Appl. Mech.*, **24**, 594-601, 1957.

31. Bird, R.B., Stewart, W.E., and Lightfoot, E.N., *Transport Phenomena*, John Wiley, New York, 1960.

32. Booker, J.R., and Savvidou, C., 'Consolidation around a spherical heat source,' *Int. J. Solids Structures*, **20**, 1079-1090, 1984.

33. Booker, J.R., and Savvidou, C., 'Consolidation around a point heat source,' *Int. J. Num. Anal. Meth. Geomech.*, **9**, 173-184, 1985.

34. Boresi, A.P., and Chong, K.P., *Elasticity in Engineering Mechanics*, Elsevier Science Publication Co., New York, 1987.

35. Bradley, W.B., 'Failure of inclined boreholes,' *J. Energy Resour. Tech., ASME*, **101**, 232-239, 1979.

36. Brownell, D.H., Jr., Garg, S.K., and Pritchett, J.W., 'Governing equations for geothermal reservoirs,' *Water Resour. Res.*, **13**, 929–934, 1977.

37. Carslaw. H.S., and Jaegar, J.C., *Conduction of Heat in Solids*, Oxford University Press, New York, 1959.

38. Carter, J.P., and Booker, J.R., 'Elastic consolidation around a deep circular tunnel,' *Int. J. Solids Structures*, **18**, 1059-1074, 1982.

39. Carter, J.P., and Booker, J.R., 'Elastic consolidation around a lined circular tunnel,' *Int. J. Solids Structures*, **20**(6), 589-608, 1983.

40. Chenevert, M.E., 'Shale alteration by water adsorption,' *J. Pet. Tech.*, **22**, 1141-1148, 1970a.

41. Chenevert, M.E., 'Shale control with balanced-activity oil-continuous muds,' *J. Pet. Tech.*, 1309-1316, October, 1970b.

42. Cheng, A.H-D., 'Material coefficients of anisotropic poroelasticity,' *Int. J. Rock Mech. Min. Sci.*, **34**, 183-193, 1997.

43. Cheng, A.H-D., 'On generalized plane strain poroelasticity,' *Int. J. Rock Mech. Min. Sci.*, **35**, 199-205, 1998.

44. Cheng, A.H-D., Abousleiman, Y., and Roegiers, J.-C., 'Review of some poroelastic effects in rock mechanics,' *Int. J. Rock Mech. Min. Sci. & Geomech. Abstr.*, **30**, 1119-1126, 1993.

45. Cleary, M.P., 'Fundamental solutions for a fluid-saturated porous solid,' *Int. J. Solids Structures*, **13**, 785-806, 1977.

46. Coussy, O., 'A general theory of thermoporoelastoplasticity for saturated porous materials,' *Transport in Porous Media*, **4**, 281-293, 1989.

47. Coussy, O., *Mécanique des milieux poreux*, Editions Technip, 1991.

48. Coussy, O., *Mechanics of Porous Continua*, John Wiley & Sons, New York, 1995.

49. Coussy, O., Dangla, P., Dormieux, L., and Lemarchand, E., 'Two-scale modelling of a swelling clay,' *Journal De Physique IV*, **9**(9), 21-33, 1999.

50. Crank, J., *The Mathematics of Diffusion*, 2nd ed., Oxford Science Publications, 1979.

51. Cryer, C.W., 'A comparison of the three-dimensional consolidation theories of Biot and Terzaghi,' *Quart. J. Mech. Appl. Math.*, **16**, 401-412, 1963.

52. Cui, L., *Poroelasticity with Application to Rock Mechanics*, Ph.D. Dissertation, University of Delaware, 1995.

53. Cui, L., and Abousleiman, Y., 'Time-dependent poromechanical responses of saturated cylinders,' *ASCE J. Engg Mech.*, **127**(4), 391-398, 2001.

54. Cui, L., Abousleiman, Y., Cheng, A.H-D., Kaliakin, V.N., and Roegiers, J.-C., 'Finite element analyses of anisotropic poroelasticity: A generalized Mandel's problem and an inclined borehole problem,' *Int. J. Numer. Anal. Meth. Geomech.*, **20**, 381-401, 1996.

55. Cui, L., Abousleiman, Y., Cheng, A.H-D., and Roegiers, J.-C., 'Time-dependent failure analysis of inclined boreholes in fluid saturated formations,' *J. Energy Resour. Tech.*, **121**, 31-38, 1999a.

56. Cui, L., Cheng, A.H-D., and Abousleiman, Y., 'Poroelastic solution of an inclined borehole,' *J. Appl. Mech., ASME*, **64**, 32-38, 1997.

57. Cui, L.,Ekbote, S., Abousleiman, Y., Zaman, M.M., and Roegiers, J.-C., 'Borehole stability analyses in fluid saturated formations with non-penetrating walls,' *Int. J. Rock Mech. Min. Sci.*, **35**(4/5), Paper No. 061, 1998.

58. Cui, L., Ekbote, S., and Abousleiman, Y., 'Effect of pore fluid conditions at the borehole wall on borehole stability,' *Proc.37th U.S. Rock Mech. Symp.*, Vail, Colorado, ed. Amadei et al., Balkema, 187-194, 1999b.

59. Davies, B., and Martin, B., 'Numerical inversion of the Laplace transform: A survey and comparison of methods,' *J. Computational Physics*, **33**, 1-32, 1979.

60. De Groot, S.R., *Thermodynamics of Irreversible Processes*, North-Holland, Amsterdam, 1952.

61. Desai, C.S., and Siriwardane, H.J., *Constitutive Laws for Engineering Materials with Emphasis on Geologic Materials*, Prentice-Hall, 1984.

62. Detournay, E., and Cheng, A.H-D., 'Fundamentals of poroelasticity,' Chap 5 in *Comprehensive Rock Engineering: Principles, Practice and Projects. Vol. II, Analysis and Design Methods*, Ed. C. Fairhurst, Pergamon Press, 113-171, 1993.

63. Dormieux, L., Bardoux, P., Coussy, O., and Dangla, P., 'Macroscopic model of the swelling phenomenon of a saturated clay,' *Eur J Mech A Solids*, 14(6), 981-1004, 1995.

64. Ekbote, S., Abousleiman, Y., Cui, L., and Zaman, M.M., 'Analyses of inclined boreholes in poroelastic media,' submitted to *Int. J. Geomechanics*, 2002.

65. Ekbote, S., Abousleiman, Y. & Zaman, M.M., 'Porothermoelastic solution for an inclined borehole in transversely isotropic porous media,'. *Fourth North American Rock Mech. Symp.*, Seattle, USA, Sep 5-10, 2000.

66. Fjær, E., Holt, R.M., Horsrud, P., Raaen A.M., and Risnes, R., *Petroleum Related Rock Mechanics*, Elsevier Science, 1992.

67. Geertsma, J., 'Problems of rock mechanics in petroleum production engineering,' *Proc. 1st Congr. ISRM*, Lisbon, **3**, 585-594, 1966.

68. Haie, A.H., Mody, F.K., and Salisbury, D.P., 'Experimental investigation of the influence of chemical potential on wellbore stability,' In *Proc. SPE/IADC Drilling Conf.*, paper 23885, New Orleans, 1992.

69. Heidug, W.K., and Wong, S.-W., 'Hydration swelling of water-absorbing rocks: A constitutive model,' *Int. J. Num. Anal. Geomech.*, **20**, 403–430, 1996.

70. Hubbert, M.K., and Willis, D.G., 'Mechanics of hydraulic fracturing,' *Petroleum Trans.*, AIME, **210**, 153-168, 1957.

71. Huyghe, J.M., and Janssen, J.D., 'Thermo-chemo-elctro-mechanical formulation of saturated charged porous solids,' *Transport in Porous Media*, **34**, 129-141, 1999.

72. Jaegar, J.C., and Cook, N.G.W., *Fundamentals of Rock Mechanics*, 2nd edition., John Wiley, New York, 1979.

73. Kanj, M. and Abousleiman, Y., 'The Generalized Lame' Problem: Coupled Poro-mechanical Solutions,' submitted to *J. App Mech.*, 2002.

74. Katsube, N., 'The anisotropic thermomechanical constitutive theory for fluid-filled porous materials with solid/fluid outer boundaries,' *Int. J. Solids Structures*, **24**(4), 375–380, 1988.

75. Kodashima, T., and Kurashige, M., 'Thermal stresses in a fluid-saturated poroelastic hollow sphere,' *Journal of Thermal Stresses*, **19**, 139-151, 1996.

76. Kümpel, H.-J., 'Poroelasticity: parameters reviewed,' *Geophys.J.Int.*, **105**, 783-799, 1991.

77. Kurashige, M., 'A thermoelastic theory of fluid-filled porous materials,' *Int. J. Solids Structures*, **25**(9), 1039-1052, 1989.

78. Kurashige, M., 'Thermal stresses of a fluid-saturated poroelastic hollow cylinder,' *JSME International Journal*, **35**(4), 386-391, 1992.

79. Lade, P.V., 'Failure criterion for frictional materials.' *Mechanics of Engineering Materials*, Eds. Desai and Gallager, Wiley, New York, 384-391, 1984.

80. Lee, C.K., and Mei, C.C., 'Re-examination of the equations of poroelasticity,' *Int. J. Engng. Sci.* , **35**(4), 329-352, 1997.

81. Lekhnitskii, S.G., *Theory of Elasticity of an Anisotropic Elastic Body*, transl. rev. 1977 Russian Ed., Mir Publishers, Moscow, 1981.

82. Li, X., 'A generalized theory of thermoelasticity for an anisotropic medium,' *Int. J. Engng. Sci.*, **30**(5), 571-577, 1992.

83. Li, X., 'Thermoporomechanical modeling of inclined borehole.' Ph.D. Dissertation, The University of Oklahoma, 1998.

84. Li, X., and Li, X., 'On the thermoelasticity of multicomponent fluid-saturated reacting porous media,' *Int. J. Engng, Sci.*, **30**(7), 891-912, 1992.

85. Lomba, R.F.T., Chenevert, M.E., and Sharma, M.M., 'The ion-selective membrane behavior of native shales,' *J. Pet. Sci. Engg.*, **25**, 9-23, 2000.

86. Lomba, R.F.T., Chenevert, M.E., and Sharma, M.M., 'The role of osmotic effects in fluid flow through shales,' *J. Pet. Sci. Engg.*, **25**, 25-35, 2000.

87. Mandel, J., 'Consolidation des sols (étude mathématique),' *Géotechnique*, **3**, 287-299, 1953.

88. McTigue. D.F., 'Thermoelastic response of fluid-saturated porous rock,' *Journal of Geophysical Research*, **91**(B9), 9533-9542, 1986.

89. McTigue, D.F., 'Flow to a heated borehole in porous, thermoelastic rock: Analysis,' *Water Resources Research*, **26**(8), 1763-1774, 1990.

90. Mitchell, J.K., 'Fundamentals of Soil Behavior,' *John Wiley*, 1993.

91. Mody, F.K., and Hale, A.H., 'A borehole model to couple the mechanics and chemistry of drilling fluid shale interaction,' In *Proc. SPE/IADC Drilling Conf.*, paper 25728, Richardson, Texas, Society of Petroleum Engineers, 1993.

92. Nair, R., Abousleiman, Y., and Zaman, M.M., 'A finite element porothermoelastic model for dual-porosity media,' in preparation, 2002.

93. Nowacki, W., *Thermoelasticity*, Addison-Wesley, 1962.

94. Nowinski, J.L., *Theory of thermoelasticity with applications* , Sijthoff & Noordhoff International Publishers, 1978.

95. Nur, A., and Byerlee, J.D., 'An exact effective stress law for elastic deformation of rocks with fluids,' *J. Geophy. Res.*, **76**(26), 641406419, 1971.

96. Palciauskas, V.V., and Domenico, P.A., 'Characterization of drained and undrained response of thermally loaded repository rocks,' *Water Resour. Res.*, **18**(2), 281-290, 1982.

97. Pender, M.J., 'Elastic solutions for a deep circular tunnel,' *Géotechnique*, **30**(2), 216-222, 1980.

98. Rice, J.R., and Cleary, M.P., 'Some basic stress diffusion solutions for fluid-saturated elastic porous media with compressible constituents,' *Reviews of Geophysics and Space Physics* **14**(4), 227-241, 1976.

99. Saada, A., *Elasticity: Theory and Applications*, Pergamon Press, NewYork, 1974.

100. Scheidegger, A.E., *The Physics of Flow through Porous Media*, 3rd edition., University of Toronto Press, Toronto, 1974.

101. Schiffman, R.L., 'A thermoelastic theory of consolidation,' in *Environmental and Geophysical Heat Transfer, ASME*, New York, pp. 78-84, 1971.

102. Sharma, J.N., and Kumar, V., 'On the axisymmetric problems of generalized anisotropic thermoelasticity,' *Journal of Thermal Stresses*, **19**, 781-794, 1996.

103. Sharma, J.N., and Kumar, V., 'Plane strain problems of transverse isotropic thermoelastic media,' *Journal of Thermal Stresses*, **20**, 463–476, 1997.

104. Sherwood, J.D., 'Biot poroelasticity of a chemically active shale,' *Proc. R. Soc. Lond. A*, **440**, 365-377, 1993.

105. Sherwood, J.D., 'A model of hindered solute transport in a poroelastic shale,' *Proc. R. Soc. Lond. A*, **445**, 679-692, 1994a.

106. Sherwood, J.D., 'A model for the flow of water and ions into swelling shale,' *Langmuir: the ACS journal of surfaces and colloids*, **10**(7), 2480-2486, 1994b.

107. Sherwood, J.D., 'Ionic transport in swelling shale,' *Advances in Colloid and Interfaces Science*, **61**, 51-64, 1995.

108. Sherwood, J.D., and Bailey, L., 'Swelling of shale around a cylindrical wellbore,' *Proc. R. Soc. Lond. A*, **444**, 161-184, 1994.

109. Stehfest, H., 'Numerical inversion of Laplace transforms,' *Comm. ACM.*, **13**, pp 47-49 and pp 624, 1970.

110. Thompson, M., and Willis, J.R., 'A reformulation of the equations of anisotropic poroelasticity,' *J. Appl. Mech., ASME*, **58**, 612-616, 1991.

111. Utsugida, Y., 'Coupled analysis of flow and heat around a high-level nuclear waste repository,' In *Proc. 5th Int. Conf. Numerical Methods in Geomechanics*, Nagoya, Balkema, Rotterdam, 711-716, 1985.

112. Van Oort, E., 'Physico-chemical stabilization of shales,' SPE Paper number 37263, presented at the *SPE Int. Symp. on Oilfield Chemistry*, Houston TX, Feb 18-21, 1997.

113. Vgenopoulou, I., and Beskos, D.E., 'Dynamic behavior of saturated poroviscoelastic media,' Acta Mechanica, **95**, 185-192, 1992.

114. Wang, H., *Theory of Linear Poroelasticity with applications to Geomechanics and Hydrogeology*, Princeton Univ. Press, New Jersey, 2000.

115. Wang, Y., and Papamichos, E., 'Conductive heat flow and thermally induced fluid flow around a wellbore in a poroelastic medium,' *Water Resources Research*, **30** (12), 3375-3384, 1994.

116. Wood Muir, A.M., 'The circular tunnel in elastic ground,' *Géotechnique*, **25**(1), 115-127, 1975.

117. Yeung, A.T., and Mitchell, J.K., 'Coupled fluid, electrical and chemical flows in soil,' *Geotechnique* **43**(1), 121-134, 1993.

118. Yuan, Y. G., Abousleiman, Y., Roegiers, J.-C., 'Fluid penetration around a borehole under coupled hydro-electro-chemico-thermal potentials,' Paper 95-72, presented at the *46th Annual Technical Meeting of The Petroleum Society of CIM*, Alberta, Canada, May 14-17, 1995.

# Appendix A

# The Generalized Plane Strain Isotropic Elastic Inclined Borehole Solution

The expressions for stress distributions around boreholes assuming an isotropic elastic medium are presented in this Appendix. These solutions employ a generalized plane strain assumption and have been presented by Bradley (*Bradley*, 1979). The far-field insitu stresses are denoted by stresses are denoted by $S_{x'}$, $S_{y'}$ and $S_{z'}$ in which $S_{x'}$ is the maximum horizontal insitu stress, $S_{y'}$ is the minimum horizontal insitu stress and $S_{z'}$ is the overburden vertical stress. The far-field stresses are transformed to a local borehole coordinate system via a stress transformation as explained in Chapter 3. In the local coordinate system, the borehole is characterized by normal as well as shear components of the insitu stress. The borehole is assumed to be of radius $R$. The wellbore fluid pressure is denoted by $p_w$ and its effect is superimposed on the stresses. Expressions for stresses are presented as functions of the radial distance, $r$, and the angle around the borehole, $\theta$. The angle $\theta$ is measured from the direction of $S_x$ in the anticlockwise direction. The radial distance $r$ is measured from the center of the borehole such that $r = R$ corresponds to the borehole wall. The expressions for the stress distributions are

given as (*Bradley*, 1979)

$$\sigma_{rr} = \left(\frac{S_x + S_y}{2}\right)\left(1 - \frac{R^2}{r^2}\right) + \left(\frac{S_x - S_y}{2}\right)\left(1 + \frac{3R^2}{r^2} - \frac{4R^2}{r^2}\right)\cos 2\theta + S_{xy}\left(1 + \frac{3R^2}{r^2} - \frac{4R^2}{r^2}\right)\sin 2\theta + p_w\left(\frac{R^2}{r^2}\right) \tag{A.1}$$

$$\sigma_{\theta\theta} = \left(\frac{S_x + S_y}{2}\right)\left(1 + \frac{R^2}{r^2}\right) - \left(\frac{S_x - S_y}{2}\right)\left(1 + \frac{3R^2}{r^2}\right)\cos 2\theta + S_{xy}\left(1 + \frac{3R^2}{r^2}\right)\sin 2\theta - p_w\left(\frac{R^2}{r^2}\right) \tag{A.2}$$

$$\sigma_{zz} = S_z - \nu\left[2\left(S_x - S_y\right)\left(\frac{R^2}{r^2}\right)\cos 2\theta + 4S_{xy}\left(\frac{R^2}{r^2}\right)\sin 2\theta\right] \tag{A.3}$$

$$\sigma_{r\theta} = \left(\frac{S_x - S_y}{2}\right)\left(1 - \frac{3R^2}{r^2} + \frac{2R^2}{r^2}\right)\sin 2\theta + S_{xy}\left(1 - \frac{3R^2}{r^2} + \frac{2R^2}{r^2}\right)\cos 2\theta \tag{A.4}$$

$$\sigma_{\theta z} = \left(-S_{xz}\sin\theta + S_{yz}\cos\theta\right)\left(1 + \frac{R^2}{r^2}\right) \tag{A.5}$$

$$\sigma_{rz} = \left(S_{xz}\cos\theta + S_{yz}\sin\theta\right)\left(1 - \frac{R^2}{r^2}\right) \tag{A.6}$$

# Appendix B

# Transversely Isotropic and Isotropic Poroelastic Borehole Solutions

Poroelastic inclined borehole solutions for the transversely isotropic and isotropic cases are presented.

## B.1 Transversely Isotropic Solution

The complete poroelastic solution for the inclined borehole for the transversely isotropic case is given by equations (3.54) - (3.61) setting $\varpi_1 = 1, \varpi_2 = 0, \varpi_3 = 0$. Expressions for $\sigma_{rr}^{(1)}$, $\sigma_{rr}^{(2)}$, $\sigma_{rr}^{(3)}$, $\sigma_{\theta\theta}^{(1)}$, $\sigma_{\theta\theta}^{(2)}$, $\sigma_{\theta\theta}^{(3)}$, $\sigma_{r\theta}^{(3)}$, $p^{(2)}$, $p^{(3)}$, and $T^{(2)}$ for permeable and impermeable boundary condition at the borehole wall are given in the following sections. Note that solutions for Case 2 and 3 are obtained in the Laplace domain and inverted to time domain using the Stehfest algorithm (*Stehfest*, 1970).

### B.1.1 Permeable Boundary Condition Model

Solutions for stress and pore pressure distributions for the transversely isotropic poroelastic permeable boundary condition model are given as follows (*Abousleiman and Cui*, 1998):

**Solutions for Case 1:**

$$\sigma_{rr}^{(1)} = H(t)\,[P_o - p_w]\left(\frac{R^2}{r^2}\right) \tag{B.1}$$

$$\sigma_{\theta\theta}^{(1)} = -H(t)\,[P_o - p_w]\left(\frac{R^2}{r^2}\right) \tag{B.2}$$

**Solutions for Case 2:**

$$s\bar{p}^{(2)} = F_1\Phi(\xi_f) \tag{B.3}$$

$$s\bar{\sigma}_{rr}^{(2)} = \alpha\left(1 - \frac{M_{12}}{M_{11}}\right)F_1\Psi(\xi_f) \tag{B.4}$$

$$s\bar{\sigma}_{\theta\theta}^{(2)} = -\alpha\left(1 - \frac{M_{12}}{M_{11}}\right)F_1\Omega(\xi_f) \tag{B.5}$$

where the functions $\xi_f$, $F_1$, $\Phi(x)$, $\Psi(x)$ and $\Omega(x)$, are given by

$$\xi_f = \sqrt{\frac{s}{c_f}} \tag{B.6}$$

$$F_1 = (p_w - p_o) \tag{B.7}$$

$$\Phi(x) = \left[\frac{\mathrm{K}_0(xr)}{\mathrm{K}_0(xR)}\right] \tag{B.8}$$

$$\Psi(x) = \left[\frac{\mathrm{K}_1(xr)}{xr\mathrm{K}_0(xR)} - \frac{R\mathrm{K}_1(xR)}{xr^2\mathrm{K}_0(xR)}\right] \tag{B.9}$$

$$\Omega(x) = \left[\frac{\mathrm{K}_1(xr)}{xr\mathrm{K}_0(xR)} - \frac{R\mathrm{K}_1(xR)}{xr^2\mathrm{K}_0(xR)} + \frac{\mathrm{K}_0(xr)}{\mathrm{K}_0(xR)}\right] \tag{B.10}$$

in which $\mathrm{K}_n$ is the modified Bessel's function of the second kind of order $n$.

**Solutions for Case 3:**

$$\bar{p}^{(3)} = \frac{S_o}{s}\left(\frac{c_f}{2G\kappa}C_1\mathrm{K}_2(\xi_f r) + A_1C_2\frac{R^2}{r^2}\right)\cos 2(\theta - \theta_r) \tag{B.11}$$

$$\bar{\sigma}_{rr}^{(3)} = \frac{S_o}{s}\left[A_1C_1\left(\frac{1}{\xi_f r}\mathrm{K}_1(\xi_f r) + \frac{6}{(\xi_f r)^2}\mathrm{K}_2(\xi_f r)\right) - A_2C_2\frac{R^2}{r^2} - 3C_3\frac{R^4}{r^4}\right]\cos 2(\theta - \theta_r) \tag{B.12}$$

$$\bar{\sigma}_{\theta\theta}^{(3)} = \frac{S_o}{s}\left[-A_1C_1\left(\frac{1}{\xi_f r}\mathrm{K}_1(\xi_f r) + \left(1 + \frac{6}{(\xi_f r)^2}\right)\mathrm{K}_2(\xi_f r)\right) + 3C_3\frac{R^4}{r^4}\right]\cos 2(\theta - \theta_r) \tag{B.13}$$

$$\tilde{\tau}_{r\theta}^{(3)} = \frac{S_o}{s}\left[2A_1C_1\left(\frac{1}{\xi_f r}\mathrm{K}_1(\xi_f r) + \frac{3}{(\xi_f r)^2}\mathrm{K}_2(\xi_f r)\right) - \frac{A_2}{2}C_2\frac{R^2}{r^2} - 3C_3\frac{R^4}{r^4}\right]\sin 2(\theta - \theta_r) \tag{B.14}$$

In the above, the Constants $C_1$, $C_2$, $C_3$ are obtained substituting the boundary conditions. For the permeable boundary condition model these are given as

$$C_1 = \frac{4}{2A_1(B_3 - B_2) - A_2B_1} \tag{B.15}$$

$$C_2 = -\frac{4B_1}{2A_1(B_3 - B_2) - A_2B_1} \tag{B.16}$$

$$C_3 = \frac{2A_1(B_2 + B_3) + 3A_2B_1}{3[2A_1(B_3 - B_2) - A_2B_1]} \tag{B.17}$$

in which

$$A_1 = \frac{\alpha M}{M_{11} + \alpha^2 M} \tag{B.18}$$

$$A_2 = \frac{M_{11} + M_{12} + 2\alpha^2 M}{M_{11} + \alpha^2 M} \tag{B.19}$$

$$B_1 = \frac{M_{11}}{2G\alpha}\mathrm{K}_2(\xi_f R) \tag{B.20}$$

$$B_2 = \frac{1}{\xi_f R}\mathrm{K}_1(\xi_f R) + \frac{6}{(\xi_f R)^2}\mathrm{K}_2(\xi_f R) \tag{B.21}$$

$$B_3 = 2\left(\frac{1}{\xi_f R}\mathrm{K}_1(\xi_f R) + \frac{3}{(\xi_f R)^2}\mathrm{K}_2(\xi_f R)\right) \tag{B.22}$$

### B.1.2 Impermeable Boundary Condition Model

Solutions for stress and pore pressure distributions for the transversely isotropic poroelastic impermeable boundary condition model are given as follows:

**Solutions for Case 1:**

Solutions for $\sigma_{rr}^{(1)}$ and $\sigma_{\theta\theta}^{(1)}$ for the impermeable boundary condition model are the same as given by equations (B.1) and (B.2) respectively.

**Solutions for Case 2:**

Case 2 for the poroelastic impermeable boundary condition model yields trivial solutions (*Cui et al.*, 1998).

**Solutions for Case 3:**

The solutions for $\sigma_{rr}^{(3)}$, $\sigma_{\theta\theta}^{(3)}$, $\sigma_{r\theta}^{(3)}$, $p^{(3)}$ are the same as given in equations (B.9) - (B.12). The constants $C_1$, $C_2$ and $C_3$ for the impermeable boundary condition model are given by

$$C_1 = \frac{8}{2A_3(B_6 - B_5) - A_4 B_4} \tag{B.23}$$

$$C_2 = -\frac{4B_4}{2A_3(B_6 - B_5) - A_4 B_4} \tag{B.24}$$

$$C_3 = \frac{2A_3(B_5 + B_6) + 3A_4 B_4}{3[2A_3(B_6 - B_5) - A_4 B_4]} \tag{B.25}$$

in which

$$A_3 = \frac{\alpha M}{M_{11} + \alpha^2 M} \tag{B.26}$$

$$A_4 = \frac{M_{11} + M_{12} + 2\alpha^2 M}{M_{11} + \alpha^2 M} \tag{B.27}$$

$$B_4 = \frac{M_{11}}{2G\alpha}\left[\mathrm{K}_2(\xi_f R) + (\xi_f R)\,\mathrm{K}_1(\xi_f R)\right] \tag{B.28}$$

$$B_5 = 2\left[\frac{1}{\xi_f R}\mathrm{K}_1(\xi_f R) + \frac{6}{(\xi_f R)^2}\mathrm{K}_2(\xi_f R)\right] \tag{B.29}$$

$$B_6 = 4\left(\frac{1}{\xi_f R}\mathrm{K}_1(\xi_f R) + \frac{3}{(\xi_f R)^2}\mathrm{K}_2(\xi_f R)\right) \tag{B.30}$$

## B.2 Isotropic Solution

The complete poroelastic solution for the inclined borehole for the isotropic case is given by equations (3.54) - (3.61) setting $\varpi_1 = 1, \varpi_2 = 0, \varpi_3 = 0$ along with $\alpha' = \alpha$ and $\nu' = \nu$. Expressions for $\sigma_{rr}^{(1)}$, $\sigma_{rr}^{(2)}$, $\sigma_{rr}^{(3)}$, $\sigma_{\theta\theta}^{(1)}$, $\sigma_{\theta\theta}^{(2)}$, $\sigma_{\theta\theta}^{(3)}$, $\sigma_{r\theta}^{(3)}$, $p^{(2)}$, $p^{(3)}$, and $T^{(2)}$ for permeable and impermeable boundary condition models are given in the following sections. Note that

solutions for Case 2 and 3 are obtained in the Laplace domain and inverted to time domain using the Stehfest algorithm (*Stehfest*, 1970).

### B.2.1 Permeable Boundary Condition Model

Solutions for stress and pore pressure distributions for the isotropic poroelastic permeable boundary condition model are given as follows (*Cui et al.*, 1997):

**Solutions for Case 1:**

Solutions for $\sigma_{rr}^{(1)}$ and $\sigma_{\theta\theta}^{(1)}$ for the isotropic permeable boundary condition model are the same as given by equations (B.1) and (B.2) respectively.

**Solutions for Case 2:**

$$s\tilde{p}^{(2)} = F_1\Phi(\xi_f) \tag{B.31}$$

$$s\tilde{\sigma}_{rr}^{(2)} = \alpha\left(\frac{1-2\nu}{1-\nu}\right)F_1\Psi(\xi_f) \tag{B.32}$$

$$s\tilde{\sigma}_{\theta\theta}^{(2)} = -\alpha\left(\frac{1-2\nu}{1-\nu}\right)F_1\Omega(\xi_f) \tag{B.33}$$

where the functions $\xi_f$, $F_1$, $\Phi(x)$, $\Psi(x)$ and $\Omega(x)$ are given by equations (B.6) - (B.10).

**Solutions for Case 3:**

$$\tilde{p}^{(3)} = \frac{S_o}{s}\left[\frac{B^2(1-\nu)(1+\nu_u)^2}{9(1-\nu_u)(\nu_u-\nu)}C_1\mathrm{K}_1(\xi_f r) + \frac{B(1+\nu_u)}{3(1-\nu_u)}C_2\frac{R^2}{r^2}\right]\cos 2(\theta-\theta_r) \tag{B.34}$$

$$\tilde{\sigma}_{rr}^{(3)} = \frac{S_o}{s}\left[\frac{B(1+\nu_u)}{3(1-\nu_u)}C_1\left(\frac{1}{\xi_f r}\mathrm{K}_1(\xi_f r) + \frac{6}{(\xi_f r)^2}\mathrm{K}_2(\xi_f r)\right) - \frac{1}{1-\nu_u}C_2\frac{R^2}{r^2} - 3C_3\frac{R^4}{r^4}\right]\cos 2(\theta-\theta_r) \tag{B.35}$$

$$\tilde{\sigma}_{\theta\theta}^{(3)} = \frac{S_o}{s}\left[-\frac{B(1+\nu_u)}{3(1-\nu_u)}C_1\left(\frac{1}{\xi_f r}\mathrm{K}_1(\xi_f r)\left[1+\frac{6}{(\xi_f r)^2}\right]\mathrm{K}_2(\xi_f r)\right) + 3C_3\frac{R^4}{r^4}\right]\cos 2(\theta-\theta_r) \tag{B.36}$$

$$\tilde{\tau}_{r\theta}^{(3)} = \frac{S_o}{s}\left[\frac{2B(1+\nu_u)}{3(1-\nu_u)}C_1\left(\frac{1}{\xi_f r}\mathrm{K}_1(\xi_f r) + \frac{3}{(\xi_f r)^2}\mathrm{K}_2(\xi_f r)\right) - \frac{1}{2(1-\nu_u)}C_2\frac{R^2}{r^2} - 3C_3\frac{R^4}{r^4}\right]\sin 2(\theta-\theta_r) \tag{B.37}$$

where the constants $C_1$, $C_2$, $C_3$ are given by

$$C_1 = -\frac{12\xi_f R(1-\nu_u)(\nu_u-\nu)}{B(1+\nu_u)(D_2-D_1)} \tag{B.38}$$

$$C_2 = \frac{2(1-\nu_u)D_2}{D_2-D_1} \tag{B.39}$$

$$C_3 = -\frac{\xi_f R(D_2-D_1)+8(\nu_u-\nu)\mathrm{K}_2(\xi_f R)}{\xi_f R(D_2-D_1)} \tag{B.40}$$

in which the constants $D_1$ and $D_2$ are given by

$$D_1 = 2(\nu_u-\nu)\mathrm{K}_1(\xi_f R) \tag{B.41}$$

$$D_2 = \xi_f R(1-\nu)\mathrm{K}_2(\xi_f R) \tag{B.42}$$

### B.2.2 Impermeable Boundary Conditon Model

Solutions for stress and pore pressure distributions for the isotropic poroelastic impermeable boundary condition model are given as follows:

**Solutions for Case 1:**

Solutions for $\sigma_{rr}^{(1)}$ and $\sigma_{\theta\theta}^{(1)}$ for the isotropic impermeable boundary condition model are the same as given by equations (B.1) and (B.2) respectively.

**Solutions for Case 2:**

Case 2 for the poroelastic impermeable boundary condition model yields trivial solutions (*Cui et al.*, 1998).

**Solutions for Case 3:**

The solutions for $\sigma_{rr}^{(3)}$, $\sigma_{\theta\theta}^{(3)}$, $\sigma_{r\theta}^{(3)}$, $p^{(3)}$ are the same as given in equations (B.34) - (B.37). The constants $C_1$, $C_2$ and $C_3$ for the impermeable boundary condition model are given

by

$$C_1 = -\frac{24\xi_f R(1-\nu_u)(\nu_u-\nu)}{B(1+\nu_u)(D_4-D_3)} \tag{B.43}$$

$$C_2 = \frac{4(1-\nu_u)D_4}{D_4-D_3} \tag{B.44}$$

$$C_3 = -\frac{\xi_f R(D_4-D_3)+16(\nu_u-\nu)\mathrm{K}_2(\xi_f R)}{\xi_f R(D_4-D_3)} \tag{B.45}$$

in which the constants $D_3$ and $D_4$ are given by

$$D_3 = 4(\nu_u-\nu)\mathrm{K}_1(\xi_f R) \tag{B.46}$$

$$D_4 = \xi_f R(1-\nu)[2\mathrm{K}_2(\xi_f R)+(\xi_f R)\,\mathrm{K}_1(\xi_f R)] \tag{B.47}$$

# Appendix C

# Isotropic Porothermoelastic Borehole Solution

The porothermoelastic isotropic inclined borehole solution is presented in this Appendix. The solutions for the stress and pore pressure fields are given by equations (3.54) - (3.61) setting $\varpi_1 = 1., \varpi_2 = 1., \varpi_3 = 0$ and $\alpha' = \alpha$, $\nu' = \nu$ and $\beta^{s'} = \beta^s$. Expressions for $\sigma_{rr}^{(1)}$, $\sigma_{rr}^{(2)}$, $\sigma_{rr}^{(3)}$, $\sigma_{\theta\theta}^{(1)}$, $\sigma_{\theta\theta}^{(2)}$, $\sigma_{\theta\theta}^{(3)}$, $\sigma_{r\theta}^{(3)}$, $p^{(2)}$, $p^{(3)}$, and $T^{(2)}$ for permeable and impermeable boundary conditions at the borehole wall are given in the following sections. Note that solutions for Case 2 and 3 are obtained in the Laplace domain and inverted to time domain using the Stehfest algorithm (*Stehfest*, 1970).

## C.1 Permeable Boundary Condition Model

Isotropic porothermoelastic solutions for the permeable boundary condition model are given as follows (*Li*, 1998)

**Solutions for Case 1:**

Solutions for mode 1, i.e. $\sigma_{rr}^{(1)}$ and $\sigma_{\theta\theta}^{(1)}$ are the same as given by equations (B.1) and (B.2) respectively.

**Solutions for Case 2:**

$$s\tilde{T}^{(2)} = (T_w - T_o)\Phi(\xi_h) \tag{C.1}$$

$$s\tilde{p}^{(2)} = F_2\Phi(\xi_f) + F_3\Phi(\xi_h) \tag{C.2}$$

$$\begin{aligned} s\tilde{\sigma}_{rr}^{(2)} &= \alpha\left(\frac{1-2\nu}{1-\nu}\right)\{F_2\Psi(\xi_f) + F_3\Psi(\xi_h)\} \\ &+\beta^s\left(\frac{1-2\nu}{1-\nu}\right)\{(T_w - T_o)\Psi(\xi_h)\} \end{aligned} \tag{C.3}$$

$$\begin{aligned} s\tilde{\sigma}_{\theta\theta}^{(2)} &= -\alpha\left(\frac{1-2\nu}{1-\nu}\right)\{F_2\Omega(\xi_f) + F_3\Omega(\xi_h)\} \\ &-\beta^s\left(\frac{1-2\nu}{1-\nu}\right)\{(T_w - T_o)\Omega(\xi_h)\} \end{aligned} \tag{C.4}$$

where the functions $\Phi(x)$, $\Psi(x)$ and $\Omega(x)$, are given by equations (B.8) - (B.10), $F_2$, $F_3$ are given by equations (4.71) and (4.72) and

$$\xi_f = \sqrt{\frac{s}{c_f}}; \qquad \xi_h = \sqrt{\frac{s}{c_h}} \tag{C.5}$$

**Solutions for Case 3:**

Solutions for Case 3 are the same as in the poroelastic case and are given by equations (B.34) - (B.42).

## C.2 Impermeable Boundary Condition Model

Solutions for stress and pore pressure distributions for the isotropic porothermoelastic impermeable boundary condition model are given as follows:

**Solutions for Case 1:**

Solutions for $\sigma_{rr}^{(1)}$ and $\sigma_{\theta\theta}^{(1)}$ for the impermeable boundary condition model are given by equations (B.1) and (B.2).

**Solutions for Case 2:**

$$s\tilde{T}^{(2)} = (T_w - T_o)\Phi(\xi_h) \tag{C.6}$$

$$s\tilde{p}^{(2)} = F_3 \left\{ -\frac{\xi_h}{\xi_f} \left[ \frac{\mathrm{K}_1(\xi_h R)}{\mathrm{K}_0(\xi_h R)} \right] \left[ \frac{\mathrm{K}_0(\xi_f r)}{\mathrm{K}_1(\xi_f R)} \right] + \Phi(\xi_h) \right\} \tag{C.7}$$

$$\begin{aligned} s\tilde{\sigma}_{rr}^{(2)} = \alpha \left( \frac{1-2\nu}{1-\nu} \right) F_3 \Bigg\{ & \left[ \frac{\xi_h}{\xi_f} \frac{1}{\xi_f r} \frac{\mathrm{K}_1(\xi_h R)}{\mathrm{K}_0(\xi_h R)} \right] \left[ \frac{R}{r} - \frac{\mathrm{K}_1(\xi_f r)}{\mathrm{K}_1(\xi_f R)} \right] \\ & + \left[ \frac{1}{\xi_h r} \frac{\mathrm{K}_1(\xi_h R)}{\mathrm{K}_0(\xi_h R)} \left( 1 - \frac{R}{r} \right) \right] \Bigg\} \\ & + \beta^s \left( 1 - \frac{M_{12}}{M_{11}} \right) (T_w - T_o) \left\{ \frac{1}{\xi_h r} \frac{\mathrm{K}_1(\xi_h R)}{\mathrm{K}_0(\xi_h R)} \left( 1 - \frac{R}{r} \right) \right\} \end{aligned} \tag{C.8}$$

$$\begin{aligned} s\tilde{\sigma}_{\theta\theta}^{(2)} = -\alpha \left( 1 - \frac{M_{12}}{M_{11}} \right) F_3 \Bigg\{ & \left[ \frac{\xi_h}{\xi_f} \frac{\mathrm{K}_1(\xi_h R)}{\mathrm{K}_0(\xi_h R)} \right] \left[ \frac{1}{\xi_f r} \frac{R}{r} - \frac{1}{\xi_f r} \frac{\mathrm{K}_1(\xi_f r)}{\mathrm{K}_1(\xi_f R)} - \frac{\mathrm{K}_0(\xi_f r)}{\mathrm{K}_1(\xi_f R)} \right] \\ & + \left[ \frac{1}{\xi_h r} \frac{\mathrm{K}_1(\xi_h r)}{\mathrm{K}_0(\xi_h R)} - \frac{R}{r} \frac{1}{\xi_h r} \frac{\mathrm{K}_1(\xi_h R)}{\mathrm{K}_0(\xi_h R)} + \Phi(\xi_h) \right] \Bigg\} \\ & - \beta^s \left( 1 - \frac{M_{12}}{M_{11}} \right) (T_w - T_o) \Bigg\{ \frac{1}{\xi_h r} \frac{\mathrm{K}_1(\xi_h r)}{\mathrm{K}_0(\xi_h R)} \\ & - \frac{R}{r} \frac{1}{\xi_h r} \frac{\mathrm{K}_1(\xi_h R)}{\mathrm{K}_0(\xi_h R)} + \Phi(\xi_h) \Bigg\} \end{aligned} \tag{C.9}$$

**Solutions for Case 3:**

The solutions for $\sigma_{rr}^{(3)}$, $\sigma_{\theta\theta}^{(3)}$, $\sigma_{r\theta}^{(3)}$, $p^{(3)}$ are the same as the poroelastic case and given by equations (B.34) - (B.37) and (B.43) - (B.47).

# Appendix D

# Isotropic Porochemoelastic Borehole Solution

The porochemoelastic isotropic inclined borehole solution is presented in this Appendix.. The solutions for the stress and pore pressure fields are given by equations (3.54) - (3.61) setting $\varpi_1 = 1, \varpi_2 = 0, \varpi_3 = 1$ and $\alpha' = \alpha$, $\nu' = \nu$ and $\gamma^{s'} = \gamma^s$. Expressions for $\sigma_{rr}^{(1)}$, $\sigma_{rr}^{(2)}$, $\sigma_{rr}^{(3)}$, $\sigma_{\theta\theta}^{(1)}$, $\sigma_{\theta\theta}^{(2)}$, $\sigma_{\theta\theta}^{(3)}$, $\sigma_{r\theta}^{(3)}$, $p^{(2)}$, and $p^{(3)}$ for permeable and impermeable boundary conditions at the borehole wall are given in the following sections. Note that solutions for Case 2 and 3 are obtained in the Laplace domain and inverted to time domain using the Stehfest algorithm (*Stehfest*, 1970).

## D.1 Permeable Boundary Condition Model

Isotropic porothermoelastic solutions for the permeable boundary condition model are given as follows:

**Solutions for Case 1:**

Solutions for Case 1, i.e. $\sigma_{rr}^{(1)}$ and $\sigma_{\theta\theta}^{(1)}$ are the same as given by equations (B.1) and (B.2) respectively.

**Solutions for Case 2:**

$$s\bar{m}^s = [(m_w^s - m_o^s)]\,\Phi(\xi_1) \tag{D.1}$$

$$s\bar{p} = F_4\Phi(\xi_1) + F_5\Phi(\xi_2) \tag{D.2}$$

$$s\bar{\sigma}_{rr}^{(2)} = 2\eta\left\{F_4\Psi(\xi_1) + F_5\Psi(\xi_2)\right\} - \gamma^s\left(\frac{(1-2\nu)}{(1-\nu)}\right)\left\{(m_w^s - m_o^s)\,\Psi(\xi_1)\right\} \tag{D.3}$$

$$s\bar{\sigma}_{\theta\theta}^{(2)} = -2\eta\{F_4\Omega(\xi_1) + F_5\Omega(\xi_2)\} + \gamma^s\left(\frac{(1-2\nu)}{(1-\nu)}\right)\left\{(m_w^s - m_o^s)\,\Omega(\xi_1)\right\} \tag{D.4}$$

where the functions $\Phi(x)$, $\Psi(x)$ and $\Omega(x)$, are given by equations (B.8) - (B.10) and $F_4$, $F_5$ are given by equations (5.89) and (5.90) respectively.

**Solutions for Case 3:**

Solutions for Case 3 are the same as in the poroelastic case and are given by equations (B.34) - (B.42) with $\xi_f = \xi_2$.

## D.2 Impermeable Boundary Condition Model

Solutions for stress and pore pressure distributions for the isotropic porothermoelastic impermeable boundary condition model are given as follows:

**Solutions for Case 1:**

Solutions for $\sigma_{rr}^{(1)}$ and $\sigma_{\theta\theta}^{(1)}$ for the impermeable boundary condition model are given by equations (B.1) and (B.2).

**Solutions for Case 2:**

$$s\bar{m}^s = [(m_w^s - m_o^s)]\,\Phi(\xi_1) \tag{D.5}$$

$$s\bar{p} = F_4\left\{\Phi(\xi_2) - \frac{\xi_1}{\xi_2}\left[\frac{\mathrm{K}_1(\xi_1 R)}{\mathrm{K}_0(\xi_1 R)}\right]\left[\frac{\mathrm{K}_0(\xi_2 r)}{\mathrm{K}_1(\xi_2 R)}\right]\right\} \tag{D.6}$$

$$s\tilde{\sigma}_{rr}^{(2)} = 2\eta F_4 \left\{ \left[ \frac{\xi_1}{\xi_2} \frac{1}{\xi_2 r} \frac{\mathrm{K}_1(\xi_1 R)}{\mathrm{K}_0(\xi_1 R)} \right] \left[ \frac{R}{r} - \frac{\mathrm{K}_1(\xi_2 r)}{\mathrm{K}_1(\xi_2 R)} \right] + \left[ \frac{1}{\xi_1 r} \frac{\mathrm{K}_1(\xi_1 R)}{\mathrm{K}_0(\xi_1 R)} \left( 1 - \frac{R}{r} \right) \right] \right\}$$
$$-\gamma^s \left( \frac{(1-2\nu)}{(1-\nu)} \right) (m_w^s - m_o^s) \left\{ \frac{1}{\xi_1 r} \frac{\mathrm{K}_1(\xi_1 R)}{\mathrm{K}_0(\xi_1 R)} \left( 1 - \frac{R}{r} \right) \right\} \tag{D.7}$$

$$s\tilde{\sigma}_{\theta\theta}^{(2)} = -2\eta F_4 \left\{ \left[ \frac{\xi_1}{\xi_2} \frac{\mathrm{K}_1(\xi_1 R)}{\mathrm{K}_0(\xi_1 R)} \right] \left[ \frac{1}{\xi_2 r} \frac{R}{r} - \frac{1}{\xi_2 r} \frac{\mathrm{K}_1(\xi_2 r)}{\mathrm{K}_1(\xi_2 R)} - \frac{\mathrm{K}_0(\xi_2 r)}{\mathrm{K}_1(\xi_2 R)} \right] + \left[ \frac{1}{\xi_1 r} \frac{\mathrm{K}_1(\xi_1 r)}{\mathrm{K}_0(\xi_1 R)} - \frac{R}{r} \frac{1}{\xi_1 r} \frac{\mathrm{K}_1(\xi_1 R)}{\mathrm{K}_0(\xi_1 R)} + \Phi(\xi_1) \right] \right\}$$
$$+\gamma^s \left( \frac{(1-2\nu)}{(1-\nu)} \right) (m_w^s - m_o^s) \left\{ \frac{1}{\xi_1 r} \frac{\mathrm{K}_1(\xi_1 r)}{\mathrm{K}_0(\xi_1 R)} - \frac{R}{r} \frac{1}{\xi_1 r} \frac{\mathrm{K}_1(\xi_1 R)}{\mathrm{K}_0(\xi_1 R)} + \Phi(\xi_1) \right\} \tag{D.8}$$

**Solutions for Case 3:**

The solutions for $\sigma_{rr}^{(3)}$, $\sigma_{\theta\theta}^{(3)}$, $\sigma_{r\theta}^{(3)}$, $p^{(3)}$ are the same as the poroelastic case and given by equations (B.34) - (B.37) and (B.43) - (B.47) again with $\xi_f = \xi_2$.

# Appendix E

# Isotropic Porochemothermoelastic Borehole Solution

The porochemothermoelastic isotropic inclined borehole solution is presented in this Appendix.. The solutions for the stress and pore pressure fields are given by equations (3.54) - (3.61) setting $\varpi_1 = 1, \varpi_2 = 0, \varpi_3 = 1$ and $\alpha' = \alpha$, $\nu' = \nu$ and $\gamma^{s'} = \gamma^s$. Expressions for $\sigma_{rr}^{(1)}$, $\sigma_{rr}^{(2)}$, $\sigma_{rr}^{(3)}$, $\sigma_{\theta\theta}^{(1)}$, $\sigma_{\theta\theta}^{(2)}$, $\sigma_{\theta\theta}^{(3)}$, $\sigma_{r\theta}^{(3)}$, $p^{(2)}$, and $p^{(3)}$ for permeable and impermeable boundary conditions at the borehole wall are given in the following sections.

## E.1 Permeable Boundary Condition Model

Isotropic porothermoelastic solutions for the permeable boundary condition model are given as follows:

**Solutions for Case 1:**

Solutions for Case 1, i.e. $\sigma_{rr}^{(1)}$ and $\sigma_{\theta\theta}^{(1)}$ are the same as given by equations (B.1) and (B.2) respectively.

**Solutions for Case 2:**

$$s\bar{m}^s = \left[(m_w^s - m_o^s)\right]\Phi(\xi_1) \tag{E.1}$$

$$\bar{p} = F_6\Phi(\xi_1) + F_7\Phi(\xi_2) + F_8\Phi(\xi_3) \tag{E.2}$$

$$
\begin{aligned}
s\tilde{\sigma}_{rr}^{(2)} &= 2\eta \left\{ F_6 \Psi(\xi_1) + F_7 \Psi(\xi_2) + F_8 \Psi(\xi_3) \right\} \\
&+ \beta^s \left( \frac{(1-2\nu)}{(1-\nu)} \right) \left\{ (T_w - T_o) \Psi(\xi_3) \right\} \\
&- \gamma^s \left( \frac{(1-2\nu)}{(1-\nu)} \right) \left\{ (m_w^s - m_o^s)\, \Psi(\xi_1) \right\} \qquad \text{(E.3)} \\
s\tilde{\sigma}_{\theta\theta}^{(2)} &= -2\eta \{ F_6 \Omega(\xi_1) + F_7 \Omega(\xi_2) + F_8 \Omega(\xi_3) \} \\
&- \beta^s \left( \frac{(1-2\nu)}{(1-\nu)} \right) \left\{ (T_w - T_o) \Omega(\xi_3) \right\} \\
&+ \gamma^s \left( \frac{(1-2\nu)}{(1-\nu)} \right) \left\{ (m_w^s - m_o^s)\, \Omega(\xi_1) \right\} \qquad \text{(E.4)}
\end{aligned}
$$

where the functions $\Phi(x)$, $\Psi(x)$ and $\Omega(x)$, are given by equations (B.8) - (B.10) and $F_6$, $F_7$ and $F_8$ are given by equations (6.103) - (6.105).

**Solutions for Case 3:**

Solutions for Case 3 are the same as in the poroelastic case and are given by equations (B.34) - (B.42) with $\xi_f = \xi_2$.